THIRD SEMI-ANNUAL TECHNICAL REPORT

ELECTRICAL and OPTICAL PROPERTIES of AMORPHOUS MATERIALS*

by

A Solid-State Group of the Physics Department
Northern Illinois University
DeKalb, Illinois 60115

*Sponsored by
Advanced Research Projects Agency
ARPA Order No. 1562

DISCLAIMER NOTICE

THIS DOCUMENT IS THE BEST QUALITY AVAILABLE.

COPY FURNISHED CONTAINED A SIGNIFICANT NUMBER OF PAGES WHICH DO NOT REPRODUCE LEGIBLY.

GENERAL INFORMATION

ARPA Order Number	1562
Program Code Number	0D10
Name of Contractor	U. S. Army Research Office
Effective Date of Contract	June 1, 1971
Contract Expiration Date	May 31, 1972
Amount of Contract	$58,000.00
Contract Number	DA-ARO-D-31-124-71-G132
Principal Investigator	Dr. Charles Wood (815) 753-1773

CONTENTS

SUMMARY

A considerable proportion of the last six months was spent on investigating in more depth the areas outlined in the last semi-annual report and published in the Bull. Amer. Phys. Soc. abstracts. This endeavor has resulted in a series of preprints which are being submitted for publication and which are appended at the end of this report.

The more significant developments in this period are summarized below:

Kramers-Kronig analysis of reflectance data is becoming a routine procedure and has been applied to amorphous and crystalline Sb_2Se_3 over a wide spectral range from 0 to 35 eV, (using synchrotron radiation for the higher energies) giving us essentially complete experimental data to characterize the material.

An accurate procedure has been developed for the computation of optical constants of thin films from reflectance and transmittance data.

We have discovered important effects relating to materials preparation e.g., the effect of compositional fluctuations on the optical properties of thin films and have developed a method to overcome this problem.

The scope of materials investigations has been enlarged to include all of the antimony chalcogenides and stoichiometric compounds of single crystal and amorphous Sb_2Te_3 and Sb_2O_3 have been prepared and are undergoing investigation.

Room-temperature photoconductivity results have been completed, essentially, and agree with optical absorption measurements.

Mossbauer studies are proving to be an extremely useful tool in studying the microstructure of amorphous material and has been utilized to investigate Sn-doped

As_2Se_3 glasses.

More details will be found on these topics in the body of this report and even more information in the appendices.

THEORETICAL RESEARCH

A) Kramers-Kronig Analysis

The development of a computational scheme for doing Kramers-Kronig analysis of optical data which was both rapid and accurate was one of the principal objectives of the theoretical work under this grant from its inception. We believe that that objective has been completely attained (1). In this report in Appendix A there are presented the results of a Kramers-Kronig analysis of reflectivity data taken in two polarizations on crystalline Sb_2Se_3 as well as on amorphous films of Sb_2Se_3 (see Optical Properties). We thus have the requisite information to compare with the results of the band calculation discussed below.

B) The Band Structure of Sb_2Se_3

With the experimental optical properties of Sb_2Se_3 in both the crystalline and amorphous states well characterized the calculation of the band structure of crystalline and amorphous Sb_2Se_3 seems a logical step. Thus we are initiating a pseudopotential band calculation on the crystalline material. Since Sb_2Se_3 has a large number of atoms in the unit cell and, as has been indicated by its optical properties, is quite anisotropic a large number of plane waves will be needed to obtain reasonably accurate results for this material. Other than the practical considerations involved in diagonalizing large matrices (an excess of 100 x 100) we foresee no difficulties in the computation of the band structure of Sb_2Se_3. We will also compute the density of states, and the joint density of states of crystalline Sb_2Se_3 for comparison with experiment through $\varepsilon_2(\omega)$ as obtained from the reflectivity and photoemission data. In addition we are planning to attempt

a computation of the density of states of the amorphous material by the correlated basis function method outlined in our previous reports. Such a computation requires the results from the calculation upon the crystalline material.

MATERIALS PREPARATION

A) Amorphous Thin Films

An intensive effort has been made to accurately control coevaporation rates of Sb and Se with limited success using Sloan Omni II A monitors and rate controllers. Although electron microprobe analysis shows reasonable correlation between rates and composition, it appears at present that some optical properties are more sensitive to slight composition changes and inhomogeneities. In particular we find that a small modulation is imposed on the maxima and minima of the interference fringes observed in transmission and reflection spectra at wavelengths longer than the absorption edge. By deliberately modulating the evaporation rate of one element, e.g., Sb, we have markedly increased the magnitude of the modulation in height of the fringes. The incorporation of two electron-beam guns for sources, instead of an electron-beam gun for Sb and a resistance heated source for Se, has not yielded much improvement.

Evaporation from a single source of Sb_2Se_3 using an electron-beam gun has produced films which do not show the interference fringe modulation. To overcome the problem of stoichiometry we have allowed equilibrium to be attained at the source surface before allowing deposition to occur on the substrate, and have examined the composition of the films at successive stages of deposition by microprobe analysis. A full report is given in Appendix B.

Amorphous Sb_2Te_3 has been produced by coevaporation in the standard system onto quartz substrates at room temperature. As in the case of antimony (2) there appears to be a dependence on the degree of amorphousness on film thickness.

Films 0.1μ thick appeared amorphous by x-ray diffraction while films 1μ thick showed signs of partial crystallinity.

B) Single Crystals

The single crystal growth apparatus using tin-oxide coated quartz tubes as furnace elements is now in operation. A report of its development and success in growing single crystals is attached in Appendix C.

This apparatus is also in use for vapor-phase growth of single crystals and small crystals of orthorhombic Sb_2O_3 suitable for optical studies have been produced.

STRUCTURAL INVESTIGATIONS

A) Mossbauer Studies

A Mossbauer study has been undertaken of amorphous semiconducting glasses $Sn_x(As_2Se_3)_{1-x}$ (x = 2.5, 5.0, 8.0 and 10.0 atomic percent tin) in order to delineate the role of the Group IV element in an analogue of a switching glass (3,4). In contrast to the findings of Shkolnikov (5), the degree of amorphousness is found to be dependent on the method of preparation of the glass. Although x-ray diffraction measurements indicate no long-range order in the amorphous samples, the Mossbauer measurements at Sn atoms show almost perfect short-range order. Tin occurs in only one phase in the amorphous samples for low tin concentrations (up to 5.0%) and in two phases at higher concentrations; further, the spectra are similar to those for crystalline $SnSe_2$ and SnSe, respectively, as predicted by Shkolnikov (5) and observed by Borisova (4). The long-range disorder in the glasses leads to small and approximately constant differences in the isomer shift and in the quadrupolar coupling at the Sn atom between glass and crystal. Debye temperatures for the Sn atom are estimated from the temperature dependence of the Mossbauer absorption at 4.2, 77.3, and 298°K. The Debye temperatures are $\sim$100±10°K for SnIV and SnII in the glassy state. Within the error of measurement the same Debye temperature fits the data between 4.2 and 77.3°K and between 77.3 and 298°K for amorphous samples; the glass to crystal transition therefore takes place above room temperature. A full report is given in Appendix D.

Future work planned includes a Mossbauer study at Sb^{121} nuclei in amorphous InSb. The presence and nature of any short-range order in the glassy state will be deter-

mined for a system which is cubic in the crystalline state.

B) X-ray and Electron Diffraction Studies

It has been our goal to determine the geometrical arrangement of substituted selenium in $Sb_2Se_xTe_{3(1-x)}$ samples of various compositions. Sb_2Te_3 is known to crystallize in a layer structure with a 15 layer sequence perpendicular to the crystallographic c-axis. Six of the tellurium layers are related to one group of symmetry operations, three of the layers to another such group. Two thirds of the tellurium can be replaced by selenium before the structure breaks down. As a first step we have attempted to determine in which of the above described layers the selenium may be found. For this purpose intensity computations for the following three cases have been made: 1) The Se is statistically distributed within the six symmetrically equivalent layers. 2) The Se is statistically distributed within the other three Te layers until these layers are completely filled up, any additional Se going into the other six layers. 3) The Se can be found with equal statistical probability in any of the nine Te layers.

In order to compare the experiment with the three models, we measured the intensities and positions of the (00ℓ) x-ray reflections of single crystals. We found none of the models to fit the experimental data as long as one assumes no change of relative distances between layers with sample composition. Such a change, expressed by the atom "parameters", is presently being investigated by means of a least square refinement. The c lattice constant was found to linearly decrease with increasing Se content. Our results agreed within 2% with those reported in the literature (6).

Thin films of Sb_xSe_y ranging from Sb_1Se_3 to $Sb_{3.5}Se_3$ have been investigated by electron microscopy and selected area electron diffraction. By variation of the electron beam intensity, crystallographic changes could be introduced to the specimen. Although the electron micrographs varied considerably in appearance, the diffraction patterns for different compositions showed striking similarities. It was observed that segregation of phases within the sample took place. Some of the changes were reversible when the electron beam intensity was reduced. A complete account of this work is reported in Appendix E.

OPTICAL PROPERTIES

A) Transmission & Reflectivity Measurements

Near normal incidence optical reflectance and transmittance of single crystal Sb_2Se_3 for E||a and E||c has been extended over a broad energy range from $\sim 3 \times 10^{-3}$ eV (300μ) to $\sim$35 eV (300Å)* to allow a Kramers-Kronig calculation of dielectric constants and hence joint densities of states. A comparison of this data over much of the energy range with amorphous Sb_2Se_3 has shown that while the absence of long range order smears out the reflectance structure associated with low energy transitions, the higher energy electronic spectra involving core electrons closely coincide for the two forms of Sb_2Se_3. The data and the results are presented in preliminary form in Appendix A.

More detailed measurements have been carried out on crystalline Sb_2Se_3 near the absorption edge, chiefly as a result of improved cleaving techniques, and analysis shows that indirect transitions are responsible for the lower energy transitions with $E_g||a = 1.15$ eV and $E_g||c = 1.19$ eV and a phonon energy of .025 eV. This work is nearly complete but has not as yet been written up for publication.

B) Modulated Reflectivity

Electro-reflectance measurements in single crystal Sb_2Se_3 proved unsuccessful because of the very low electric fields ($\sim$300 v/cm) at which breakdown occurs.

* We gratefully acknowledge the cooperation and assistance of many groups, in particular: Dr. P. Yuster, Solid State Division, Argonne National Laboratory, Dr. L. Basile, Chemistry Division, Argonne National Laboratory, Dr. H. Fritsche, University of Chicago, W. Osmun, University of Chicago, J. Freeoff, University of Chicago and Dr. E. Rowe, Physical Sciences Lab., University of Wisconsin.

Thermally modulated reflectivity cannot be used because the high resistivity precludes the use of direct Joule heating and, because of the low thermal conductivity, indirect heating is not suitable. An alternative approach is being tried i.e., piezoreflectance which has the inherent advantage that uniaxial strain is more amenable as a modulating parameter for theoretical analysis.

C) Computation of Optical Constants of Thin Films

In order to characterize the type of optical transition occurring at the absorption edge and/or possible "band-tailing" in amorphous materials prepared as thin films, it is essential to obtain the optical constants n and k of the thin films from their normal incidence reflectance and transmittance for wavelengths near to and above the fundamental absorption edge. In Appendix F is presented a preprint of a paper which describes in detail a method we have devised for obtaining the optical constants of thin films mounted upon substrates. The technique has been extensively tested upon thin films of amorphous Se as well as hypothetical systems whose reflectance and transmittance have been generated by computer.

Some difficulty has been experienced with the exact determination of optical constants at energies below the absorption edge from reflectance and transmittance measurements on amorphous thin films of Sb_2Se_3 because of a modulation in the height of maxima and minima in the interference fringes. This has now been associated with slight fluctuations in deposition rates during coevaporation (see Materials Section). Films without this modulation are at present being analyzed using the above procedure.

D) Photoconductivity

An intensive investigation has been carried out of the effect of long-range disorder and composition on the photoconductive spectral response of amorphous $Sb_{1-x}Se_x$ films. Measurements on many samples of variable composition indicate that stoichiometric Sb_2Se_3 films have a photoconductivity activation energy E_g of about 1.4 eV as determined from the Moss' criterion. An increasing excess of Sb results in a decrease of E_g (e.g. for $x = 0.52$, $E_g = 0.95$ eV), while the excess of Se resulted in an increase of E_g (e.g. $E_g = 1.65$ eV for $x = 0.86$). In all cases the photoconductivity onset coincides with the optical absorption edge. To our knowledge, this has been the first attempt to investigate the effect of composition of amorphous compound films on physical properties in the case where the compound cannot be prepared by quenching from the melt.

We have also investigated the absolute photoconductivity at $h\nu = 1.65$ eV, from which we obtained the values of the internal photosensitivity ($\mu\tau$) in the range of 6×10^{-10} up to 2×10^{-9} cm^2/V, which is a typical order of magnitude for disordered films. The measured response times* of the order of 10^{-3} sec show the trapping effects are rather strong. Estimates of the density of the trapping states at the quasi-Fermi level E_F^* range from $10^{20}/cm^3$ eV for $E_F^* = 0.35$ eV to $10^{18}/cm^3$ eV for $E_F^* = 0.5$ eV.

We conclude that while the spectral dependence of the photoconductivity implies for the amorphous $Sb_{1-x}Se_x$ films the same density of states in the pseudogap as does optical absorption, a study of the steady state photoconductivity kinetics yields much higher densities of states inside the pseudogap, comparable with values obtained from transport measurements. This fact is stressed even more by comparison

* The method of measuring response times is described in Appendix G and has been accepted for publication in Rev. Sci. Inst.

of amorphous Sb_2Se_3 with single crystal Sb_2Se_3, which has a lower density of trapping states inside the gap by a factor of 10^4 to 10^5, but the sharpness of the photoconductive spectral response onset is comparable to that in the amorphous material. Full details of this work are given in Appendix H.

The photoconductivity of amorphous $Sb_{1-x}Se_x$ films is reasonably well understood at room temperature. The logical extension is to investigate the temperature dependence of the photoconductivity as well as the IR photoconductivity at low temperature. The next material for photoconductivity measurements will be probably amorphous Sb_2Te_3.

Other types of measurements suitable for determining states inside the band are thermally stimulated conductivity and space-charge limited currents. The feasibility of these measurements for our materials will be studied in detail.

E) Photoemission

The energy distribution of the joint density of states was measured using the photoemission spectroscopy technique for both crystalline and amorphous Sb_2Se_3. Although the crystals exhibited more structure in the spectra (this structure is usually associated with the critical points of the Brillouin Zone) than the amorphous films, the onset of photoemission process corresponding to transitions between the maximum in the valence band and the minimum in the conduction band had the same sharpness for both modifications. This lack of band tailing could be explained however, by suppression of the matrix elements for transitions from localized to extended states as suggested by Dow (7). These results were presented at the Fifth International Conference on Amorphous and Liquid Semiconductors at Ann

Arbor, Michigan, (see Appendix I), together with the finding that the photoemission spectrum of amorphous Sb_2Se_3 films could be explained in terms of nondirect transitions while direct transitions are mostly responsible for the spectrum of crystalline Sb_2Se_3.

Future plans include a detailed study of the possible effect of band tailing on the photoemission spectra. In order to perform this experimental study, a high sensitivity detector system for measurements of electron energy will be constructed (the work has already begun). The technique of measuring the higher derivatives of photoemission spectrum will be used to compare the critical point structure in amorphous and crystalline materials.

An arrangement has been made to use the high intensity continuum from the storage ring cynchrotron radiation at the University of Wisconsin at Madison.

F) Transport Properties

A considerable effort has been expended on the measurement of the thermal activation energy of single crystal Sb_2Se_3. Adequate heat sinking of samples and placement of thermocouple appear critical. An average activation energy at 0^oK of 1.26 eV for E||c has been obtained which compares well with the optical value of $\sim$1.2 eV at room temperature if allowance is made for the shift of absorption edge with temperature (-7×10^{-4} eV/^oC) (8). Measurements are proceeding for other orientations of the single crystal and then it is planned to measure the amorphous films as a function of composition. Preliminary measurements on stoichiometric films of Sb_2Se_3 show a thermal activation energy of $\sim$0.5 eV.

I-V characteristics of several contact materials (e.g. Au and Sb) on single

crystal Sb_2Se_3 are under examination. Comparison will be made with similar contact measurements on amorphous material.

References

1. R. Afshar, F. M. Mueller and J. C. Shaffer, (to be published).

2. G. A. Kurov and Z. G. Pinsker, Kristallografiia 1 407 (1956).

3. A. D. Pearson, W. R. Northover, J. F. Dewald and W. F. Peck (1962). Advances in Glass Technology, Plenum Press, New York; B. T. Kolomiets, E. A. Levedev (1963). Radiotechnika i Electronika, 8, 2097; E. L. Eaton (1964). J. Am. Ceram. Soc. 47, 554; Ovshinsky, S. R. (1968). Phys. Rev. Letters, 21, 1450.

4. Z. V. Borisova, L. N. Vasilev, P. P. Seregin and V. T. Shipatov, (1970). Soviet Physics - Semiconductors, 4 (3), 433.

5. E. V. Shkolnikov, (1966). Solid State Chemistry, p. 142 (Edited by E. V. Borisova) Consultants Bureau, New York.

6. Iwao Teramoto and Shigetoshi Takayanagi, J. Phys. Chem. Sol. Vol. 19 1 J24 (1961).

7. J. D. Dow and Y. Y. Hopfield, Proc. of 4th Inter. Conf. on Amorphous and Liquid Semiconductors, Ann Arbor, Michigan, 1971 (to be published).

8. J. Black, E. M. Conwell, L. Seigle and C. W. Spenser, J. Phys. Chem. Solids 2 240 (1957).

FISCAL STATUS

	Amount Allocated	Amount Spent	Balance
Personnel	$44,595	$30,154	$14,441
Supplies, Expenses and Services	10, 984	2,283	8,701
Travel	1,500	657	843
		TOTAL BALANCE	$23,985

Appendix A

Electronic Structure of Single Crystal and Amorphous Sb_2Se_3

J. C. Shaffer, B. Van Pelt and C. Wood
Physics Department
Northern Illinois University
DeKalb, Illinois 60115

and

J. Freeouf and J. W. Osmun
Physics Department
University of Chicago
Chicago, Illinois

The optical properties of single crystal and amorphous Sb_2Se_3 have been measured in the energy range 0 to 30 eV in order to determine the influence of long range order on the electronic structure.

Sb_2Se_3 is orthorhombic ($a = 11.62\text{Å}$ $b = 11.77\text{Å}$ $c = 3.96\text{Å}$)[1] of space group D_{2h}^{16}, type D_8^5, with 20 atoms, i.e., 4 molecules/unit cell. The atoms are arranged in a layer structure with layers $\perp b$ and van der Waals bonding between layers and, therefore, the crystals exhibit natural cleavage $\perp b$. Excellent mirror-like surfaces for $\vec{E}||a$ and $\vec{E}||c$ optical studies can be prepared by cleaving. However, great difficulty is experienced in preparing good surfaces perpendicular to the cleavage plane because the crystals are soft and easily deformed. Slight surface oxidation occurs if the crystals are exposed to air for long periods (days). Hence, all optical samples were either freshly cleaved or kept under an argon atmosphere prior to measurement.

* This work was supported by the Advanced Research Projects Agency of the Department of Defense and was monitored by the Army Research Office, Durham, under Contract No. DA-ARO-D-31-124-71-G132.

Also, we wish to acknowledge the support of the Synchrotron Radiation Laboratory under Air Force Contract No. F44620-70-C-0029.

Single crystals of Sb_2Se_3 were grown in a zone refiner[2] from 6-9's purity elements after extensive zone refining of the compound. Amorphous films of Sb_2Se_3 were prepared by controlled coevaporation of the elements[3].

Various spectrophotometers having overlapping energy ranges were used to cover the energy range 0 to 30 eV and comprised: Beckman IR 11 (0.003 to 0.04 eV)[4]; Beckman IR 12 (0.02 to 0.4 eV); Cary 14R (0.4 eV to 6 eV); McPherson 225 with Hinteregger Light Source[5] (4 to 12 eV); McPherson with Synchrotron Radiation Source (4 to 30 eV). Optical reflectivity was measured using the following apparatus: Beckman Micro-reflectance Accessory (0.04 to 0.4 eV); Cary Model 1413 Reflectance Attachment (0.4 to 6 eV); McPherson Reflectance Attachment (4 to 12 eV); apparatus described in Ref. 6 (4 to 30 eV). Sheet polarizers were used in the range 0.4 to 6 eV (Polaroid HR linear polarizers and Polarcoat ultraviolet polarizers). The naturally occurring polarization in the Synchrotron radiation obviated the need for polarizers in the range 4 to 30 eV.

The room-temperature reflectivity at near normal incidence of single crystal Sb_2Se_3 in the energy range 0 to 5 eV is shown in Fig. 1 for both $\vec{E}||a$ and $\vec{E}||c$. This data represents the average of measurements taken on five different single crystal samples of Sb_2Se_3. Similar data is shown for an amorphous film of Sb_2Se_3 using unpolarized light. The magnitude of the reflectance of the single crystal in the region 0.05 - 0.5 eV is somewhat undertain, due to the fact the measurement was taken with respect to an aluminum mirror. This mirror could not be measured absolutely in our IR reflectance attachment but was taken to be equivalent to a standard evaporated mirror.[7] A strong lattice absorption band was observed beginning at a wavelength of $\sim$23 microns or $\sim$ 0.05 eV for unpolarized radiation.

The structure displayed by the single crystals in the range of the broad reflectivity maxima, 1 to 6 eV, is in good general agreement with the data of Shutov et. al.[8] (see Table 1) and is a result of singularities associated with symmetry points in the Brillouin zone. The fundamental absorption edge spectrum of Sb_2Se_3 indicates that the extremes of the valence and conduction bands occur at different points in the zone and absorption begins with an indirect transition at 1.16 eV[9]; this is appreciably higher than the value of 0.89 eV reported by Sobolov et. al.[10] From symmetry considerations on isostructural Sb_2Se_3, Audzijonis et. al.[11] have suggested that the maximum in valence band at the center of the Brillouin Zone Γ was split into subbands Γ_2, Γ_6 and Γ_4. Correspondingly, Sobolov et. al have associated transitions between $\Gamma_2(\vec{E}||a)$ $\Gamma_6(\vec{E}||b)$ and $\Gamma_4(\vec{E}||c)$ and the state Γ_1 at the conduction band minimum with the lowest direct transition in Sb_2Se_3. No assignments have been made for the higher energy structure in this broad maximum.

In marked contrast, the broad reflectivity maximum of the amorphous form of Sb_2Se_3 is featureless showing that the selection rules for these transitions are broken in the absence of long range order.

The near normal incidence reflectance was measured in the range 4 to 30 eV and is shown in Figure 2. At energies greater than 8 eV, a marked similarity exists between the crystalline and amorphous forms. The minima at 8 eV closely corresponds to that of As_2S_3 and As_2Se_3[12] and similarly, by Kramers-Kronig analysis appears to be associated with the threshold of a new absorption process from a deeper lying valence band. In the region of this second broad maxima, two marked peaks are observed at 10 and 12.4 eV independent of the orientation of the $\vec{E}$ vector or the absence of long-range order.

Beyond 23 eV the reflectivity appears to rise again. However, the data here is not reliable because of the presence of a gold mirror in the reflectivity apparatus which begins to absorb strongly in this region, with consequent diminuition of the signal.

The normal incidence reflectivity data described above have been Kramers-Kronig analyzed by the method described by Afshar et. al.[13,14]. The method essentially consists of two steps. First the Kramers-Kronig relation between the phase the modulus of the complex reflection coefficient

$$\phi(\omega) = \frac{P}{\pi} \int_{-\infty}^{+\infty} \frac{\ell n\, r(\omega')\, d\omega'}{\omega' - \omega} \qquad (1)$$

is separated into two portions, i.e.,

$$\phi(\omega) = \chi(\omega) + \theta(\omega)$$

where

$$\chi(\omega) = \frac{P}{\pi} \int_{-\infty}^{+\infty} \frac{\ell n \rho(\omega')\, d\omega'}{\omega' - \omega} \qquad (2)$$

and

$$\theta(\omega) = \frac{P}{\pi} \int_{-\infty}^{+\infty} \frac{\Delta(\omega')\, d\omega'}{\omega' - \omega} \qquad (3)$$

In these relations $\rho(\omega')$ is the modulus of the complex reflectivity for some system of charged classical harmonic oscillators chosen to have a reflectivity $\rho^2(\omega')$ which closely fits the measured reflectivity data at the high and low frequency

extremes of the measured data range. $\rho^2(\omega')$ thus extrapolates the data into the unmeasured spectral regions. The $\chi(\omega)$ can easily be computed from the appropriate dielectric function (which gives rise to $\rho^2(\omega')$ of the form

$$\hat{\varepsilon}(\omega) = 1 + \sum_{i=1}^{N} \frac{f_i}{(\omega^2 - \omega^2) + i\Gamma_i\omega}$$

where the constants (f_i, τ_i) paramertize the strength and linewidth of the classical oscillators with resonant frequency ω_i. We find in the analysis of the data presented here that three oscillators are sufficient to fit the data at the extremes of the data range. $\theta(\omega)$ is computed by expanding $\Delta(\omega')$, the residual portion of $\ln r(\omega')$ in Hermite functions, and using the Hermite representation of the Hilbert Transform operator developed by Afshar[14] et. al. to compute the integral in (3). All optical functions are obtainable from $\rho(\omega)^{i\phi(\omega)}$ the complex reflection coefficient.

Here we give the complex dielectric function for $\vec{E}||a$, $\vec{E}||c$, and for an amorphous film as computed from the normal incidence reflectivity data described above. In addition, the energy loss function $-\mathrm{Im}\,\frac{1}{\hat{\varepsilon}}$ is also displayed. In Fig. 3 the imaginary part of the dielectric function, $\varepsilon_2(\omega)$, is shown for the two polarizations $\vec{E}||a$, and $\vec{E}||c$ and for the amorphous film as computed from reflectivity data. In Fig. 4 the same display is made for $\varepsilon_1(\omega)$ and Fig. 5 shows a plot of the energy loss function in each case.

An additional interesting feature is the comparison of the sum rule on $\sigma_1(\omega) = \omega\varepsilon_2(\omega)$ for the three cases. Thus we have computed

$$\frac{2}{\pi} \int_0^{\omega} \omega' \, \varepsilon_2 \, (\omega') \, d\omega' = \frac{4\pi e^2}{m} N \, (\omega)$$

in each case. In Fig.6 the (relative) dependences of $N(\omega)$ upon ω are shown in each of the three cases. One can estimate the number of valence electrons in each case from the "valence-band plasma frequency" peaks in the respective energy loss functions.

In conclusion we conjecture that transitions occurring up to approximately 8 eV involve transitions from the valence to conduction bands in the crystalline and amorphous samples and the structure beyond this energy is associated with transitions from core electron states.

References

1. N. W. Tideswell, F. H. Kruse and J. D. McCullough, Acta Cryst. 10 99 (1957).

2. C. Wood, B. Van Pelt and E. Hyland, (to be published).

3. R. Mueller and C. Wood, (to be published).

4. Instrument loaned by Dr. Basil, Chemistry Div., Argonne National Laboratory.

5. Instrument loaned by Dr. P. Yuster, Solid State Div., Argonne National Laboratory.

6. U. of Chicago reflectance apparatus at the U. of Wisconsin Synchrotron.

7. American Institute of Physics Handbook, 2nd. Ed., McGraw Hill, p. 619, New York (1963).

8. S. D. Shutov, V. V. Sobolov, Y. V. Popov and S. N. Shestatskii, Phys. Stat. Sol. 31 K23 (1969).

9. B. Van Pelt and C. Wood (to be published).

10. V. V. Sobolov, S. D. Shutov and S. N. Shestatskii, Moldavian Academy of Sciences U.S.S.R. 183 (1969).

11. A. Audzijonis, J. Batarunas, A. Karpus and S. Kuḍzmanskas, Lietuvos Fizikos Rinkiny 5 481 (1965).

12. R. Zallen, R. E. Drews, R. L. Emerald and M. L. Slade, Phys. Rev. Lett. 26 1564 (1971).

13. R. Afshar, F. M. Mueller and J. C. Shaffer, (submitted to J. Comp. Phys.).

14. R. Afshar, F. M. Mueller and J. C. Shaffer, (submitted to J. Opt. Soc. America).

Table 1 Reflectivity peaks energies (eV) of Sb_2Se_3

Polarization	A_1	A_2	A_3	A_4	A_5	A_6	A_7	A_8	A_9	A_{11}	A_{12}	A_1
$\vec{E}\|\|a$	1.36 (1.36)	2.30 (1.97)	- -	- -	3.30 (3.15)	4.15 (3.95)	- (4.56)	-	7.4	10.0	-	12.4
$\vec{E}\|\|c$	- -	- (1.90)	2.30 (2.30)	3.00 (2.95)	- (3.20)	4.0 (4.0)	4.52 4.52	(5.6)	(7.4)	(9.5)	(10.8)	-

Figure Captions

Figure 1 Optical Reflectance of Amorphous and Single Crystal Sb_2Se_3 (0-5 eV).

Figure 2 Optical Reflectance of Amorphous and Single Crystal Sb_2Se_3 (4-30 eV).

Figure 3 Imaginary Part of Dielectric Function versus Photon Energy.

Figure 4 Real Part of Dielectric Function versus Photon Energy.

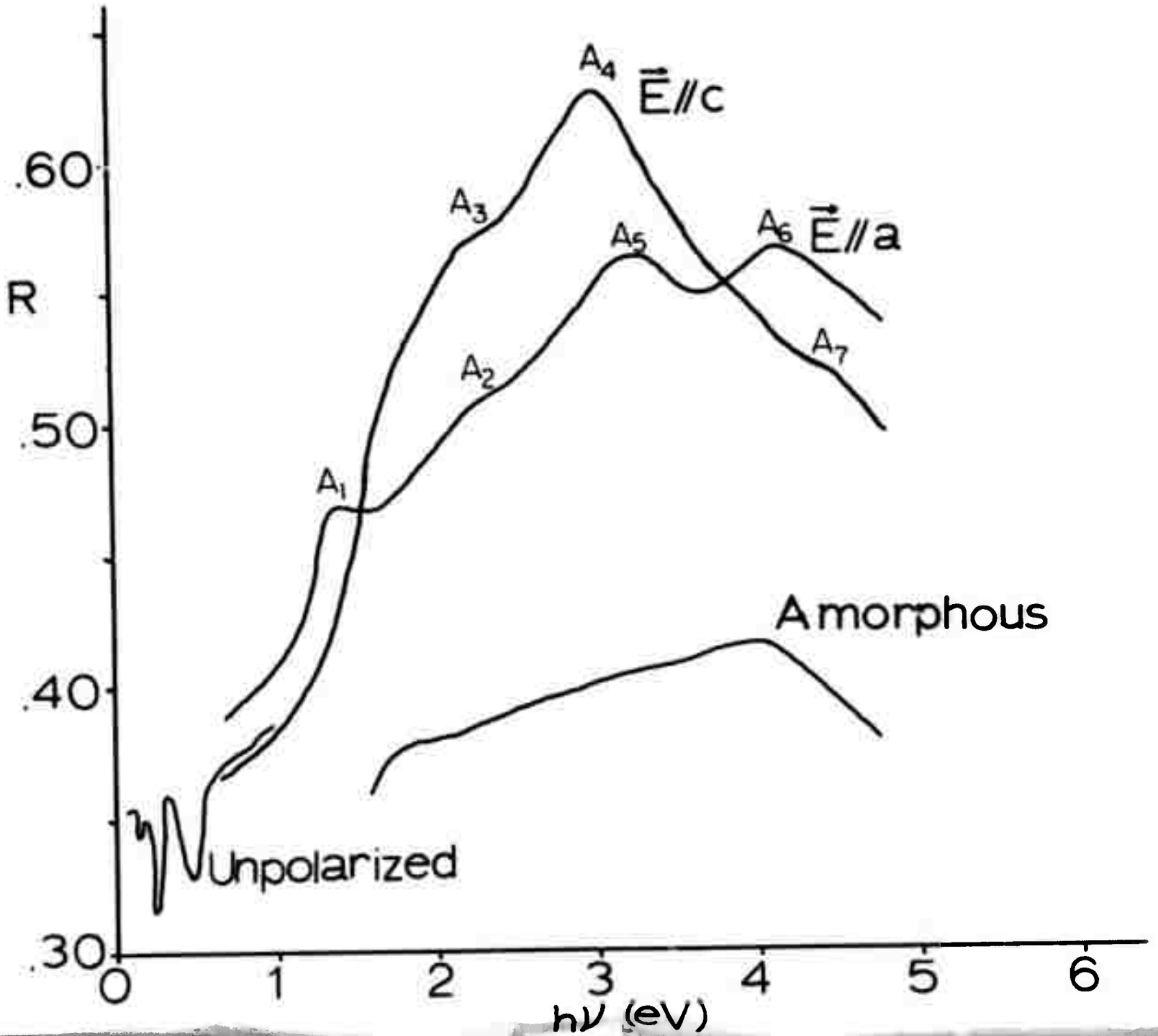
A4
E//c
A3
A5
A6
E//a
A7
A2
A1
R
.60
.50
.40
.30
Amorphous
Unpolarized
0
1
2
3
4
5
6
hν (eV)

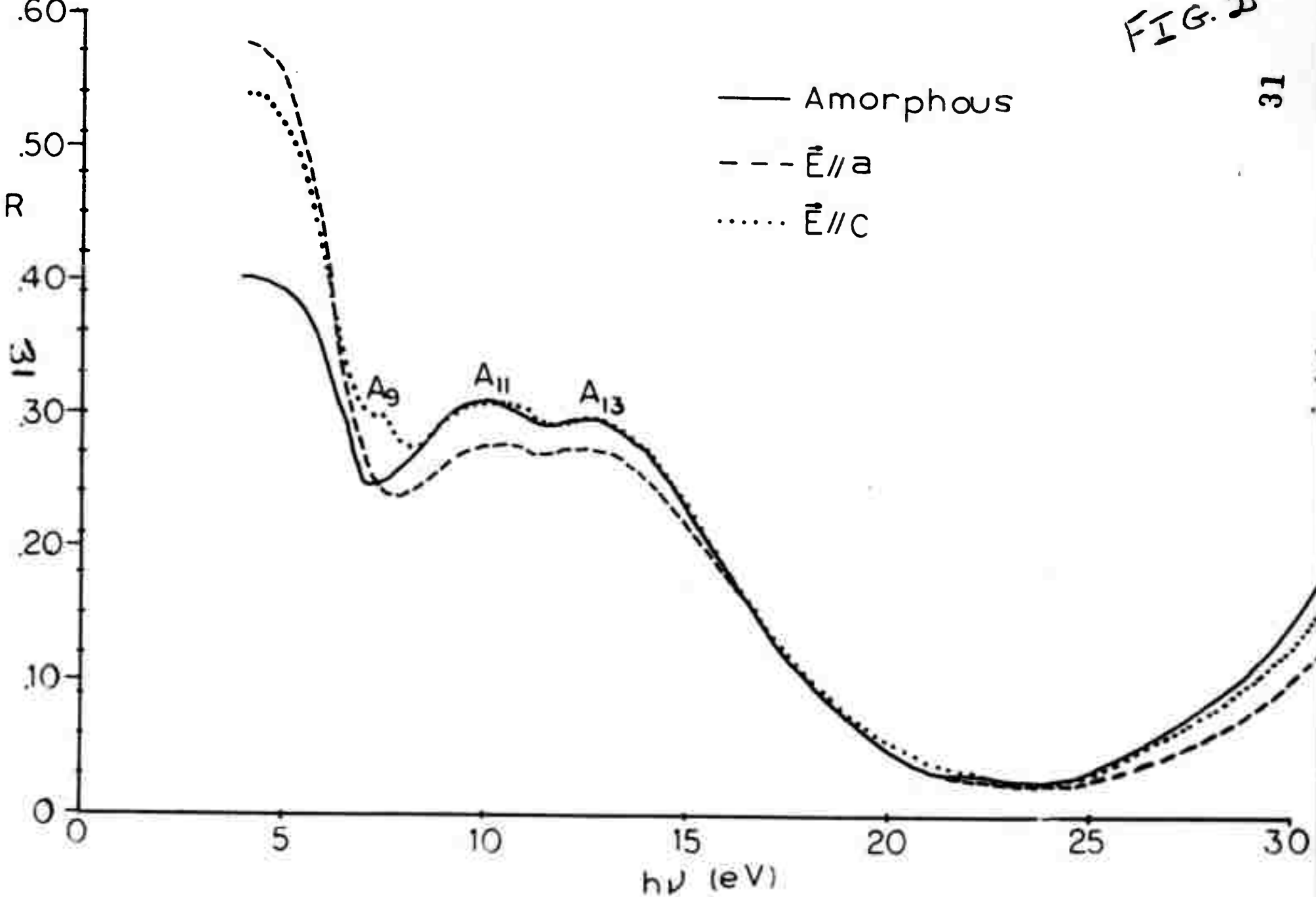
FIG. 2
31
Amorphous
$\vec{E}$ // a
$\vec{E}$ // C
R
.60
.50
.40
.30
.20
.10
0
A_9
A_{11}
A_{13}
0
5
10
15
20
25
30
hν (eV)

FIG. 3

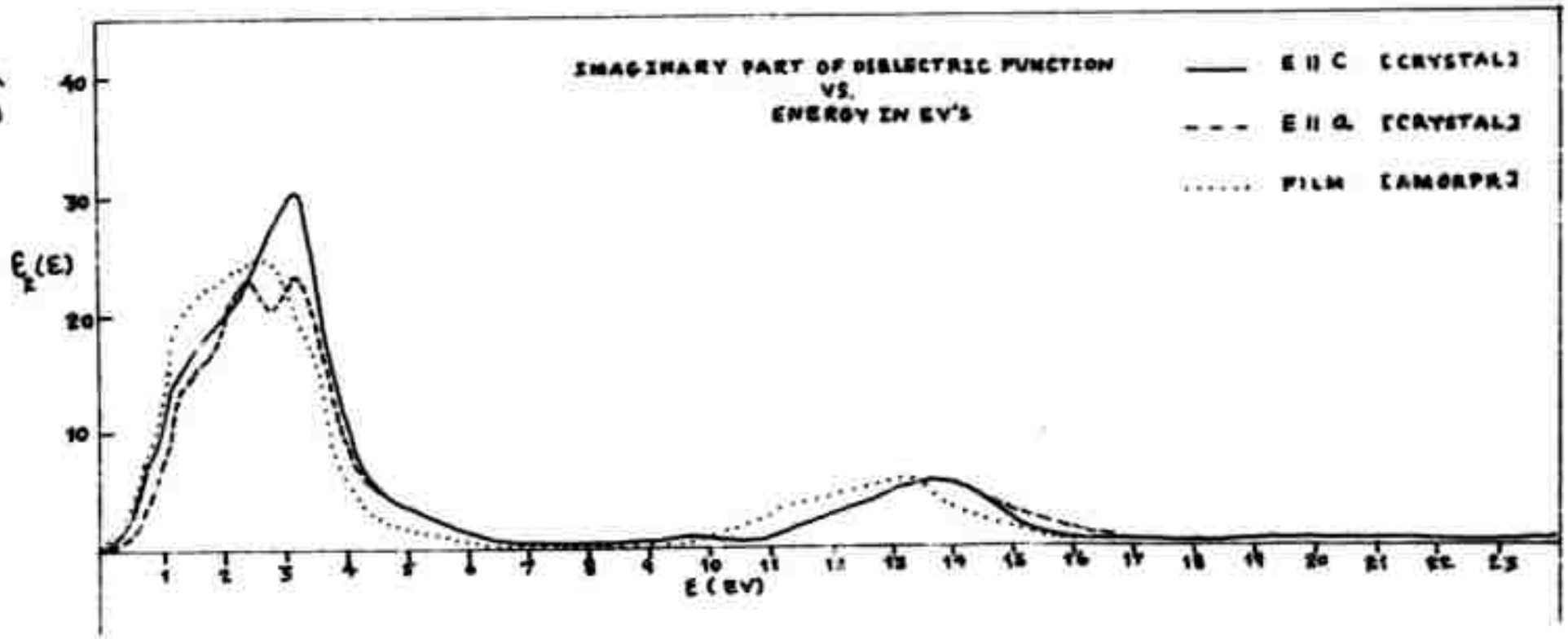
IMAGINARY PART OF DIELECTRIC FUNCTION
VS.
ENERGY IN EV'S
E II C [CRYSTAL]
E II a [CRYSTAL]
FILM [AMORPH]
$\epsilon_2(E)$
40
30
20
10
1
2
3
4
5
6
7
8
9
10
11
12
13
14
15
16
17
18
19
20
21
22
23
E (EV)

32

FIG. 4

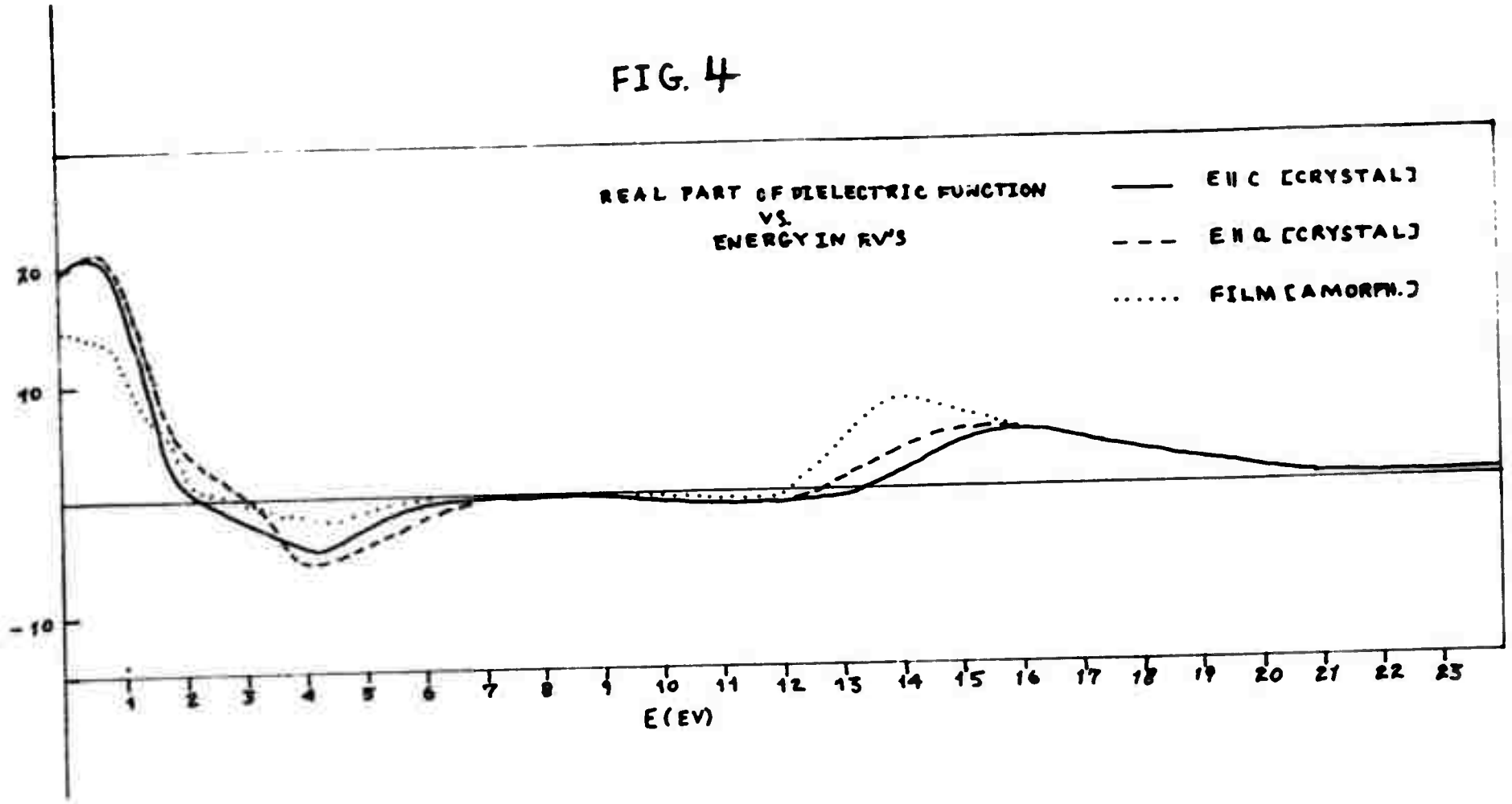
REAL PART OF DIELECTRIC FUNCTION
VS.
ENERGY IN RY'S
E ⊥ C [CRYSTAL]
E ∥ C [CRYSTAL]
FILM [AMORPH.]
20
10
-10
1
2
3
4
5
6
7
8
9
10
11
12
13
14
15
16
17
18
19
20
21
22
23
E(EV)

33

Appendix B

The Preparation of Amorphous Thin Films

R. Mueller and C. Wood

Physics Department, Northern Illinois University, DeKalb, Illinois

Abstract

Amorphous thin films of antimony selenide of controlled composition have been prepared by vacuum evaporation. Various evaporation techniques are compared and their influence on optical properties is discussed. The optical energy gap is shown to increase with increasing selenium content.

1. Introduction

Certain semiconductors can be made amorphous only under drastic quenching conditions, such as vapor deposition onto a cold (compared to the melting point) substrate. Classic examples of such materials are Ge and Se amongst the elemental semiconductors and As_2Te_3 and Sb_2Se_3 amongst the compound semiconductors.

A serious problem, which has received little attention in the literature, arises with the latter group, i.e., one of controlling stoichiometry or of maintaining a constant predetermined composition of deposited material. In most cases the vapor above a solid or melt source is not a single species and varies with the temperature and environment of the source and vapor, e.g., whether the vapor is allowed to be in equilibrium with the source. Even if complete dissociation of the compound source occurs on evaporation it is rare that the elements have a sufficiently close vapor pressure at the chosen evaporation temperature to insure that the components impinge on the substrate in the desired concentration ratios. We have, of course, ignored the problem of sticking coefficients onto the specific substrate material. This, however, is generally of secondary consideration only, since once

the first few monolayers of the compound cover the substrate, one is concerned only with the sticking coefficient onto the compound itself.

Compositional variations have often gone undetected in amorphous materials since x-ray diffraction measurements only show lack of structure. Electron microprobe measurements are rarely employed and at best can only show variations on a gross scale (greater than microns) perpendicular to the substrate where the compositional gradient is likely to be greatest and, further, the analysis is not accurate to better than ~1 at. %. A saving grace is that amorphous materials are often not markedly compositional dependent over deviations of a few atomic %, but it is inexcusable that much data in the literature is reported on compound amorphous films with gross deviations from stoichiometry with the implication that the films are stoichiometric and, what is more, no details are given on preparation.

2. Preparation of Antimony Selenide

Let us consider the specific case of antimony selenide in the light of the above discussion. Mass spectometric measurements by Sullivan et. al.[1]) have shown that the equilibrium vapor species over Sb_2Se_3 is predominantly SbSe and most other species present are Sb-rich compared to stoichiometry. However, this analysis applies to the condition of dynamic equilibrium between a melt and its vapor and does not correspond to the conditions applying in a conventional vacuum evaporation experiment where the vapor is immediately removed from above an open crucible. Rather, one is concerned with the dissociation vapor pressure of the element of highest vapor pressure, i.e., Se above a solid or melt of antimony selenide [2]) whose composition is varying as a function of time. Thus as the

evaporation proceeds the source is gradually depleted of selenium and consequently, the composition of the deposit changes with time [3]) and with thickness.

Our initial approach to solving this problem was to force a given deposit composition by using a selenium-rich source. As an example we found by trial and error that a source composition of $\sim SbSe_{0.9}$ at a temperature of $\sim 720^{\circ}C$ was required in order to produce a deposit of Sb_2Se_3 as determined by microprobe analysis. This further necessitated using a large source of material compared with the amount of deposit required so that the composition of the source did not significantly alter with time.

A more satisfactory and convenient technique from a control viewpoint was to coevaporate Sb and Se from separate crucibles. The relative rates were monitored and controlled by two Sloan Onmi II A rate-controllers. Collimating tubes were employed as shown in Fig. 1 to avoid cross-contamination of the quartz crystal oscillators. By using electron-beam heating for Sb and resistance heating for Se it was possible to obtain a fairly good degree of control at a deposition rate of 35-40Å/sec. However, we were not able to reduce the fluctuations on the rates below ± 2Å/sec. The Se resistance-heater was in the form of a thin (5 mil) stainless steel tube, through which the current passed, totally enclosing the Se and having a small aperture with baffle (see insert) so that no direct vapor path occurred between substrate and heater. Occasionally a vapor surge from the Se source would ruin an evaporation run. To avoid such surges, we later employed electron-beam heating for the Se source as well as for Sb. This did reduce large excursions in rates but fluctuations were at least as bad as with the resistance heater. Electron microprobe analysis showed the composition to approximately

correspond to the set evaporation rates as plotted on x-t recorders by this coevaporation technique.

3. Optical Properties

One of the purposes of this study was to examine the optical properties of amorphous antimony selenide films deposited on fused quartz substrates, as a function of composition and the optical absorption coefficient (α) versus photon energy is shown in Fig. 2. It is seen that the absorption edge obeys an approximate $\alpha h\nu \propto (h\nu - E_g)^2$ variation with energy as observed by Tauc et. al. [4]) for amorphous Ge, suggesting the optical transitions conserve energy but not crystal momentum (Fig. 3). The position of the edge decreases in energy as the Sb content increases; a variation observed previously for other elements in selenium [5]). Extrapolation of the curve for amorphous Sb_2Se_3 to $\alpha = 0$ gives a value of $E_g = 1.25$ eV which is slightly larger than the value of 1.15 eV obtained for the i: direct edge in single crystal Sb_2Se_3 [6]).

The absorption coefficient (α) was determined from the observed transmittance (T_{obs}) and reflectance (R_{obs}) using the following equations: [7,8])

$$T_f = T_{obs.} \frac{(1 - R_f' R_s')}{(1 - R_s')} \qquad (1)$$

$$R_f = R_{obs.} \frac{T_f^2 R_s'}{(1 - R_f' R_s')} \qquad (2)$$

assuming $R_f' \simeq R_{obs}$, where the subscripts f and s refer to film and uncoated substrate, respectively, and

$$T_f = \frac{(1 - R_s)^2 \, e^{-\alpha\chi}}{1 - R_f^2 \, e^{-2\alpha\chi}} \qquad (3)$$

where χ is the film thickness. Equation 3 could be used only in the region where interference effects could be ignored i.e., where the absorption was high. Attempts to use exact equations [9]), which included interference effects, over the whole energy range failed because of a slight modulation imposed on the height of the interference fringes observed beyond the absorption edge (see Fig. 4). By deliberately increasing the rate fluctuations (see Fig. 4) this modulation was traced to be due to the slight fluctuations in the relative evaporation rates of Sb and Se.

Accordingly, it was decided to revert to the single source evaporation process and to attempt stoichiometry control by the following means. Evaporation from melt-quenched ingot of Sb_2Se_3 was carried out by electron-beam gun heating from a water-cooled hearth at sufficiently slow rates such that evaporation proceeded only from the surface, the rest of the ingot remaining solid. Initially, the higher vapor pressure element (Se) is preferentially evaporated from the surface. The process then becomes rate limited by the evaporation rate of Sb from the Sb-enriched surface and the rate of diffusion of Se to the surface. A dynamic equilibrium is thus established such that the rate at which Se is removed is controlled by the rate of evaporation of Sb; forcing the relative evaporation rates to be equal to the elemental ratio in the solid.

By examining the composition of a sequence of films prepared from a single source in this manner, it was established that the first few films were selenium-rich but, towards the middle of the run, equilibrium was established with the films being close to stoichiometry. At the latter stages, when the electron beam had

penetrated through the source, the films reverted to non-stoichiometry again. The optical reflectance and transmittance of a typical film prepared in this fashion; Fig. 3, shows complete regularity of height of the interference fringes. The optical absorption edge obtained by analysis of the data (Fig. 3) shows reasonable coincidence with those obtained on coevaporated films of similar composition.

4. Conclusions

It is concluded that conventional evaporation is unsatisfactory as a method of producing amorphous films of controlled composition; that with the current state-of-the-art of rate control, coevaporation is suitable only for exploratory work on composition; and surface evaporation, although more laborious for a phase-diagram type study, does yield homogeneous films of desired composition at equilibrium. Furthermore, the optical absorption edge of amorphous antimony selenides has been shown to strongly depend on composition and, hence, on the method of preparation. The optical energy gap of amorphous Sb_2Se_3 closely corresponds to the indirect gap in the single crystal.

References

1. C. Sullivan, J. E. Prusaczyk and K. D. Carlson, J. Chem. Phys. 53 1289 (1970).

2. N. Kh. Abrikosov, V. F. Bankina, L. V. Poretskaya, L. E. Shelimova, and E. V. Skudnova, Semiconducting II-VI, IV-VI and V-VI Compounds, Plenum Press, New York, (1969) p. 194.

3. A. Efstathiou , D. M. Hoffman and E. R. Levin, J. Vac. Sci. Tech. 6 383 (1969).

4. J. Tauc, R. Grigorovici and A. Vanen, Phys. Stat. Sol. 15 627 (1966).

5. J. C. Schottmiller, D. L. Bowman and C. Wood, J. Appl. Phys. 39 1663 (1968).

6. B. Van Pelt and C. Wood, (to be published).

7. H. E. Bennett and J. M. Bennett, Physics of Thin Films ed. G. Hass and R. E. Thun, Academic Press, New York, (1967) p. 31.

8. T. S. Moss, Optical Properties of Semiconductors, Butterworths, London (1961).

9. L. R. Gilbert J. C. Shaffer and F. M. Mueller, (to be published).

Figure Captions

Figure 1 Coevaporation System.

Figure 2 Optical Absorption Coefficient versus Photon Energy

Figure 3 Variation of Absorption Coefficient with Photon Energy

Figure 4 Interference Peaks in Sb_2Se_3 Amorphous Thin Films

FIG. 1

Coevaporation System

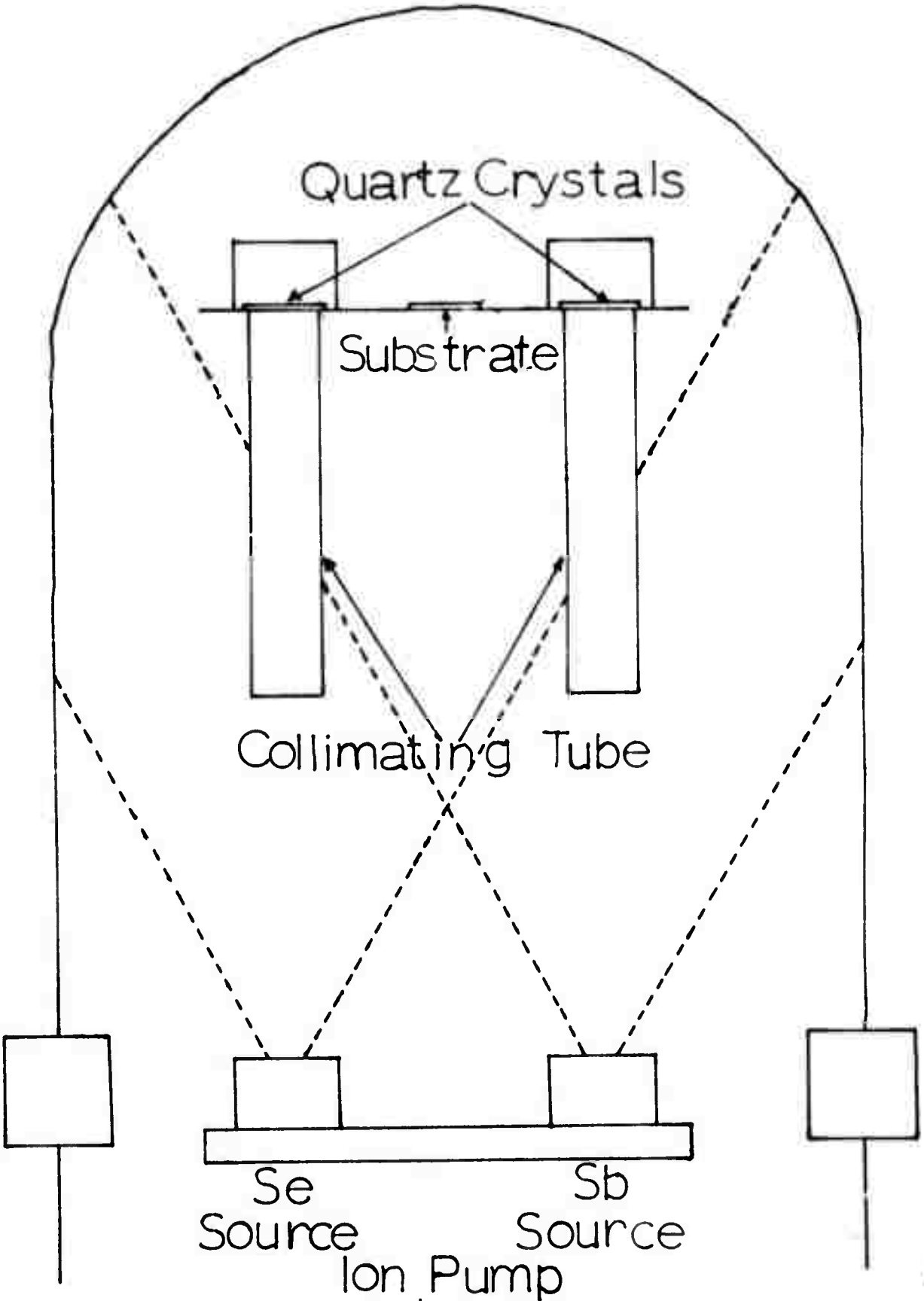

FIG. 2

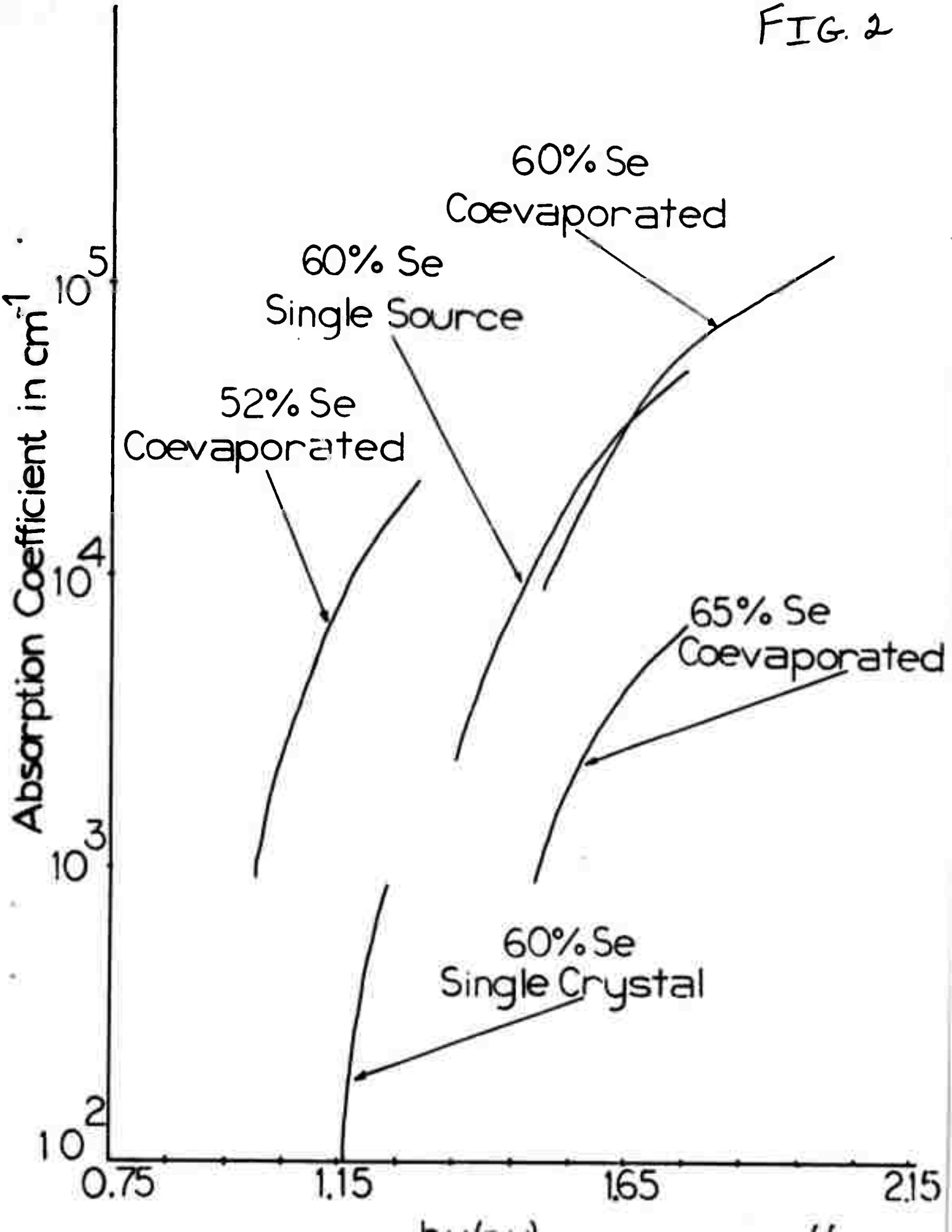
60% Se
Coevaporated
60% Se
Single Source
52% Se
Coevaporated
65% Se
Coevaporated
60% Se
Single Crystal
Absorption Coefficient in cm⁻¹
10⁵
10⁴
10³
10²
0.75
1.15
1.65
2.15

FIG. 3

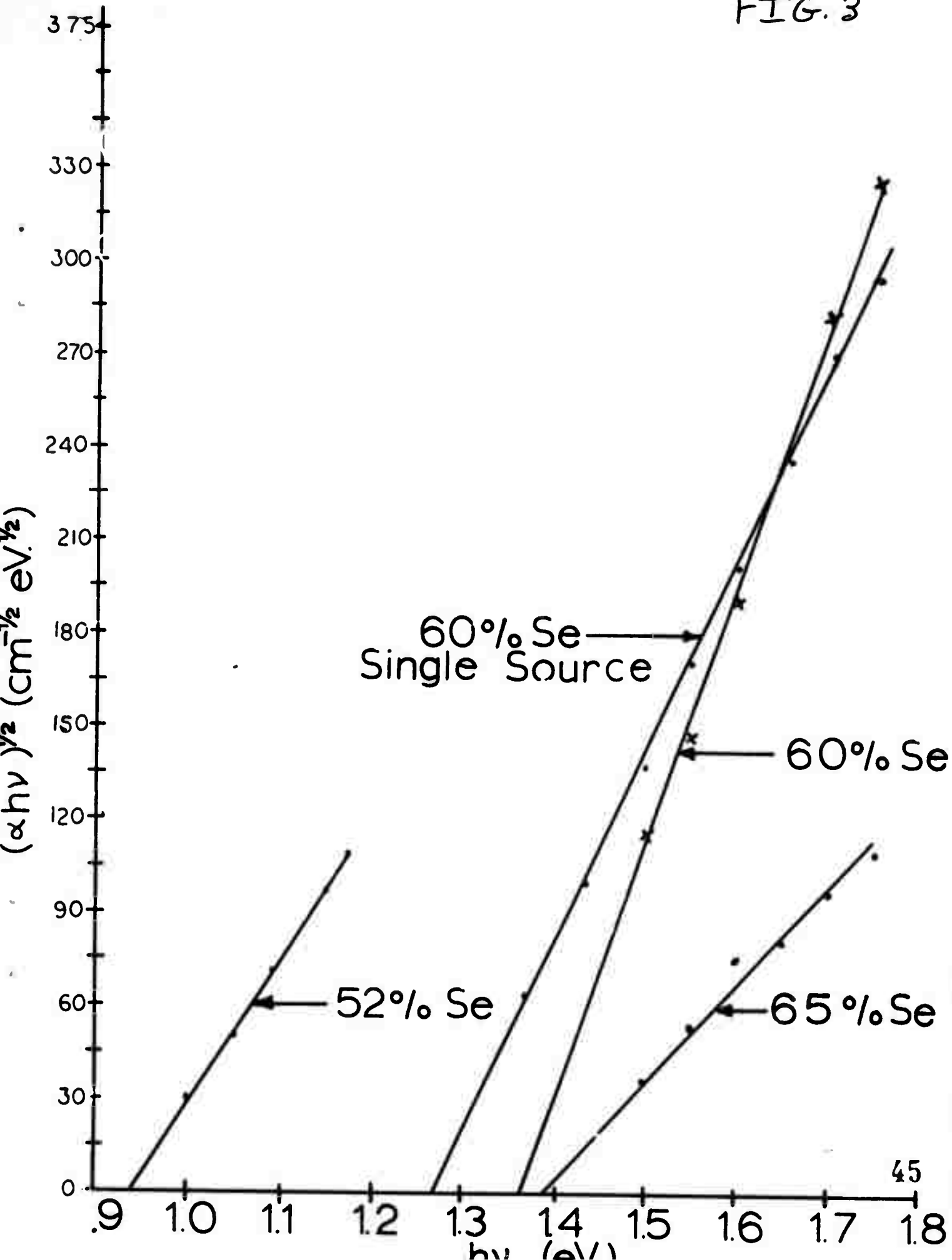
375
330
300
270
240
210
180
150
120
90
60
30
0
$(\alpha h\nu)^{1/2}$ $(cm^{-1/2} eV^{1/2})$
60% Se
Single Source
60% Se
52% Se
65% Se
.9
1.0
1.1
1.2
1.3
1.4
1.5
1.6
1.7
1.8
hν (eV)
45

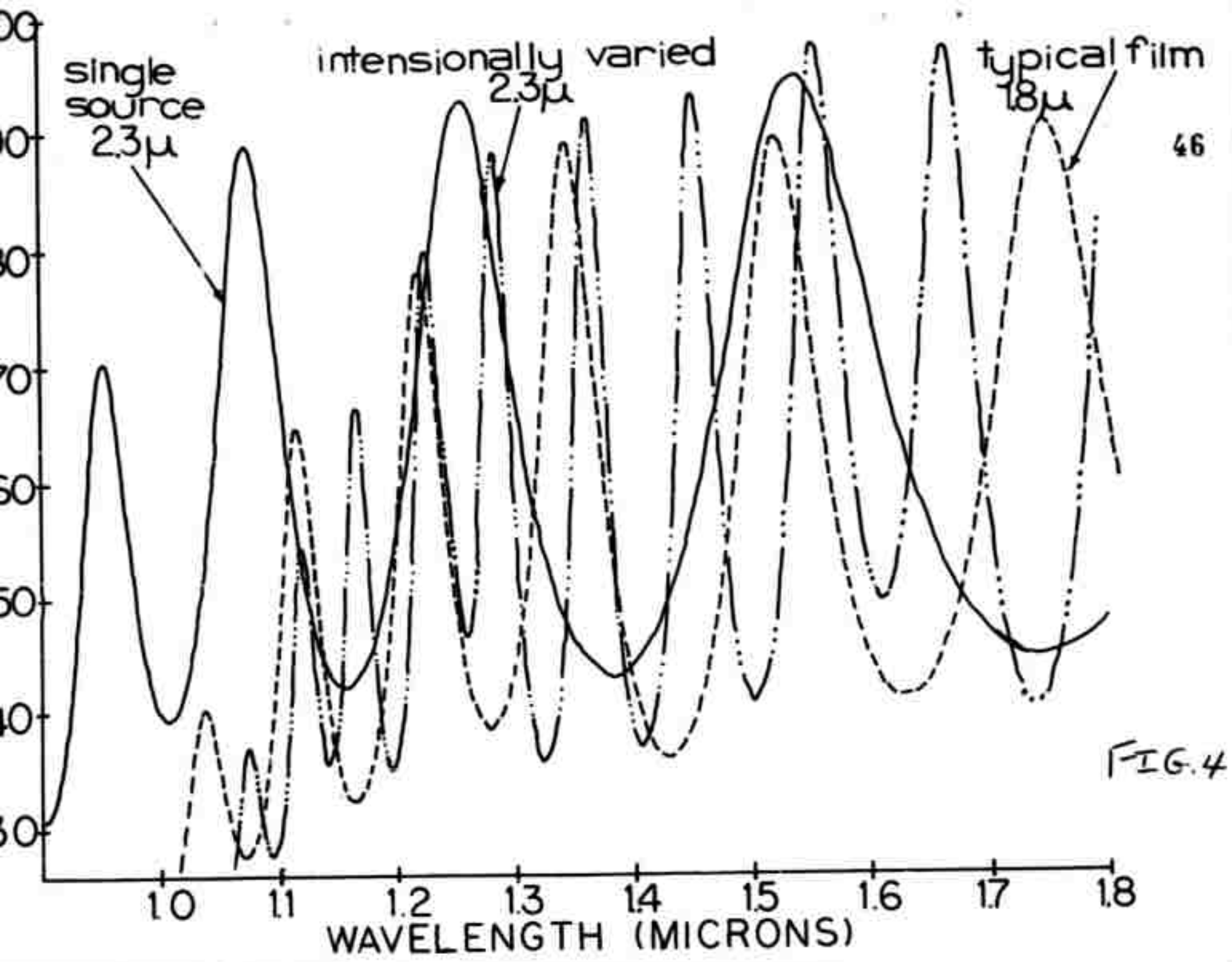
single source 2.3μ
intensionally varied 2.3μ
typical film 1.8μ
1.0
1.1
1.2
1.3
1.4
1.5
1.6
1.7
1.8
WAVELENGTH (MICRONS)

FIG. 4

Appendix C

A Zone Refiner for Crystal Growth*

C. Wood, B. Van Pelt and E. Hyland
Department of Physics
Northern Illinois University
DeKalb, Illinois 60115

It is fairly common practice to utilize a horizontal zone-refiner to grow single crystals.[1] Not only can the shape of the freezing interface be conveniently viewed (almost an essential for good crystal growth) but there is the additional convenience that some purification can be effected before attempting to grow a crystal. It may be added that superior zone purification is effected if the conditions encourage good crystal growth since it is well known that impurities tend to segregate at grain boundaries.

If the material has a high vapor pressure at the melting point or is a compound with a tendency to dissociate at the melting point, then it becomes necessary to control the temperature of the whole environment of the material in order to suppress evaporation or dissociation. Evaporation or dissociation still occurs but a dynamic equilibrium is set up between the melt and walls of the vessel enclosing the ingot. In the case of dissociation of a compound, the element having the highest vapor pressure tends to evaporate preferentially. The walls of the enclosure are thus maintained at a temperature which corresponds to a higher vapor pressure for the free element than the pressure of that element above the compound at its melting point. This furnace enclosure also acts as an after-heater, which greatly assists in the growth of single crystals, but often obstructs clear

viewing of the freezing interface.

We have been growing single crystals of antimony chalcogenides, e.g., Sb_2S_3, Sb_2Se_3, Sb_2Te_3, which tend to dissociate on melting (melting points in the range 600°C to 700°C) and have devised a system which overcomes the difficulty of viewing. A schematic diagram is shown in Fig. 1. The temperature of the hot zone is sensed by a chromel-alumel thermocouple junction positioned in the center of the zone and suspended inside the inner furnace tube. The arms of the thermocouple extend from opposite ends of the furnace tube and are supported by a frame attached to the travelling zone carriage. The thermocouple controls the power supplied to the furnaces, which are wired in series, through a Leeds and Northrup Speedomax W Azar Recorder. The compounds are sealed-off inside an evacuated fused-quartz capsule which is placed inside the furnace tube.

The central feature of the apparatus is a tin-oxide conductive coating on the exterior of fused quartz tubing.[2] This has been utilized to provide both the stationary furnace tube enclosing the whole ingot and the shorter travelling heater which supplies the additional heat necessary for the molten zone. The tin-oxide coating can be made thick (~30-170Ω/square) while still remaining very transparent (the growth interface can be clearly seen through both tubes) and can be operated continuously at temperatures up to 700°C without deterioration.

Silver paste supplied by Engelhard Industries, Inc. painted in strips around the tube and fired on at ~600°C provides a suitable electrical contact to the tin-oxide. It is essential not to contact the tin-oxide directly

since hot spots are formed which craze the oxide coating. Stainless steel foil wrapped and bolted around the silver paste contact or stainless steel U-shaped bars (preferably gold coated) in which the tube can be nestled are satisfactory.

The main difficulty experienced in the development of this apparatus was non-uniformity of the tin-oxide coating. For good crystal growth it is essential that the temperature conditions do not vary at different parts of the tube, which implies uniformity of conductive coating. A coated tube supplied by Corning Glass Works, although remarkably uniform considering it was hand-coated, was inadequate for our purposes. Since better uniformity of coating was not available, we, therefore, set up a spray coating system (using the formula described in Ref. 2) on a travelling lathe. The problem of maintaining the tube surface at $\sim 520^{\circ}C$ during spraying was overcome by inserting a nichrome wound furnace tube inside the fused quartz tube to be coated and relying mainly upon radiant heat to maintain the surface temperature. Best results were obtained with freshly mixed solutions of tin-chloride.

As is well known, the ideal shape of a freezing front is slightly concave, i.e., the molten zone forms the shape of a slightly concave lens, so that the first part of the front to freeze does so on the crystal nuclei and not on foreign nuclei on the walls of the tube. This condition is easily achieved by lowering the heat input to the molten zone and thus increasing the relative contribution of the thermal conduction along the bar to the heat losses. Too small a heat input will cause the axis along the center of the molten zone to freeze across completely while the edges still remain

molten. Too large a heat input will give rise to a convex shape.

Examples of some of the crystals grown in this type of apparatus are shown in Fig. 2. The shape of the freezing front used on a single crystal of Sb_2Se_3 can be seen in the figure. The ingot was not uniform in cross-section and shows the freezing front shape in a height step.

The tin-oxide coating is quite versatile as a heating element and specially shaped heating zones can easily be fabricated by painting the electrodes to the desired configuration. Also, it is comparatively simple to construct a heater with multiple heating zones for rapid zone refining by painting many electrodes on a tin-oxide coated tube and shorting out alternate coatings.

The authors are indebted to B. Hanson for assistance with temperature control and construction of an electrical power supply for the tin-oxide tubes.

* This research was supported by the Advanced Research Projects Agency of the Department of Defense and was monitored by the Army Research Office, Durham, under Contract No. DA-ARO-D-31-124-71-G132.

[1]W. G. Pfann, Zone Melting (Wiley, New York, 1959) p. 153.

[2]Proceedings of the Eleventh Symposium on the Art of Glassblowing, (1966) American Scientific Glassblowers Society, p. 128.

Fig 2 not available

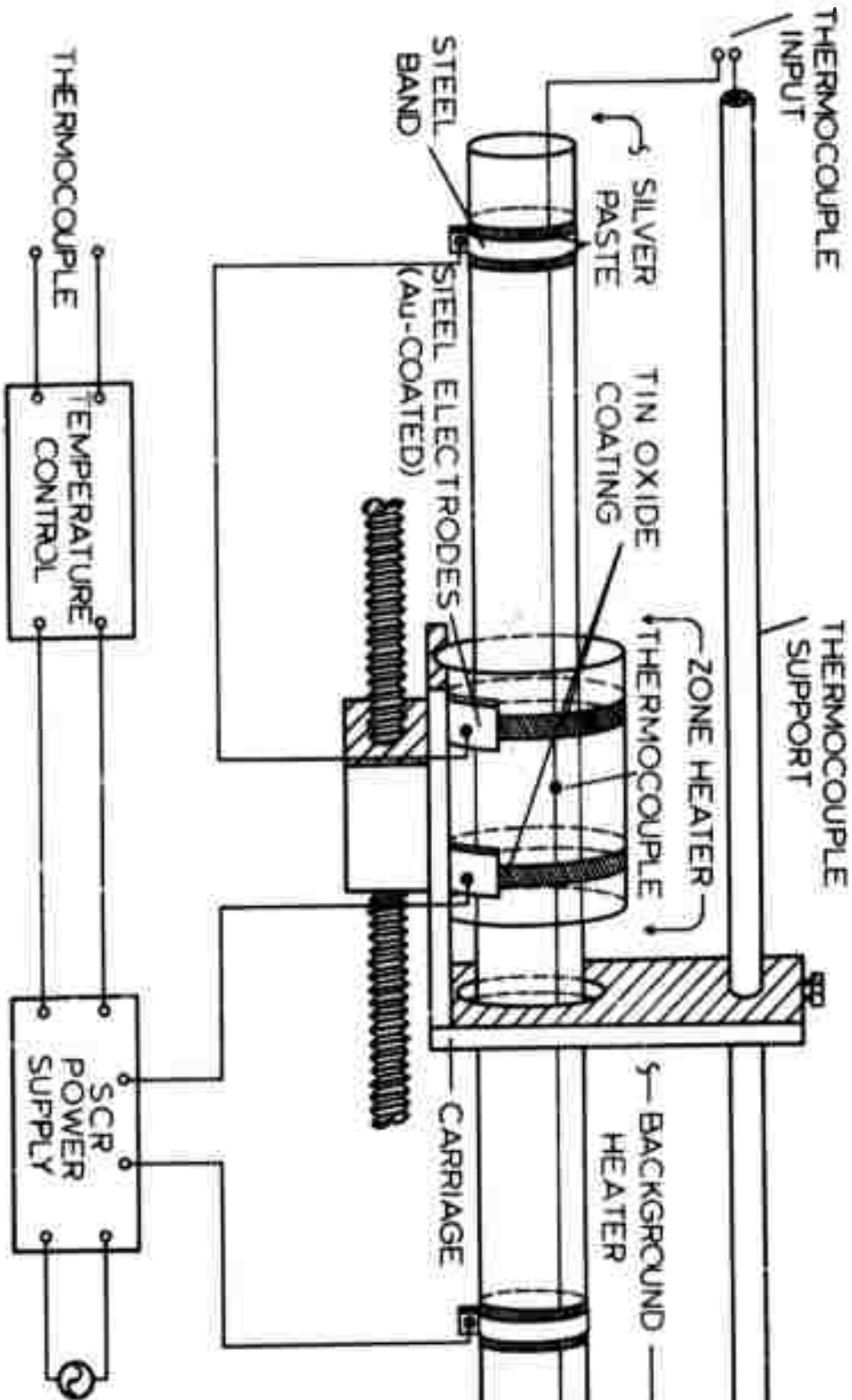
THERMOCOUPLE INPUT
SILVER PASTE
STEEL BAND
TIN OXIDE COATING
STEEL ELECTRODES (Au-COATED)
ZONE HEATER
THERMOCOUPLE
THERMOCOUPLE SUPPORT
BACKGROUND HEATER
CARRIAGE
THERMOCOUPLE
TEMPERATURE CONTROL
SCR POWER SUPPLY

Fig 1

Appendix D

Mossbauer Investigations of $Sn_x(As_2Se_3)_{1-x}$ Glasses*

S. P. Taneja, A. E. Dwight, L. Gilbert,
W. C. Harper, C. W. Kimball and C. Wood
Physics Department
Northern Illinois University
DeKalb, Illinois

Mossbauer measurements on ^{119}Sn nuclei in $Sn_x(As_2Se_3)_{1-x}$ (x = 2.5, 5.0 8.0 and 10.0 atomic percent) glasses have been made at 4.2, 77.3 and 298°K. The chemical reactions suggested by Shkolnikov are confirmed. Contrary to the findings of Shkolnikov, these results, combined with those of Borisova et al., show that the chemical kinetics are sensitive to the method of preparation of the glass. Although x-ray measurements indicate that no long-range order exists, the Mossbauer results show that the short-range order about Sn atoms is almost complete. In the glass the long-range disorder affects the isomer shift and quadrupolar coupling at Sn atoms only to second order. The Debye temperature for Sn atoms differs in crystal (~140°K) and glass (~100°K), however, by ~40°K.

* This research was supported by the Advanced Research Projects Agency of the Department of Defense and was monitored by the Army Research Office, Durham, under Contract No. DA-ARO-D-31-127-71-G132.

The ternary systems of amorphous chalcogenide semiconductors have been the subject of intensive investigation in the past.[1,2] This class of materials has taken on more significance recently with the discovery of switching effects and possible device applications.[3] The addition of Group IV elements to the arsenic chalcogenides has been found to have significant effects on softening temperature, microhardness and electrical conductivity. These changes in the physical properties have been ascribed to the crosslinking of the chain-like structure by the Group IV element.[1]

A Mossbauer study of ^{119}Sn in $Sn_x(As_2Se_3)_{1-x}$ glasses, where x = 2.5, 5.0, 8.0 and 10 atomic percent Sn has been made at 298, 77.3 and 4.2°K to further study the nature of the glass-crystal transition and the role of the Group IV element in a switching glass. The isomer shift, the centroid of the absorption pattern, reflects the electronic structure of the Sn atom and its vibrational energy. The quadrupolar interaction reflects both the electronic structure and the noncubic nature of the environment of the Sn atom. In a disordered system distributions of both isomer shift and quadrupolar coupling should occur; the line breadth and shape should reflect the dispersion of these distributions. The Debye temperature can be obtained by measuring the temperature dependence of the Mossbauer absorption.

Experimental

The samples of $Sn_x(As_2Se_3)_{1-x}$ were prepared with 99.9999% grade materials. Arsenic and selenium were outgassed by subliming in a vacuum and then sealed in a fused quartz ampoule, in proper ratio, under a pressure of $\sim 10^{-5}$ mm of Hg.

The ampoule was placed in a rocking furnace at 630°C for ∿12 hours and then quenched in a brine solution at ∿200°K.

To prepare a single crystal of $SnSe_2$, high purity Sn and outgassed Se were mixed and sealed off in an evacuated quartz ampoule; excess Se was used in order to avoid a mixed phase of SnSe and $SnSe_2$. The ingot was placed in a three zone furnace and the temperature was slowly raised to 680°C over a period of four days. The end and middle zones were lowered at 4°C/hr to solidify the ingot from one end. Crystalline SnSe was prepared in a similar fashion using equal percentages of Sn and Se.

All samples were tested by x-ray analysis. Debye-Sherrer patterns, using a Cu target, show diffuse bands characteristic of amorphous systems for x = 2.5, 5.0 and 8.0 at. % Sn. Similar patterns for the 10 at. % Sn samples show the amorphous phase, and have, in addition, five lines of a crystalline phase, of which four can be indexed as lines of SnSe as shown in Table I. The crystallized specimens of 10 at. % Sn are found to be predominantly in the SnSe phase.

The Mossbauer absorbers were prepared by powdering the amorphous compounds and encapsulating in a cold-setting plastic. The sample thicknesses were 5-10 mg/cm^2 of natural tin. The Mossbauer source was ^{119}Sn in $BaSnO_3$ at 298°K. Mossbauer spectra were recorded with a conventional spectrometer in the constant acceleration mode. All data was least squares fitted by computer to Lorentzian lines.

Results and Discussion

The effect of tin on the micro-hardness and conductivity of semiconducting glasses of As_2Se_3 has been studied by Shkolnikov.[4] The hardness and conductivity change significantly after 5% Sn is added and Shkolnikov suggests that such behavior can be accounted for by a chemistry in which $SnSe_2$ occurs at low tin concentration and SnSe at high concentration. None of his suggested reactions contains any compound of tin with arsenic. Also, Shkolnikov found no essential difference in the degree of amorphicity between air cooled and quenched Sn-As-Se glasses. Borisova et al.[5] have examined the ^{119}Sn Mössbauer effect in $Sn_x(As_2Se_3)_{1-x}$ glasses formed by cooling in air and concluded that SnIV occured in the glassy state but that the glass-crystal mixtures exhibited both SnII and SnIV absorption lines. Our Mössbauer measurements on Sn-As-Se glasses quenched to low temperature from the melt show quantitative differences in the chemical kinetics from those observed by Borisova et al.[5]

Typical Mössbauer spectra for amorphous samples at 77.3°K for 2.5, 5.0 and 8.0 atomic percent Sn are shown in Fig. I and for 10% Sn in Figure II. Tin occurs in only one phase for concentrations of 2.5 and 5.0%, but a second phase appears in the spectra for both the 8.0 and 10.0 samples. Although the limit of solubility of tin in the quenched glassy state has been set by Kolomiets [6] as ∿7%, the second phase does not correspond to either α- or β-Sn. The reaction chemistry given by Shkolnikov[4] for low Sn concentrations is

$$(xSn + AsSe_{1.5} \rightarrow xSnSe_2 + (1 - \frac{8}{3}x)\ AsSe_{1.5} + 2xAsSe + \frac{2}{3}xAs) \quad ,$$

and for higher Sn concentrations

$$xSn + AsSe_{1.5} \rightarrow xSnSe + (1-2x)\ AsSe_{1.5} + 2xAsSe \quad .$$

As the Sn concentration increases, the Sn atom changes valence from +4 to +2 and the free As combines with Se to further increase the $AsSe_{1.5}$ content.

Crystalline $SnSe_2$ is trigonal (CdI_2 - C6 type) and all Sn atoms are in equivalent sites; crystalline SnSe is orthorhombic (GeS-B16 type) and all Sn atoms are in equivalent sites. A doublet is expected for both SnSe and $SnSe_2$; the spectra for $SnSe_2$ and SnSe are shown in Fig. III. Indeed, the spectra for low tin concentrations in the amorphous samples is similar to that for $SnSe_2$; for higher tin concentration a spectrum characteristic of SnSe appears. Slight but significant differences between the patterns for amorphous and crystalline samples are discussed below. The spectra are similar to those of Borisova et al. but the relative quantities of $SnSe_2$ and SnSe for similar concentrations of tin differ. Apparently the chemical kinetics are dependent on method of sample preparation in contrast to Shkolnikov's findings. The dominant phase in the crystalline samples is SnSe, but this phase also appears in the amorphous samples. X-ray analysis shows no crystallinity for the 8% samples quenched to low temperatures but the Mossbauer patterns show the presence of both SnSe and $SnSe_2$.

The Mossbauer results are given in Table IIand show that the short-range order about Sn atoms is almost complete. The isomer shift and quadrupolar coupling for SnIV and SnII in the amorphous solid are very close to their values for Sn in $SnSe_2$ and SnSe, respectively. The long-range disorder results in systematic and almost constant differences in the isomer shift and

quadrupolar coupling between Sn atoms in amorphous and crystalline systems. The absorption lines for Sn in the glass are symmetrical and only slightly broadened which indicates that the electronic structure of the Sn atom and the electric field gradient at Sn atom are affected to only second order by composition changes in the glasses.

Debye temperatures are estimated for the Sn in crystalline $SnSe_2$ ($\theta_D \simeq 145 \pm 10^oK$), in crystalline SnSe ($\theta_D \simeq 130 \pm 10^oK$) and in the Sn-As-Se glass, SnIV ($\theta_D \simeq 100 \pm 10^oK$) and SnII ($\theta_D \simeq 90 \pm 10^oK$), from the temperature dependence of the Mossbauer absorption. Within the error of the measurement ($\pm 10^o$) the same Debye temperature fits the data from 4.2 to 77.3°K and from 77.3 to 298°K; it is therefore inferred that the glass to crystal transition takes place above room temperature.

Table 1

Analysis of x-ray film for the 10 at. % Sn amorphous sample.

I_o	d_o	Source
m	2.90Å	2.98 for SnSe on ASTM Card
m	2.86	2.87 for SnSe on ASTM Card
w	2.35	2.39 for SnSe on ASTM Card
w	1.98	Uncertain, also not seen on SnSe sample
w	1.82	1.84 for SnSe on ASTM Card

Table II

Results of the analysis of Mossbauer Spectra of $Sn_x(As_2Se_3)_{1-x}$

(δ is the isomer shift relative to $BaSnO_3$, ΔE_Q is the quadrupole splitting)

Temperature (°K)	Composition x (atomic %)		δ_1 mm/sec	δ_2 mm/sec	ΔE_{Q_1} mm/sec	ΔE_{Q_2} mm/sec
77.3	2.5	Amorphous	1.68 ± .04	-	0.42 ± .10	-
77.3	5.0		1.69 ± .14	-	0.33 ± .14	-
77.3	8.0		1.69 ± .02	3.49 ± .06	0.46 ± .06	0.96 ± .08
298.0	10.0		1.66 ± .02	3.32 ± .02	0.51 ± .06	0.82 ± .04
77.3	10.0		1.67 ± .02	3.39 ± .02	0.50 ± .06	0.93 ± .04
4.2	10.0		1.69 ± .02	3.43 ± .02	0.50 ± .06	0.96 ± .04
298.0	10.0		0.53 ± .13	3.27 ± .02	0.99 ± .22	0.74 ± .02
77.3	10.0		1.62 ± .08	3.32 ± .02	0.50 ± .18	0.78 ± .02
298.0	$SnSe_2$	Crystalline	1.33 ± .02	-	∿0.0	-
77.3	$SnSe_2$		1.35 ± .02	-	∿0.0	-
298.0	SnSe		-	3.28 ± .02	-	0.74 ± .10
77.3	SnSe		-	3.33 ± .02	-	0.79 ± .02

References

1. Kolomiets, B. T. (1964). Phys. Stat. Sol. 7, 359.

2. Hilton, A. R., Jones, C. E. & Brau, M. (1966). Phys. Chem. Glasses 7, 105.

3. Pearson, A. D., Northover, W. R., Dewald, J. F. & Peck, W. F. (1962). Advances in Glass Technology, Plenum Press, New York; Kolomiets, B. T. & Levedev, E. A. (1963). Radiotechnika i Electronika, 8, 2097; Eaton. E. L. (1964). J. Am. Ceram. Soc. 47, 554; Ovshinky, S. R. (1968). Phys. Rev. Letters, 21, 1450.

4. Shkolinikov, E. V. (1966). Solid State Chemistry, p. 142 (Edited by E. V. Borisova) Consultants Bureau, New York.

5. Borisova, Z. V., Vasilev, L. N., Seregin, P. P. & Shipatov, V. T. (1970). Soviet Physics - Semiconductors, 4 (3), 433.

6. Kolomiets, B. T. Goryanova, N. A. & Shilo, V. P. (1960). Collection: The Glassy State Izd. Akad. Dauk. SSSR. Moscow. p. 456.

Figure Captions

Fig. I The Mossbauer spectra at 77.3°K for amorphous samples of $Sn_x(As_2Se_3)_{1-x}$ with x = 2.5, 5.0 and 8.0 at. %. The solid line is a least-squares fit to the model described in the text.

Fig. II The Mossbauer spectra at 77.3°K for amorphous and crystalline samples $Sn_x(As_2Se_3)_{1-x}$ with x = 10 at. %.

Fig. III The Mossbauer spectra at 77.3°K for $SnSe_2$ and SnSe crystalline samples.

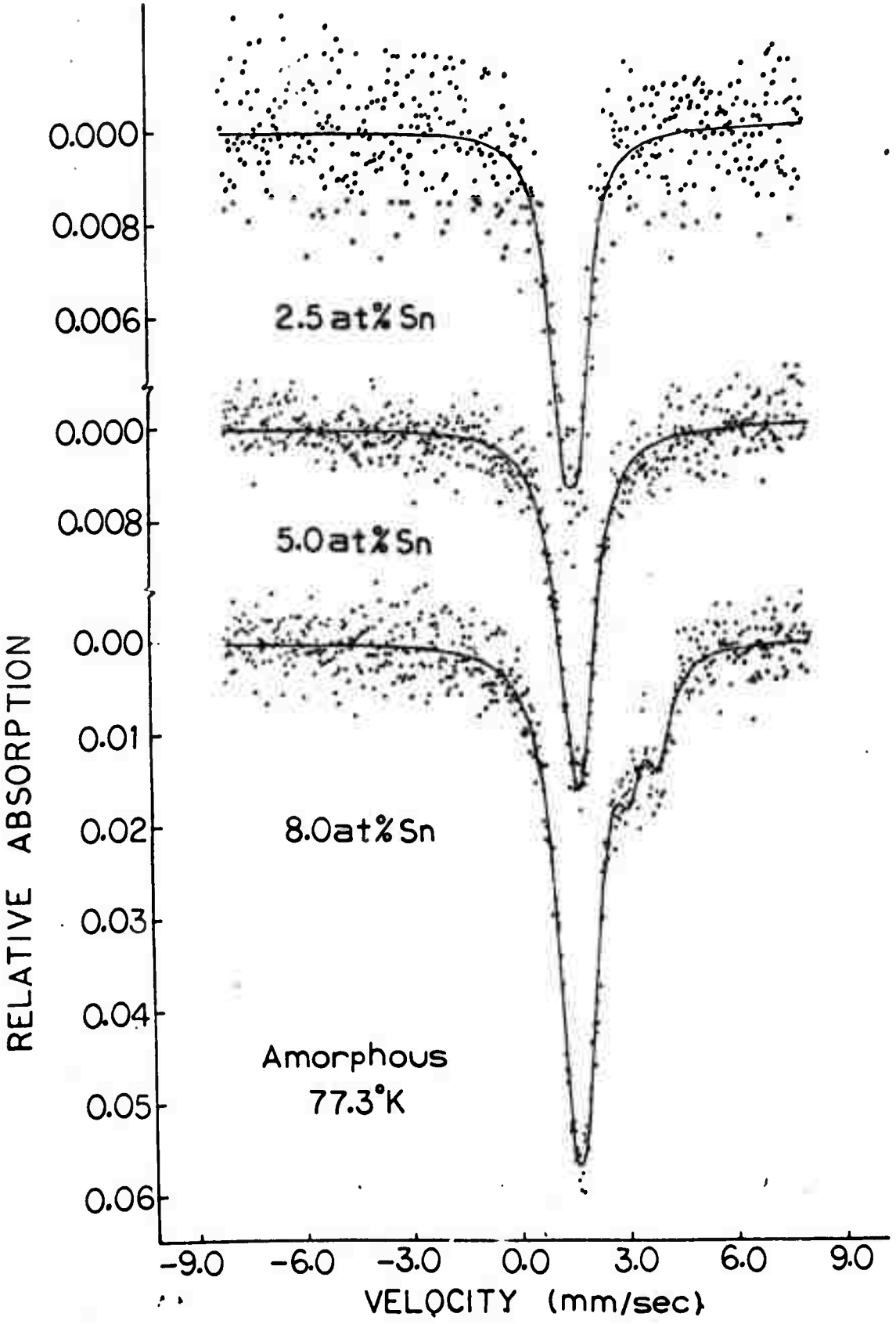
0.000
0.008
0.006
2.5 at% Sn
0.000
0.008
5.0 at% Sn
0.00
0.01
0.02
8.0 at% Sn
0.03
0.04
Amorphous
77.3°K
0.05
0.06
RELATIVE ABSORPTION
-9.0
-6.0
-3.0
0.0
3.0
6.0
9.0
VELOCITY (mm/sec)

FIG 1

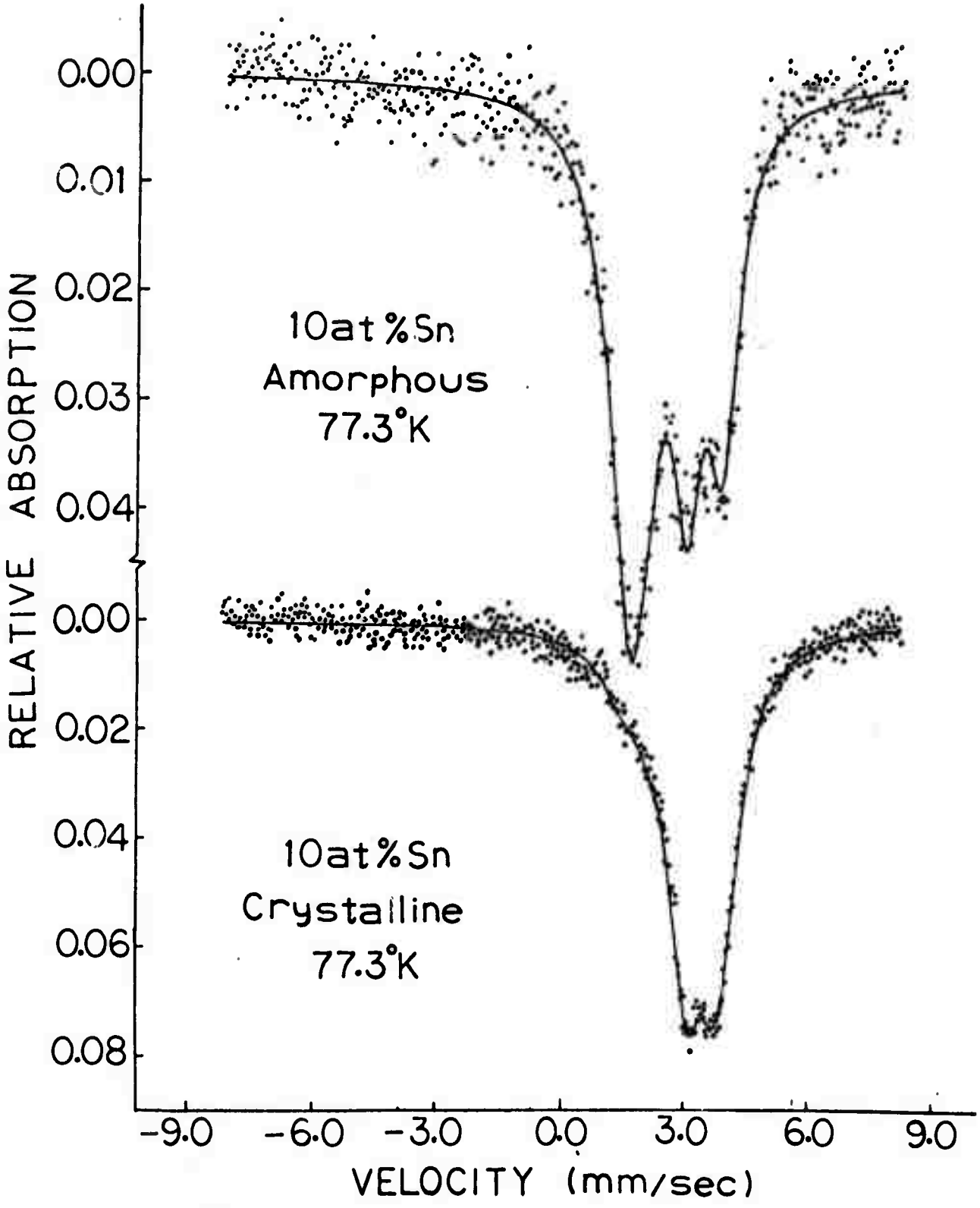
0.00
0.01
0.02
0.03
0.04
0.00
0.02
0.04
0.06
0.08
RELATIVE ABSORPTION
10at%Sn
Amorphous
77.3°K
10at%Sn
Crystalline
77.3°K
-9.0
-6.0
-3.0
0.0
3.0
6.0
9.0
VELOCITY (mm/sec)

FIG 2

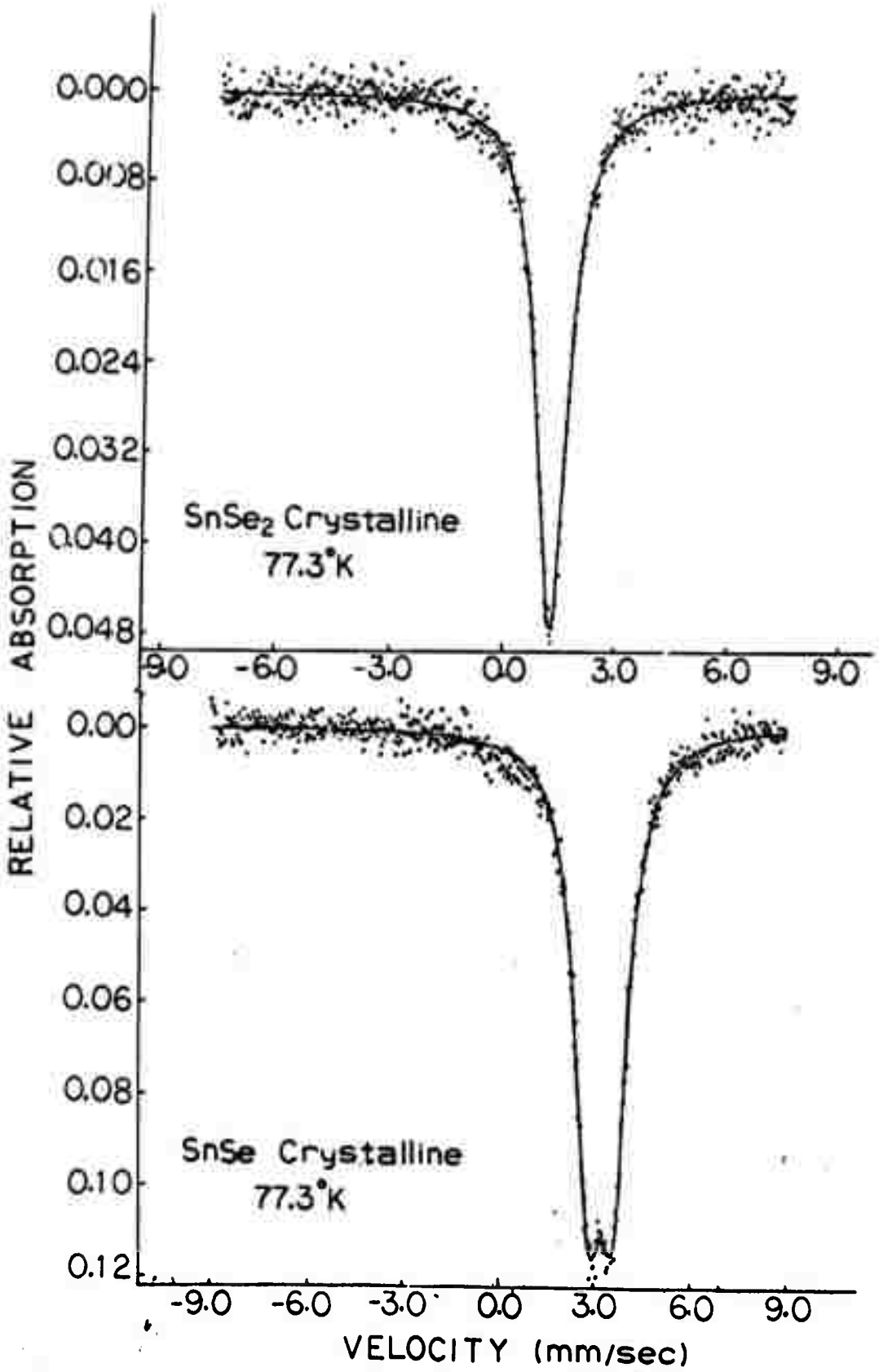
0.000
0.008
0.016
0.024
0.032
0.040
0.048
SnSe2 Crystalline
77.3°K
-9.0
-6.0
-3.0
0.0
3.0
6.0
9.0
RELATIVE ABSORPTION
0.00
0.02
0.04
0.06
0.08
0.10
0.12
SnSe Crystalline
77.3°K
-9.0
-6.0
-3.0
0.0
3.0
6.0
9.0
VELOCITY (mm/sec)

Fig 3

Appendix E

Mechanism of Crystal Growth in Thin Films of Sb_xSe_y

H. Brigitte Krause
Physics Department
Northern Illinois University
DeKalb, Illinois

Abstrect

Thin films of Sb_xSe_y ranging from Sb_1Se_3 to $Sb_{3.5}Se_3$ have been investigated by electron microscopy and selected area electron diffraction. By variation of the electron beam intensity, crystallographic changes could be introduced to the specimen. Although the electron micrographs varied considerably in appeerence, the diffraction patterns for different compositions showed striking similarities. It was observed that segregation of phases within the sample took place. Some of the changes were reversible when the electron beam intensity was reduced.

Introduction

Sb_2Se_3 crystallizes in the space group Pbnm[1] by forming endless chains parallel to the c-axis[1]. The lattice constants of the orthorhombic unit cell are: a = 11.62Å, b = 11.77Å and c = 3.96Å.[1] Because of the large a and b dimensions and because of the rather low crystal symmetry, the Sb_2Se_3 diffrection

* This research was supported by the Advanced Research Projects Agency of the Department of Defense and was monitored by the Army Research Office, Durham, under Contract No. DA-ARO-D-31-127-71-G132.

pattern consists of many reflections. In the case of partially ordered Sb_2Se_3 or nonstoichiometric Sb_xSe_y, one may expect even considerably more complexity of the diffraction pattern: line shifts, line broadening and additional lines. Thus one may not be able to resolve the various diffraction lines by conventional x-ray diffraction techniques and consider a material amorphous when, in fact, some ordering on a micro scale exists. Any anisotropy , even on a small scale, affects the physical transport properties drastically. In order to avoid any wrong conclusions one has to resort to some micro technique such as high resolution electron microscopy and selected area electron diffraction. These methods have the additional advantage that they can be used almost simultaneously on the same micro area, thus allowing a more reliable interpretation of the data than would one method alone.

While our work was in progress, the results of an identical approach by I. E. Bolotov, A. V. Kozhir and S. B. Fisheleva[2] became available. Our results agree in many aspects with those of the Russians. But our observations suggest a more complicated mechanism of crystal growth and show a greater variety of crystal appearances.

Results

The thin films were prepared by direct evaporation of antimony and selenium[3] on parlodion covered electron microscope grids. These samples were examined in a Hitachi electron microscope, equipped with a liquid nitrogen cooled anti-contamination device. Such a device also prevents heating of the sample by the

electron beam. In spite of this device, it was observed that the samples appearance considerable changes in the electron beam, especially when the beam intensity is high.

Most of the specimens were about 200-250Å thick. In the beginning of the experiment they had a rather uniform appearance, similar to that of the bulk part in Fig. 1, showing no anisotropy. The corresponding diffraction pattern taken from an area 50μ in diameter, is shown in Fig. 2. It consists of four broad bands and appears to be independent of the sample composition. (An exception found for antimony rich samples will be discussed later). A very crude estimate from the half width of those bands and of the primary beam spot indicates particle sizes of about 30Å. In view of the large unit cell it seems rather philosophical to decide whether or not these particles are crystalline.

Increase of the electron beam intensity caused all samples to change. These changes occurred either spontaneously within fractions of a second or slowly within about 30 minutes depending on the sample composition. With increasing percentage of antimony the process slowed down. Although many of the results were similar for all sample compositions, some typical differences seem to exist. We will, therefore, distinguish between three cases: 1) antimony rich samples ($Sb_{2.5}Se_3$ and $Sb_{3.5}Se_3$), 2) stoichiometric samples and 3) antimony poor samples (Sb_1Se_3 and $Sb_{1.5}Se_3$).

Fig. 1 shows the initial stage of crystallization in antimony rich samples near the margin of one of the grid holes (left in the picture). The diffraction pattern is a hexagonal single crystal pattern (Fig. 3) and may be attributed to antimony. The bulk of the material crystallizes in fibers as shown in Fig. 4.

As already pointed out by Bolotov et. al.[2] these fibers sometimes spiral around each other. This may also be concluded from the directional change of interference fringes shown in Fig. 5. While, typically, the fibers lie within the film plane, they may occasionally stick out of the film.

The appearance of stoichiometric samples of Sb_2Se_3 after crystallization is quite different. One often observes well defined crystallites from about several thousand Å to a few microns in diameter (Fig. 6). Within the particles one can see subdomains, about 30 by 500Å in size. Typically, within these subdomains one observes interference fringes. These domains probably have an orientation parallel to the chain structure of Sb_2Se_3, which sometimes can be detected in individual crystallites. A transition from the fiber structure in Fig. 4 and Fig. 5 to the domain structure in Fig. 6 is shown in Fig. 7. The domain boundaries appear rather fuzzy. Antimony poor samples sometimes seem to be crystallized even before irradiation with electrons, but the crystals remain smaller, somewhere around 500Å and the subdomains seem even closer to one another (Fig. 8). In some cases no distinct crystals develop even after prolonged irradiation (Fig. 9).

The appearance of the films does not always follow one or the above described cases. Very thin samples, for instance, show complicated systems of thickness fringes.(Fig. 10), but even from the irregularities of these fringes, one may detect the fibrous character of the sample. Sometimes the uniform Sb_xSe_y film disintegrates in favor of individual crystals (Fig. 11). Very thick samples show well developed needle-like crystals (Fig. 12).

As different as the appearance of the samples is also the appearance of the diffraction patterns. The most frequently observed Sb_2Se_3 single crystal pattern,

Fig. 13, corresponds to an a*-c* reciprocal plane. The crystallographic b-direction is perpendicular to the thin film plane. The space group extinction law for h0l reflections is violated. The forbidden reflections, however, have relatively low intensities. Such patterns have been observed for almost all sample compositions although it is difficult to get them for extreme compositions of either antimony poor or antimony rich samples. The c to a ratio calculated from different diffraction patterns, varies between 2.78 and 2.96 and does not change systematically with the sample composition. Occassionally one can see multiple spots, probably caused by double diffraction from domains with slightly varying lattice dimensions (Fig. 14). Other variations of this pattern are obtained from fibers orientated parallel to one another but rotated various amounts about the fiber axis (Fig. 15). Often observed is the pattern from the superposition of two or more sets of fibers (Fig. 16). Each set of reflections on parallel lines originates from a bundle of fibers with the fiber direction perpendicular to these lines. In many cases the fibers are not perfectly parallel as can be deduced from the conical appearance of layer lines (Fig. 7).

The transition from the amorphous stage (Fig.1) to the polycrystalline stage (Fig. 6) occurs in more than one way. Fig. 18, for instance, shows a powder pattern with preferred orientation of the crystallites in addition to amorphous rings. The preferred orientation is the same as discussed above for fibers.

Antimony poor samples tend to yield powder patterns of great complexity (Fig. 19) which can be verified as Sb_2Se_3. When the crystallites grow larger in the electron beam, most crystals are orientated with b perpendicular to the film plane. But occasionally other projections have been observed such as [100](Fig. 20)

and possibly [001] (Fig. 21). If, indeed, Fig. 21 represents an [001] projection, the extinction law: h = 2n is not observed.

Perhaps the most interesting observation is the fact that the crystallites, grown in the electon beam, are unstable. If the beam intensity is turned off, the crystals disintegrate. Upon renewed irradiation one observes diffusion processes until renewed crystallization takes place. Typical for the intermittent stage are diffuse boundaries between domains and interference fringes at the interfaces (Fig. 22).

Discussion

The data indicate that a rearrangement of atoms takes place if the electron beam intensity is increased. In particular, there is a segregation of different elements and compounds such as Sb, Se and Sb_2Se_3. The segregation of Sb in antimony rich samples has actually been observed whereas the segregation of Se in selenium rich samples is only suspected. It is not known to what extent such a segregation takes place and whether or not the remaining sample is stoichiometric. The fact that segregation of antimony has even been observed in stoichiometric samples suggests the crystallization of antimony to occur independently from the composition of the remaining sample as long as sufficient antimony is present. Nonetheless, the remaining Sb_xSe_y from which the Sb_2Se_3 diffraction patterns are obtained may be nearly stoichiometric. The domains in "stoichiometric" and selenium rich samples, for instance could be due to segregation of Se. The domains are so small that the diffraction from these domains would contribute only to the background.

In spite of the cooling of the sample by the anti-contamination device, there may be a periodic temperature gradient within the sample due to poor conductivity. The temperatures near the grid are expected to be lower than in the center of the grid. While the antimony segregates at the cooler temperature regions, the Sb_2Se_3 crystals form at higher temperatures. Excess of Se seems to reduce the temperature at which crystallization takes place, but both excess antimony and excess Se inhibit the crystal growth.

Perhaps most interesting is the deterioration of crystals once the electron beam is turned off. Additional work is needed to understand this phenomenon.

Figure Captions

Fig. 1 Initial Stage of Crystallization of an amorphous rich Sb_xS_y film.

Fig. 2 Diffraction Pattern of an Amorphous Sb_xSe_y film.

Fig. 3 Diffraction Pattern of Antimony.

Fig. 4 Fiber Structure of antimony rich samples.

Fig. 5 Interference fringes indicating spiraling of fibers around one another.

Fig. 6 Appearance of stoichiometric samples.

Fig. 7 Transition from fibrous sample appearance to distinct domains.

Fig. 8 Appearance of antimony poor film after crystallization.

Fig. 9 Appearance of antimony poor polycrystalline film.

Fig. 10 Appearance of very thin sample showing thickness fringes.

Fig. 11 Small Sb_xSe_y crystals on amorhpous substrate.

Fig. 12 Needle-like crystals in 500Å to 1000Å thick film.

Fig. 13 Diffraction pattern of Sb_2Se_3.

Fig. 14 Diffraction pattern showing multiple-spots due to domains with different lattice constants.

Fig. 15 Diffraction patterns of fibers with ordering only in the direction of the fiber axis.

Fig. 16 Diffraction pattern originating two sets of fibers with fiber axis perpendicular to the predominant lines.

Fig. 17 Diffraction pattern from fibers showing misalignment also with respect to zone axis.

Fig. 18 Diffraction pattern showing transition from amorphous to crystalline state.

Fig. 19 Powder pattern of Sb_2Se_3.

Fig. 20 [100] projection of Sb_2Se_3.

Fig. 21 [001] projection of Sb_2Se_3.

Fig. 22 Transition stage after interruption of electron irradiation.

Acknowledgement

The author wishes to thank Dr. Charles Wood and Mr. Robert Mueller for supplying the samples and Miss Dian Molsen for her help in relation to the electron microscope.

References

1. N. W. Tideswell, F. H. Kruse and J. D. McCullough, The Crystal Structure of Antimony Selenide, Sb_2Se_3, Acta. Cryst. 10, 99 (1957).

2. I. E. Bolotov, A. V. Kozhin and S. B. Fisheleva, Branching-Induced Formation Of Spherulites in In_2Se and Sb_2Se_3 Films, Soviet Phys. - Crystallography, Vol. 15 3, (1970).

3. R. Mueller and C. Wood, (to be published).

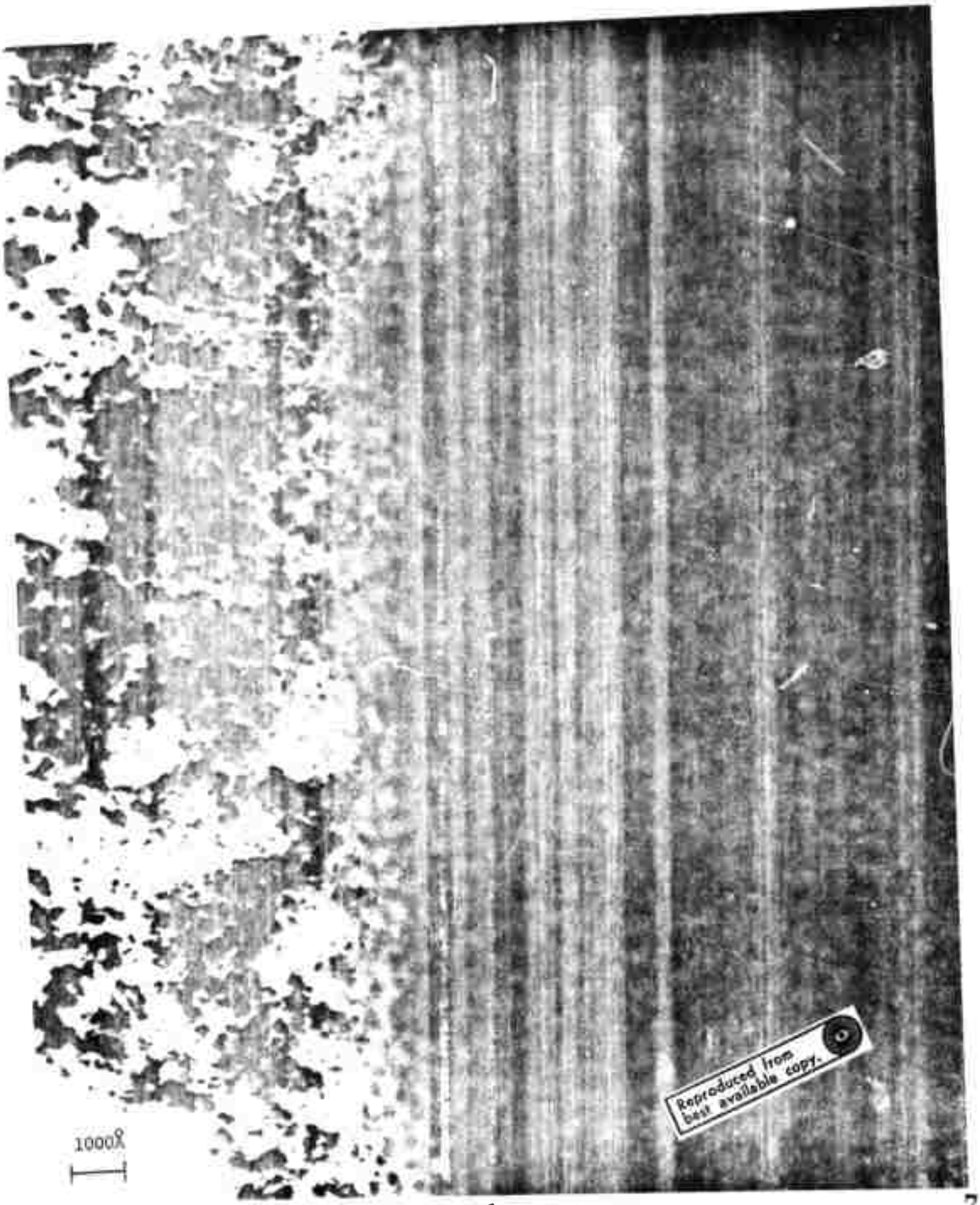

FIG. 1

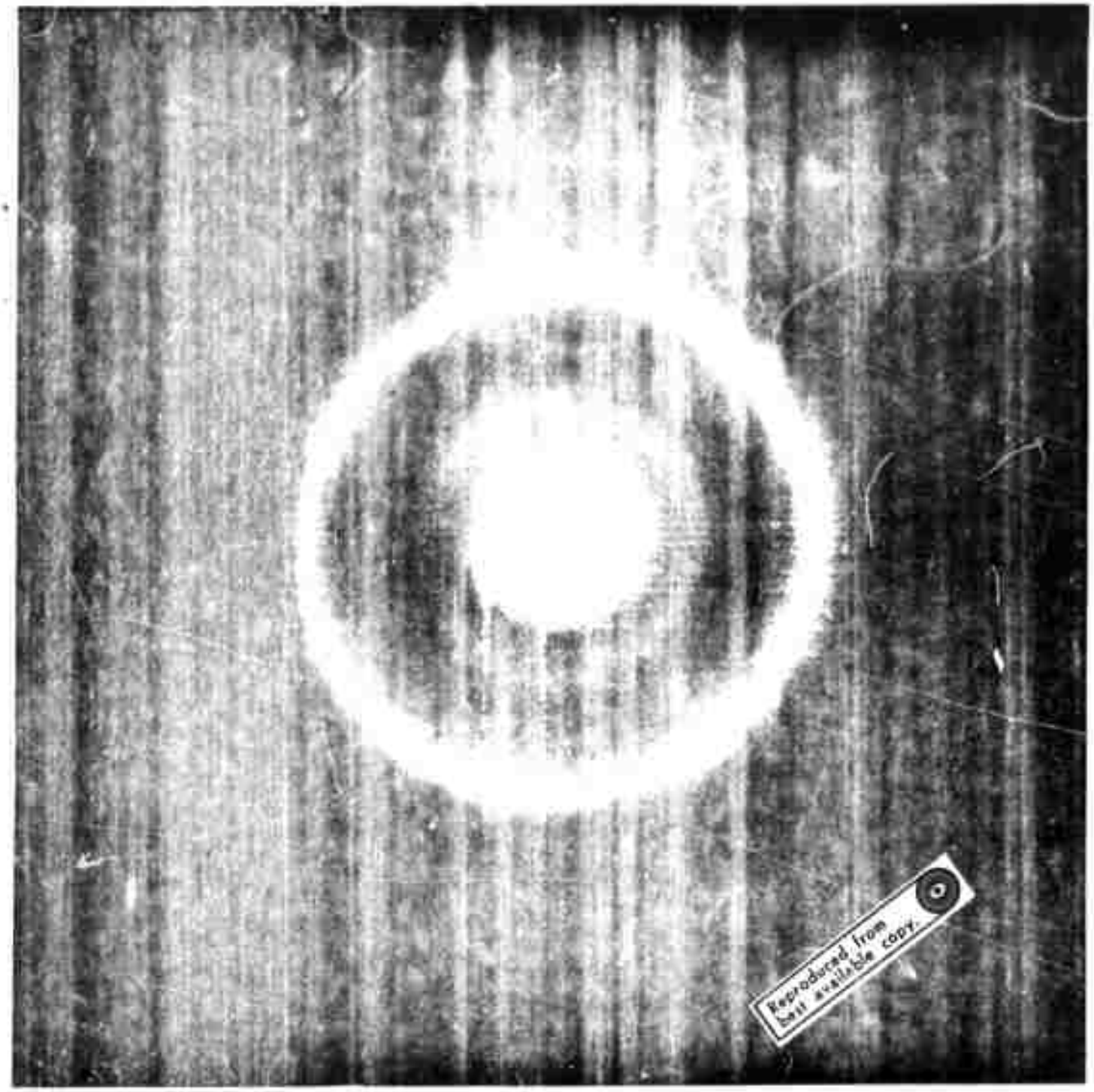

0.25Å^{-1}

FIG. 2

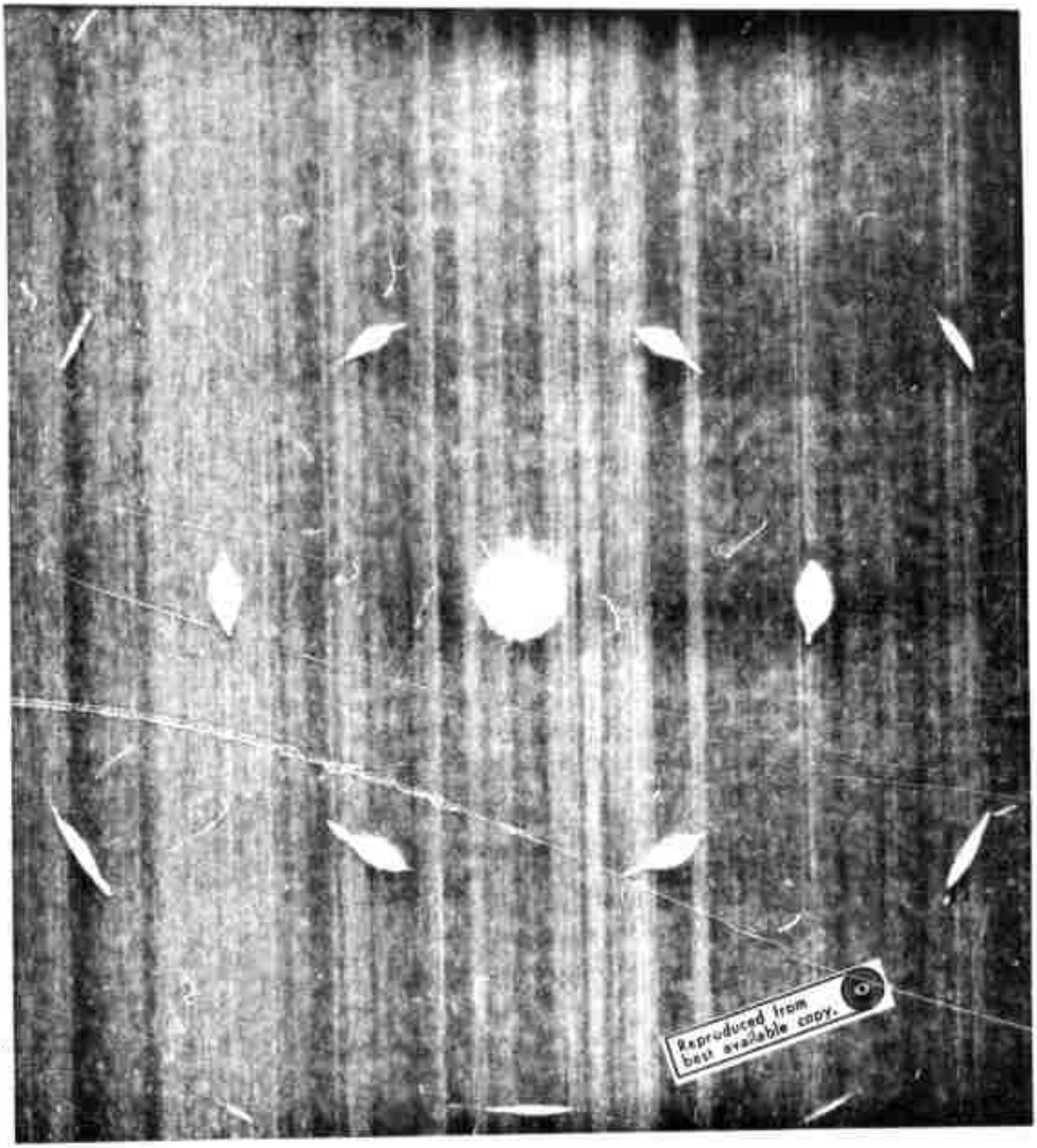

0.25Å^{-1}

FIG. 3

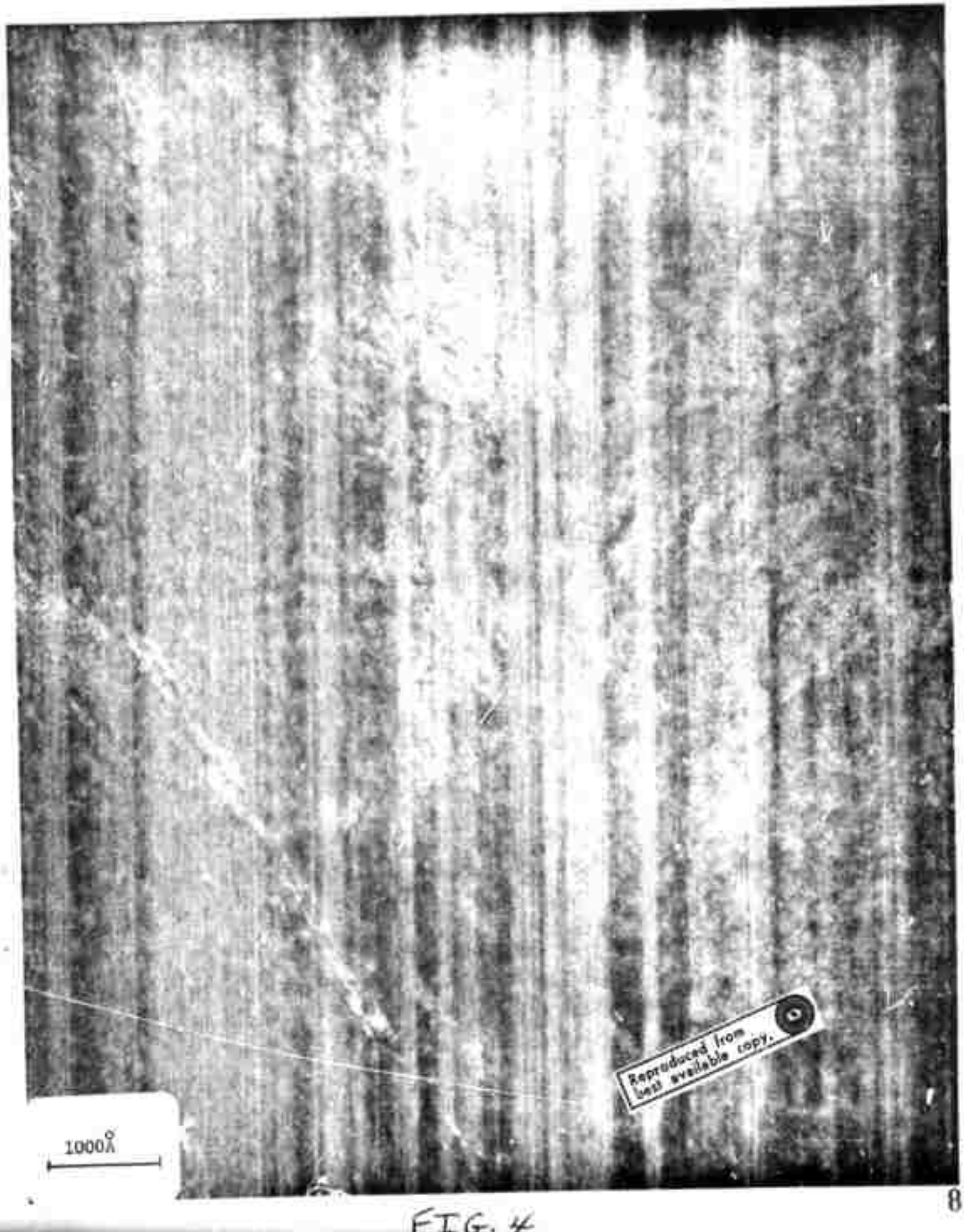

FIG. 4

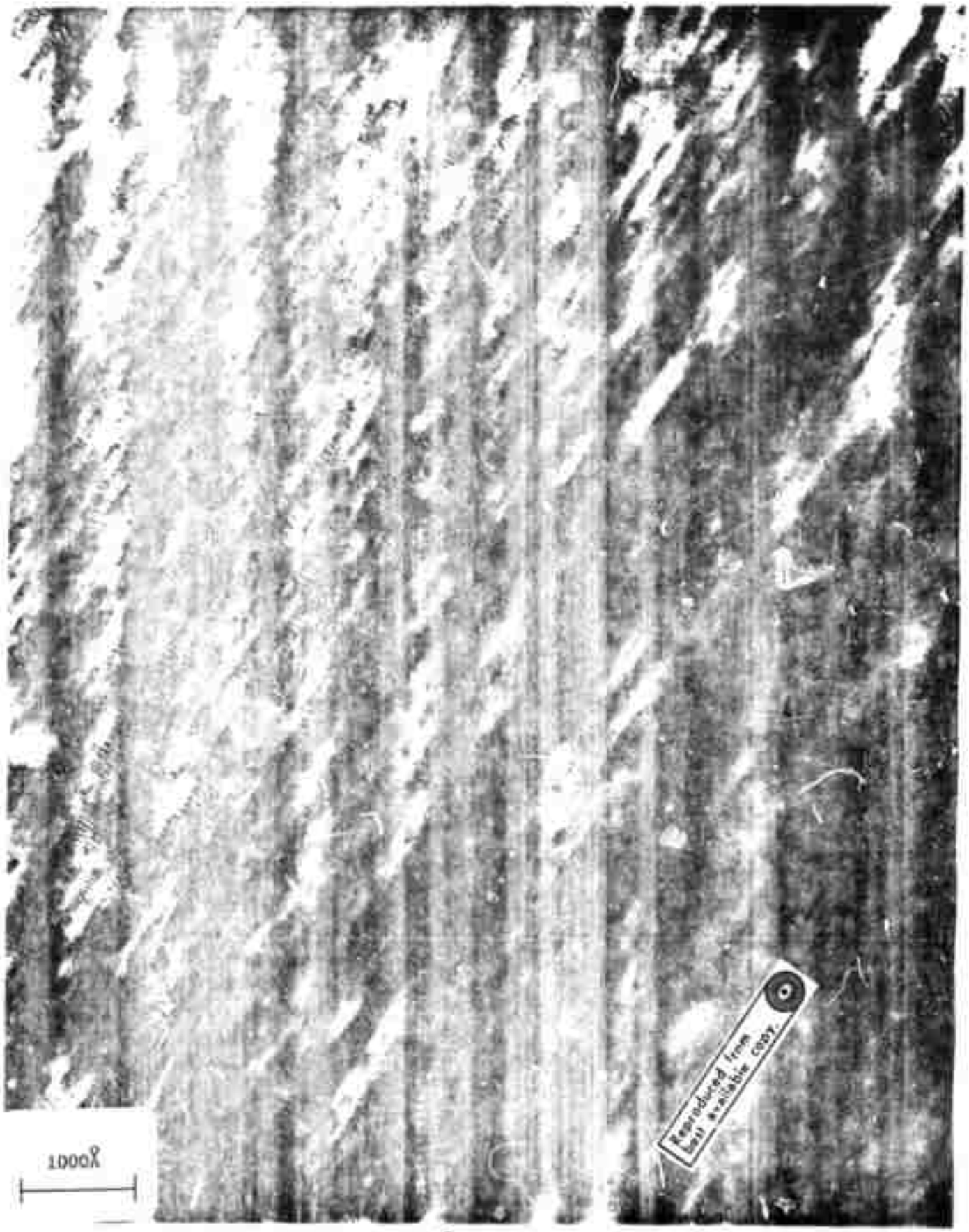

FIG. 5

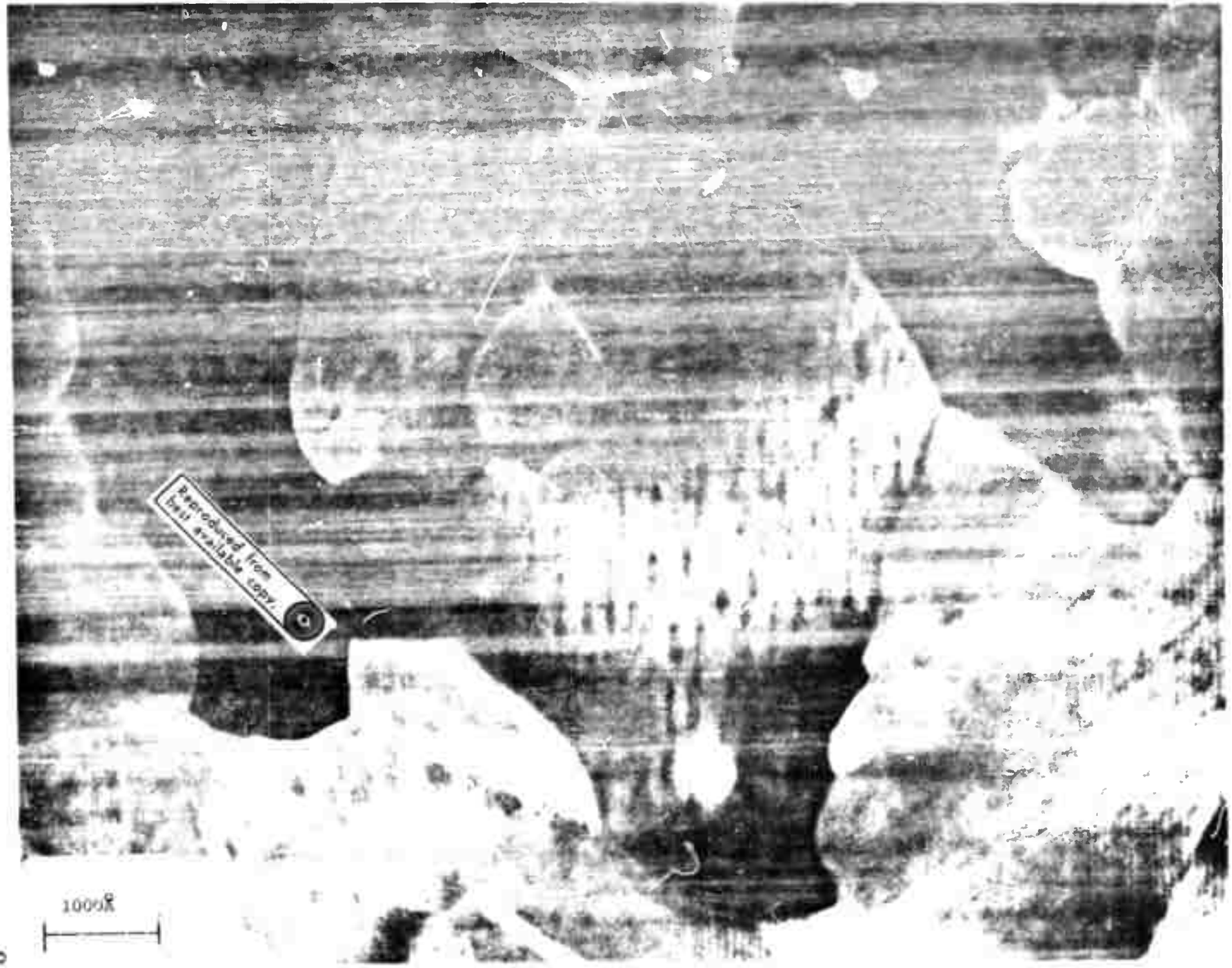

FIG. 6

FIG. 7

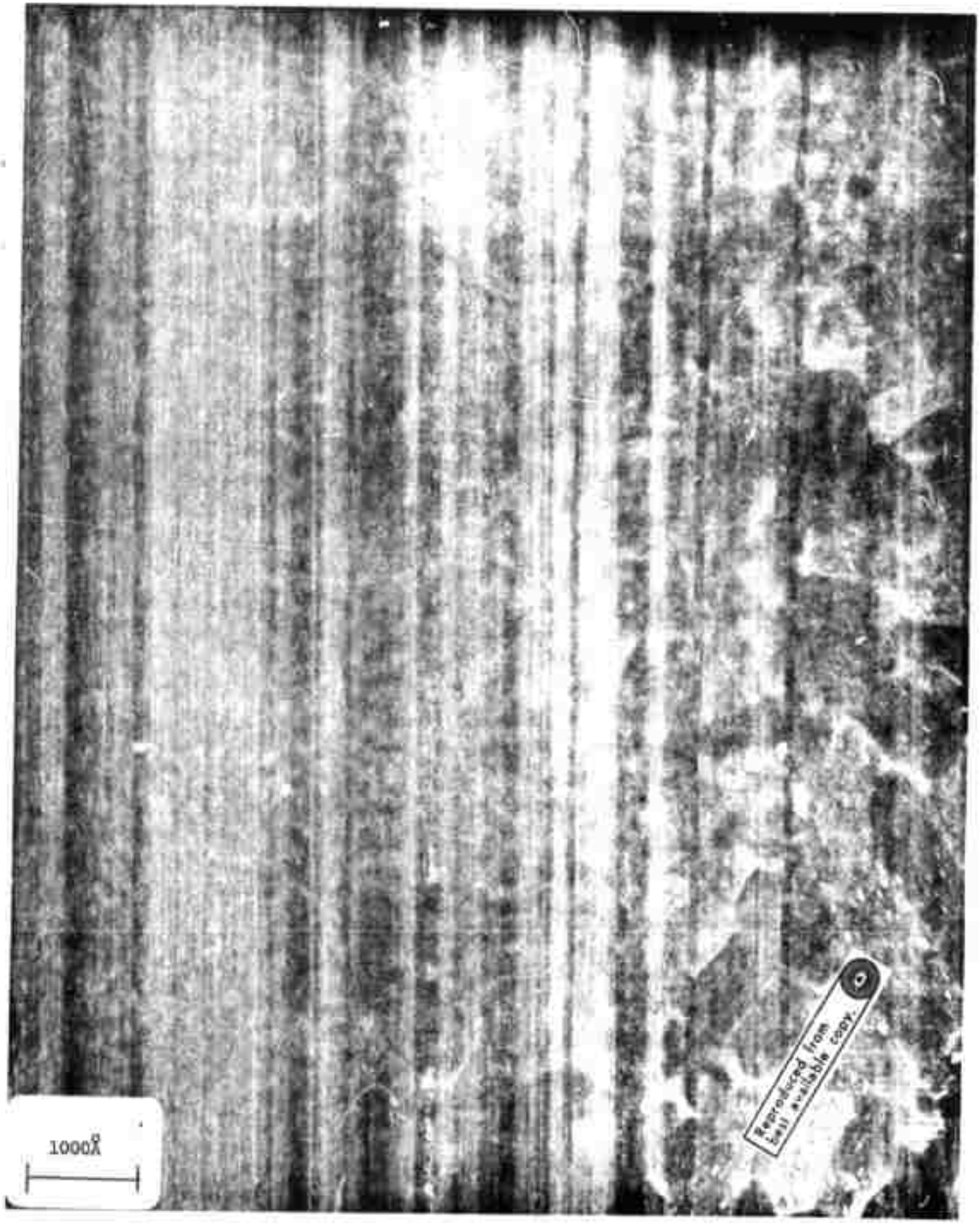

FIG. 8

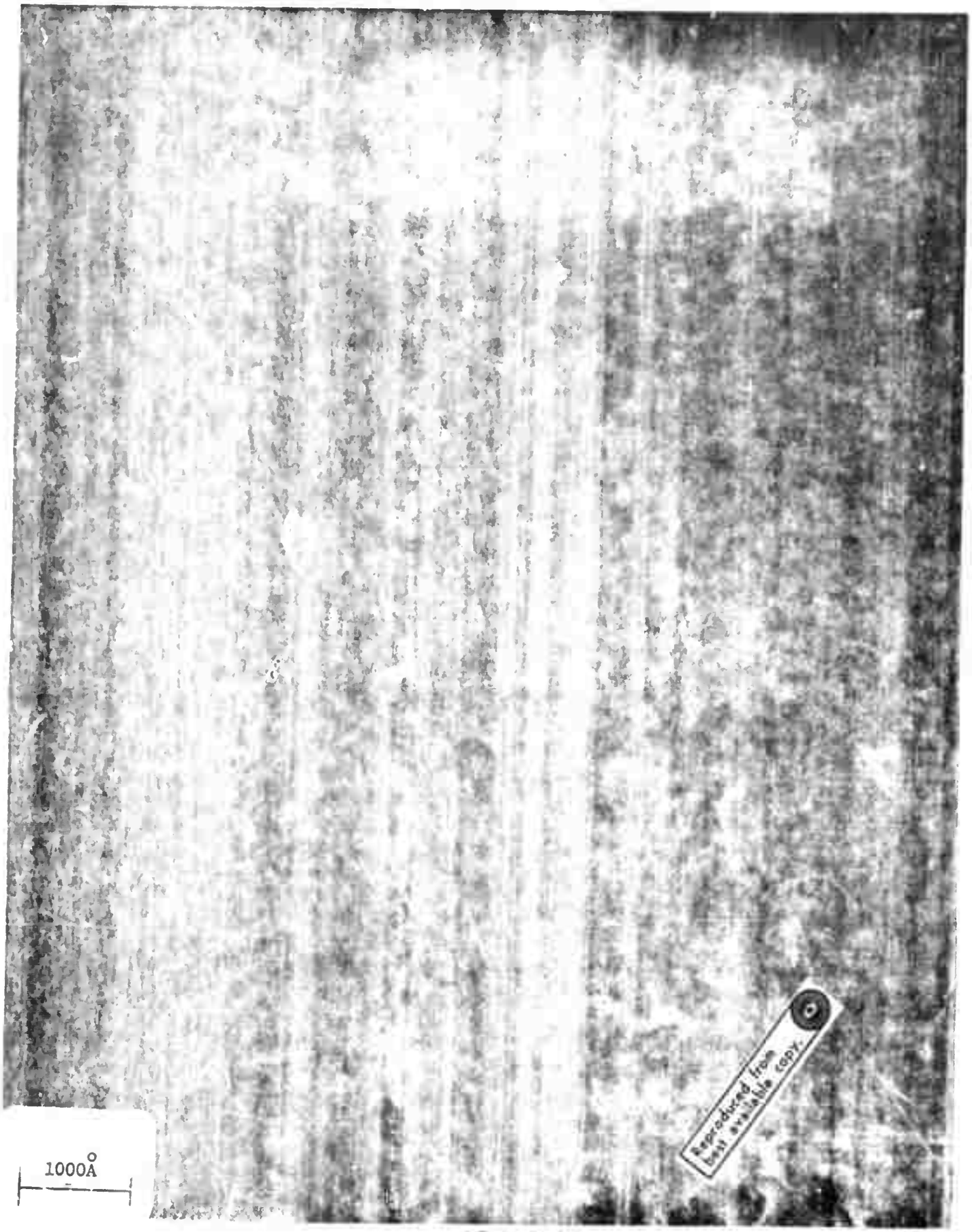

FIG. 9

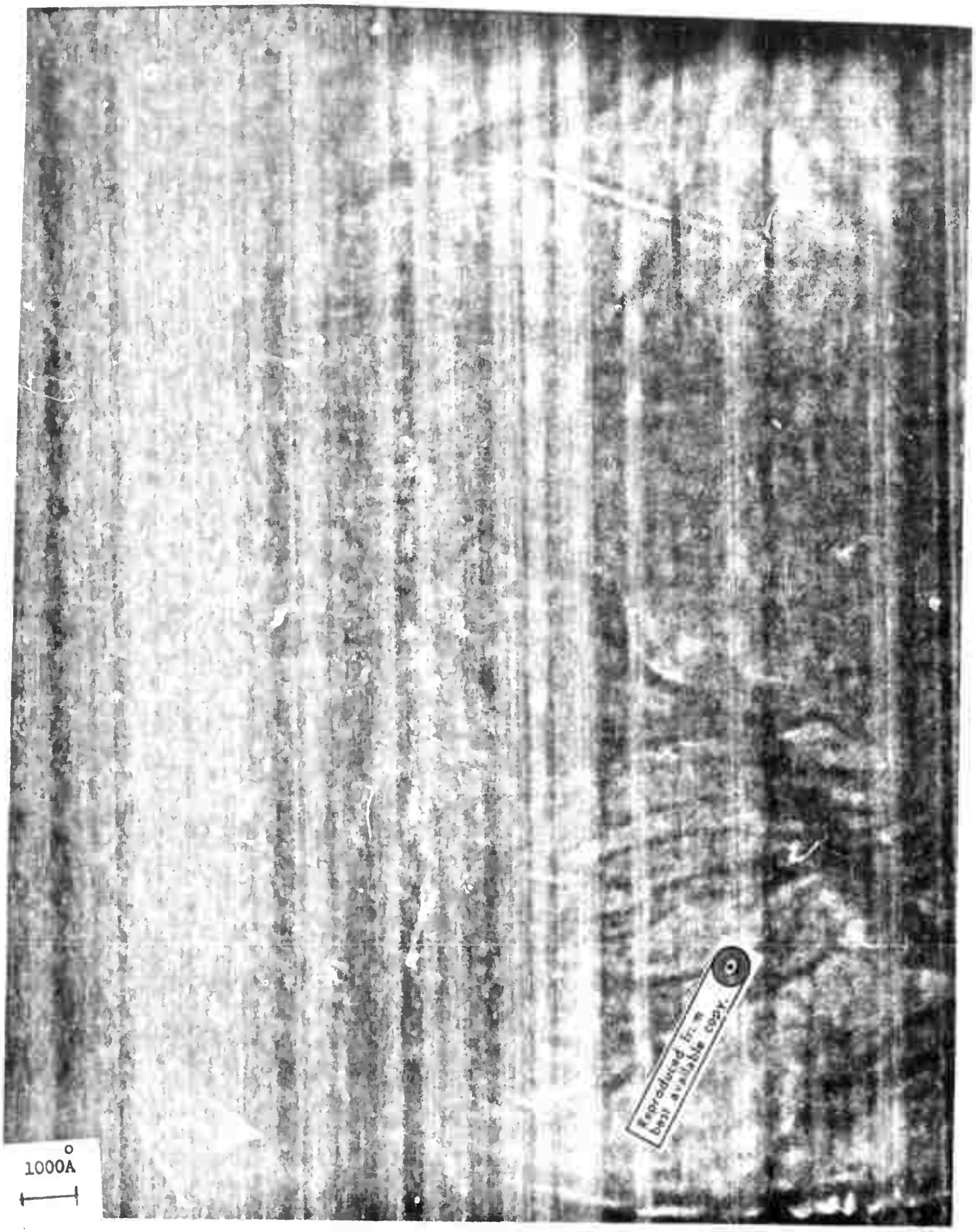

FIG. 10

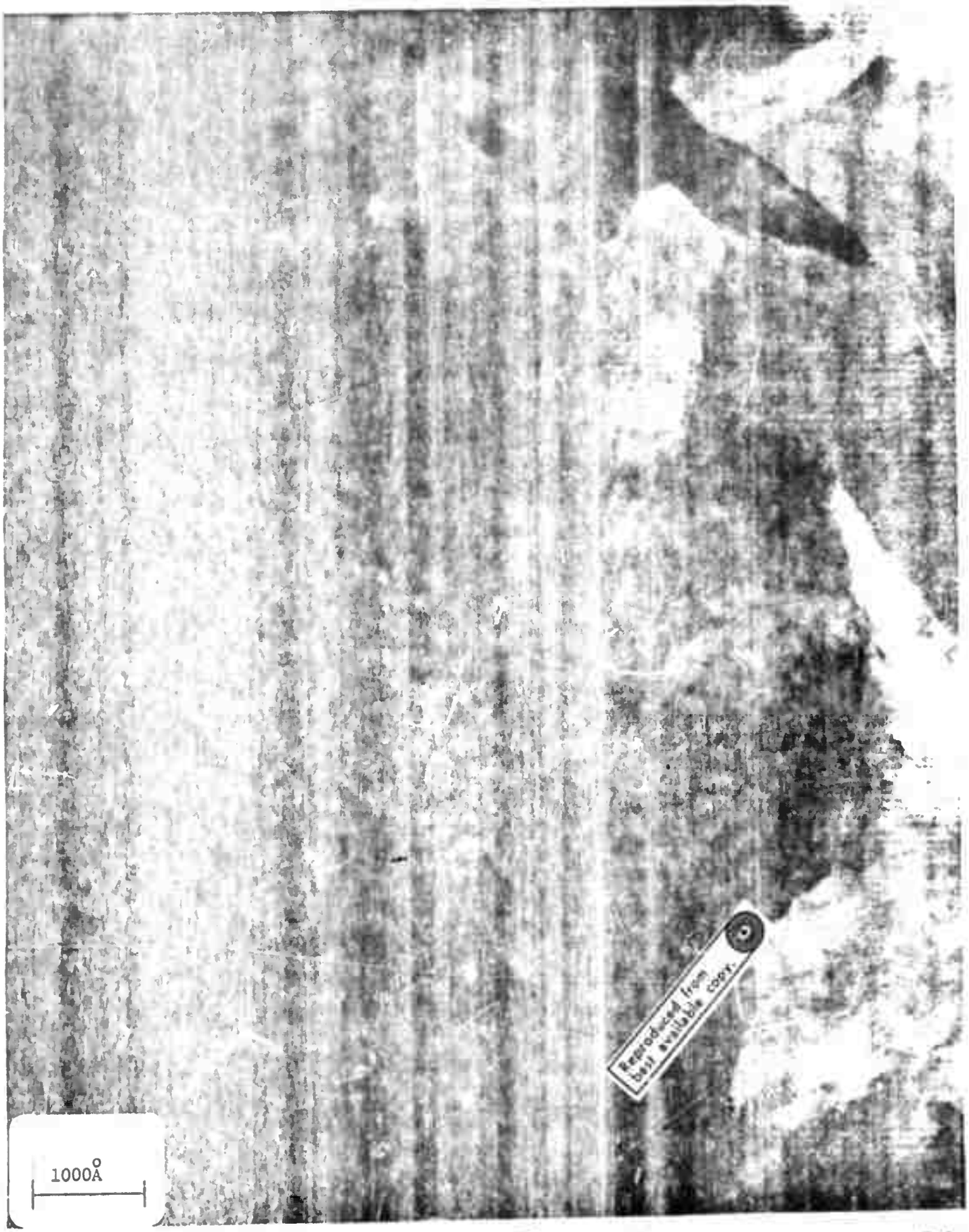

FIG. 11

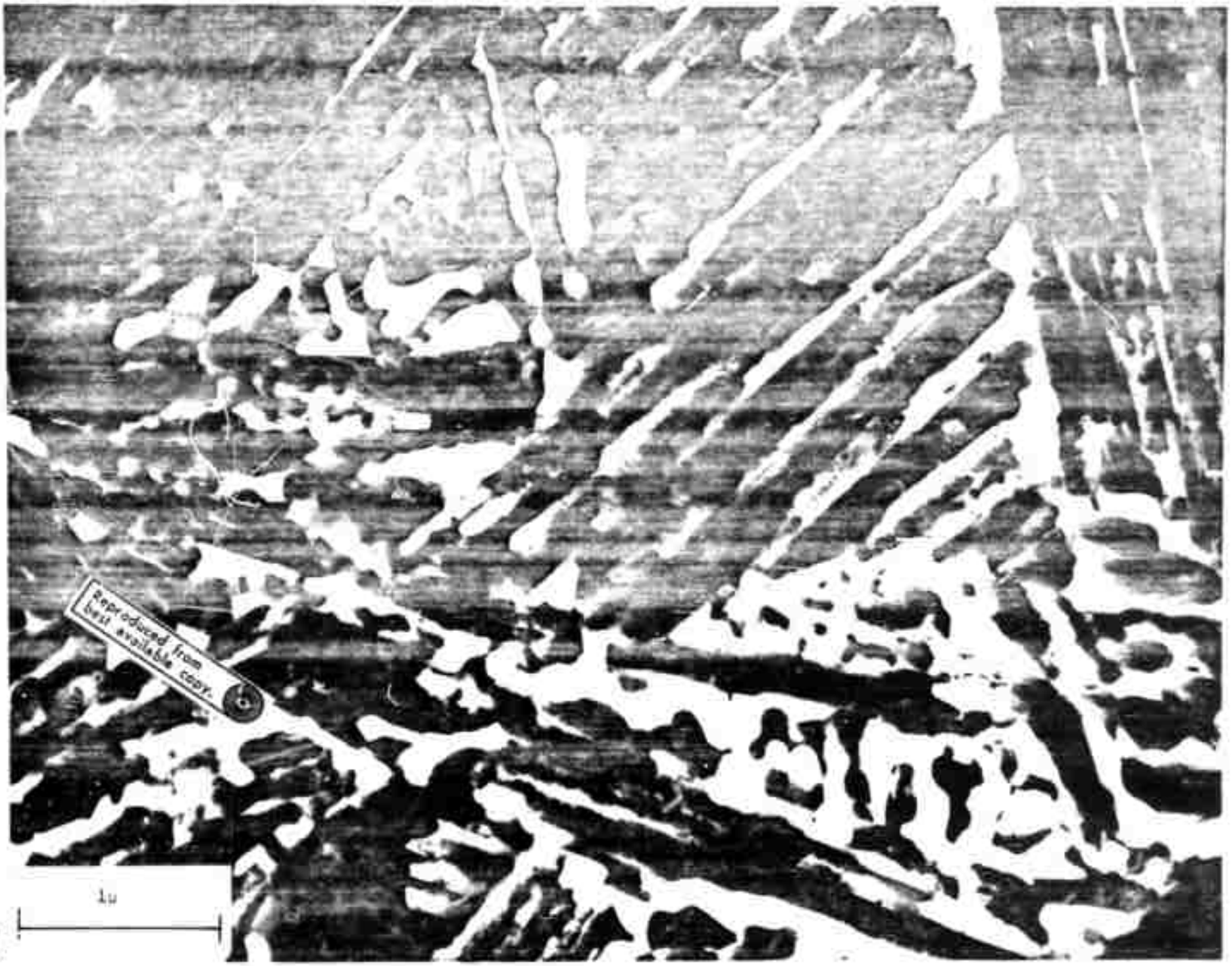

FIG. 12

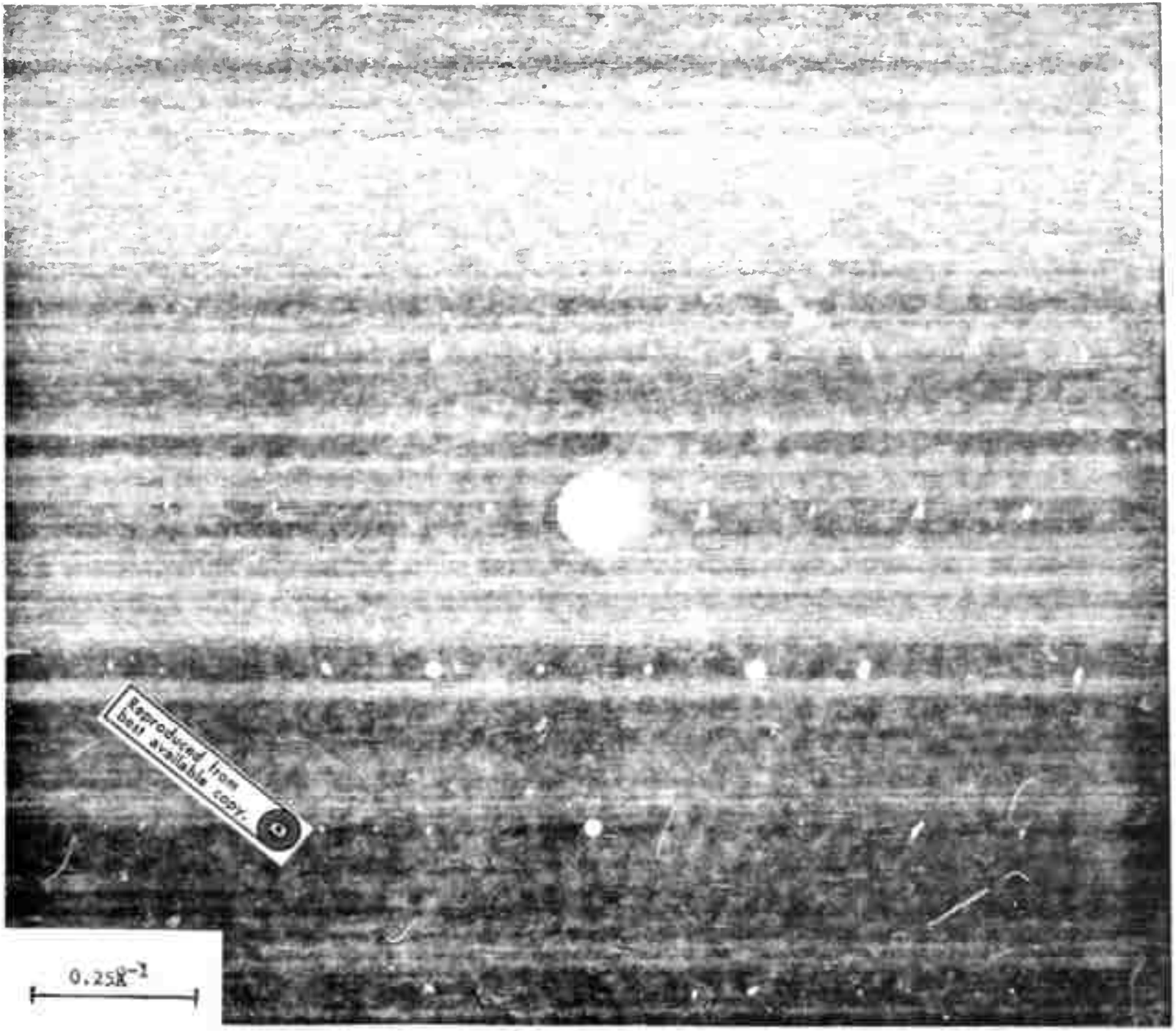

FIG. 13

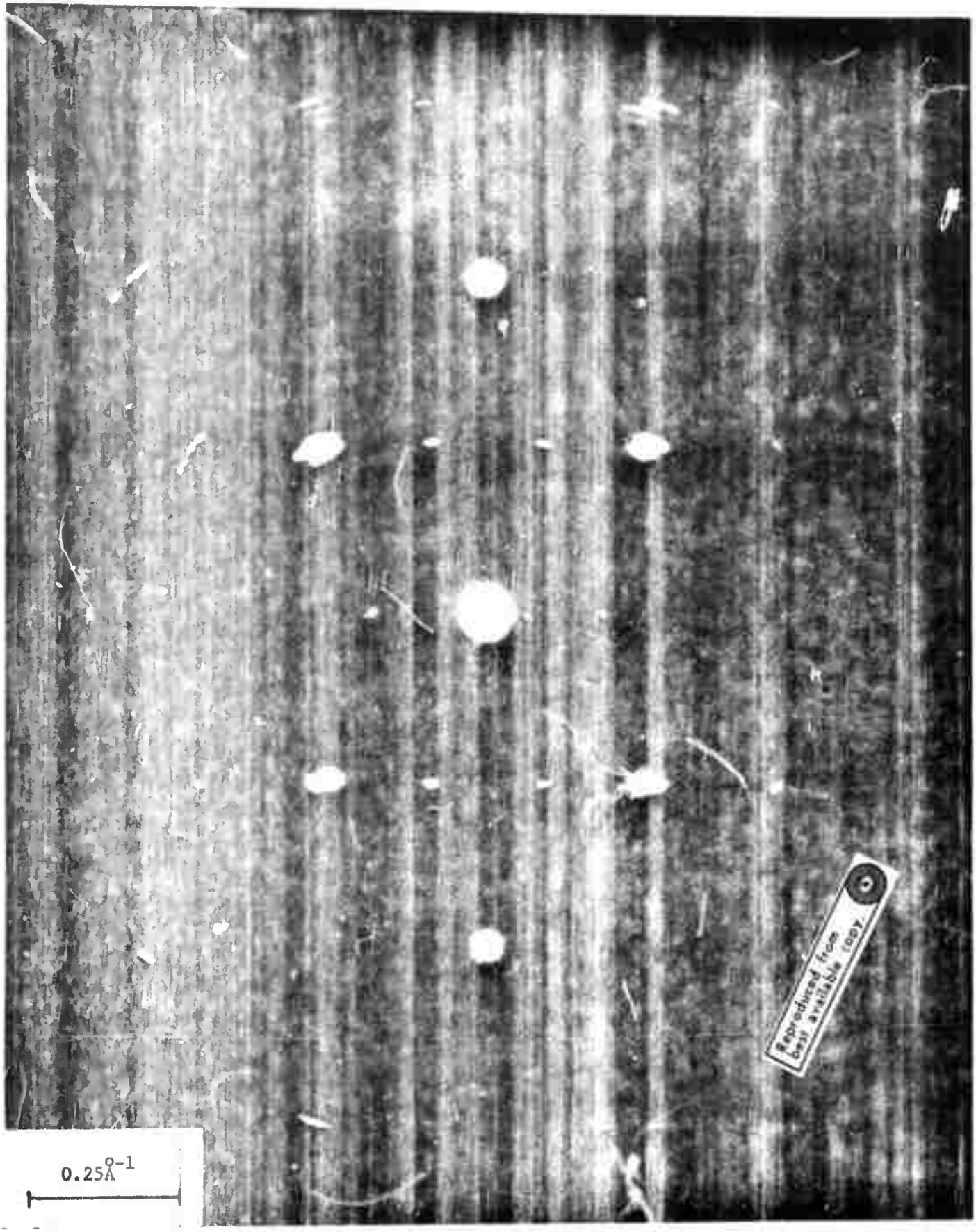

FIG. 14

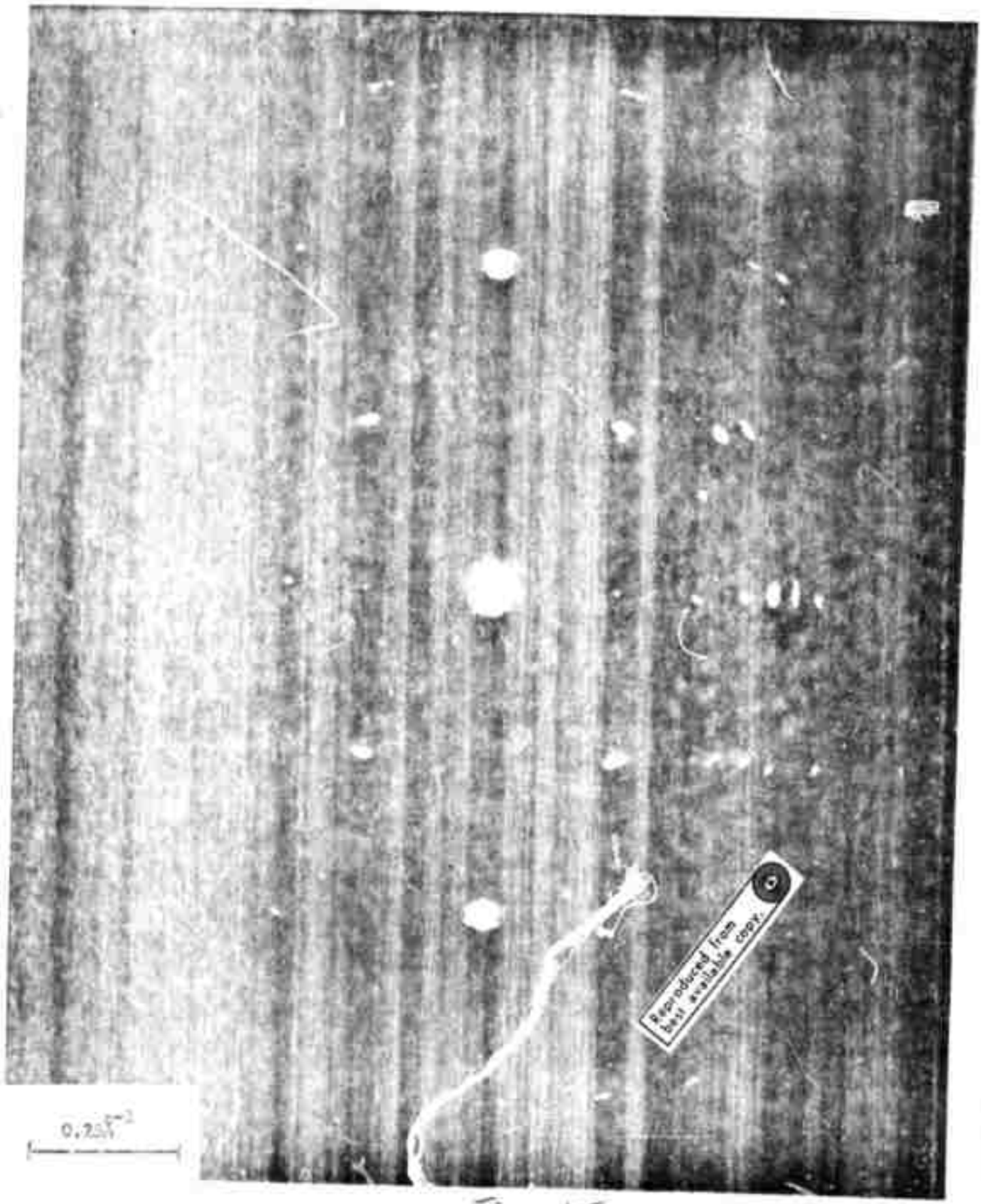

Fig. 15

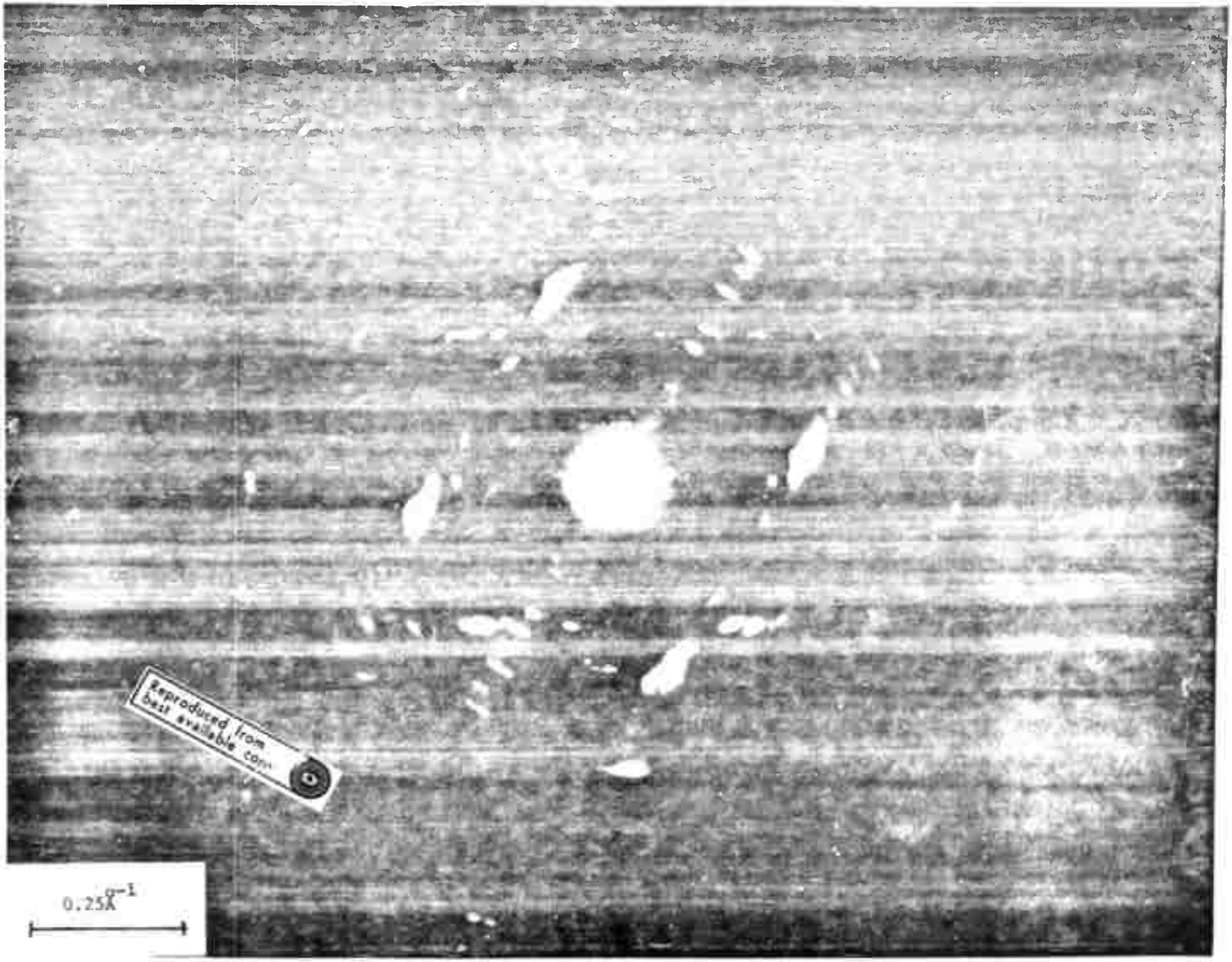

FIG. 16

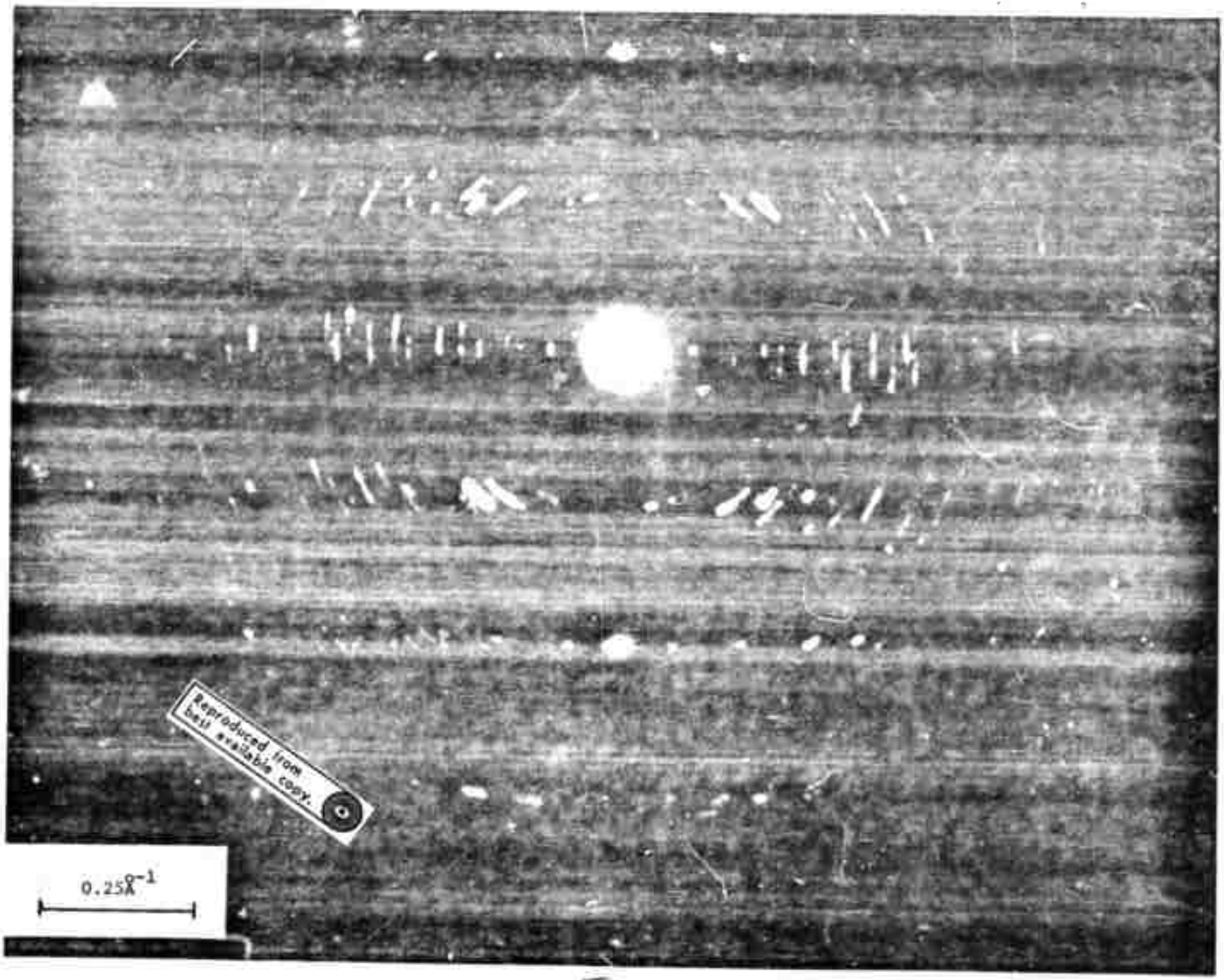

FIG. 17

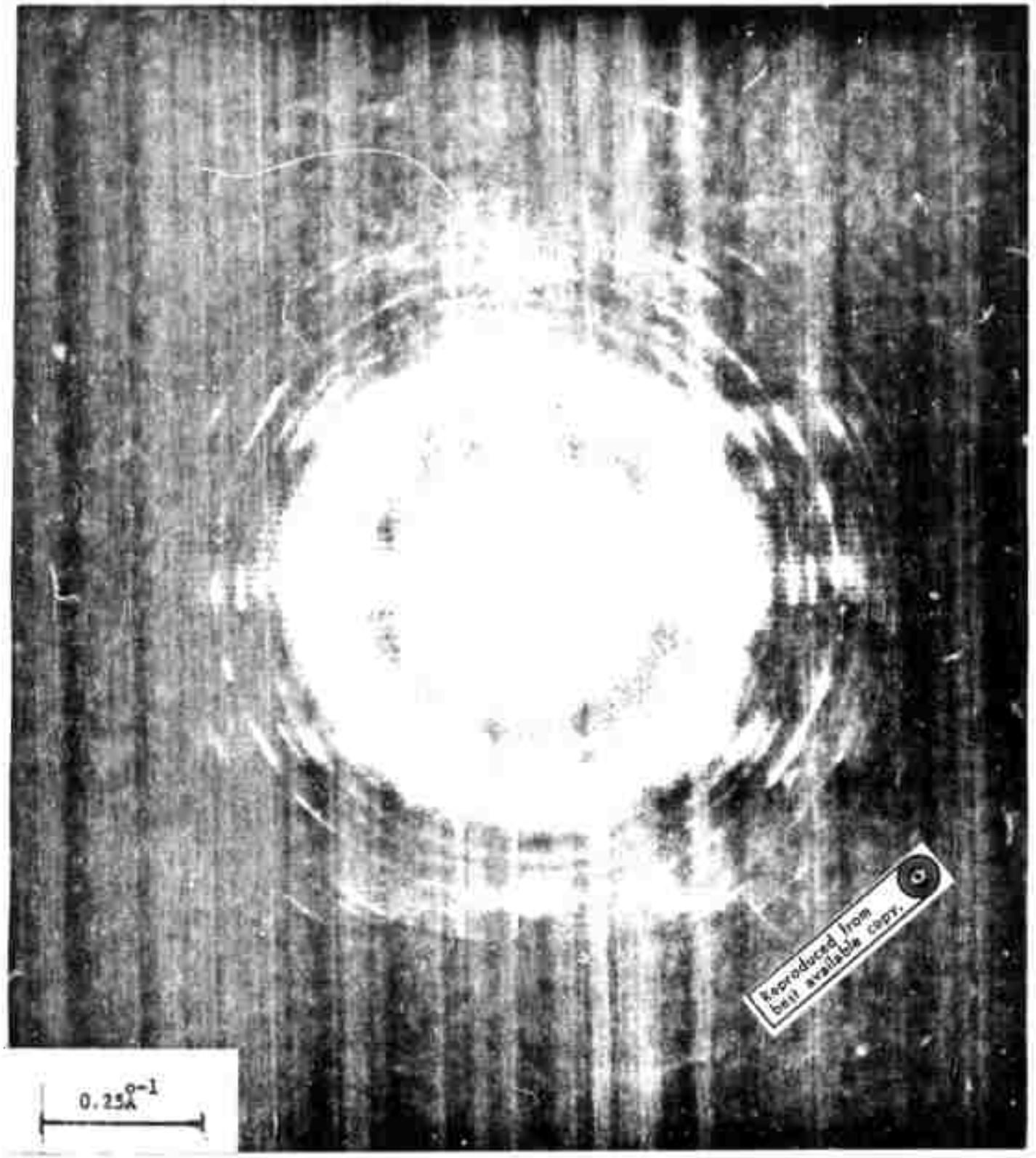

FIG. 18

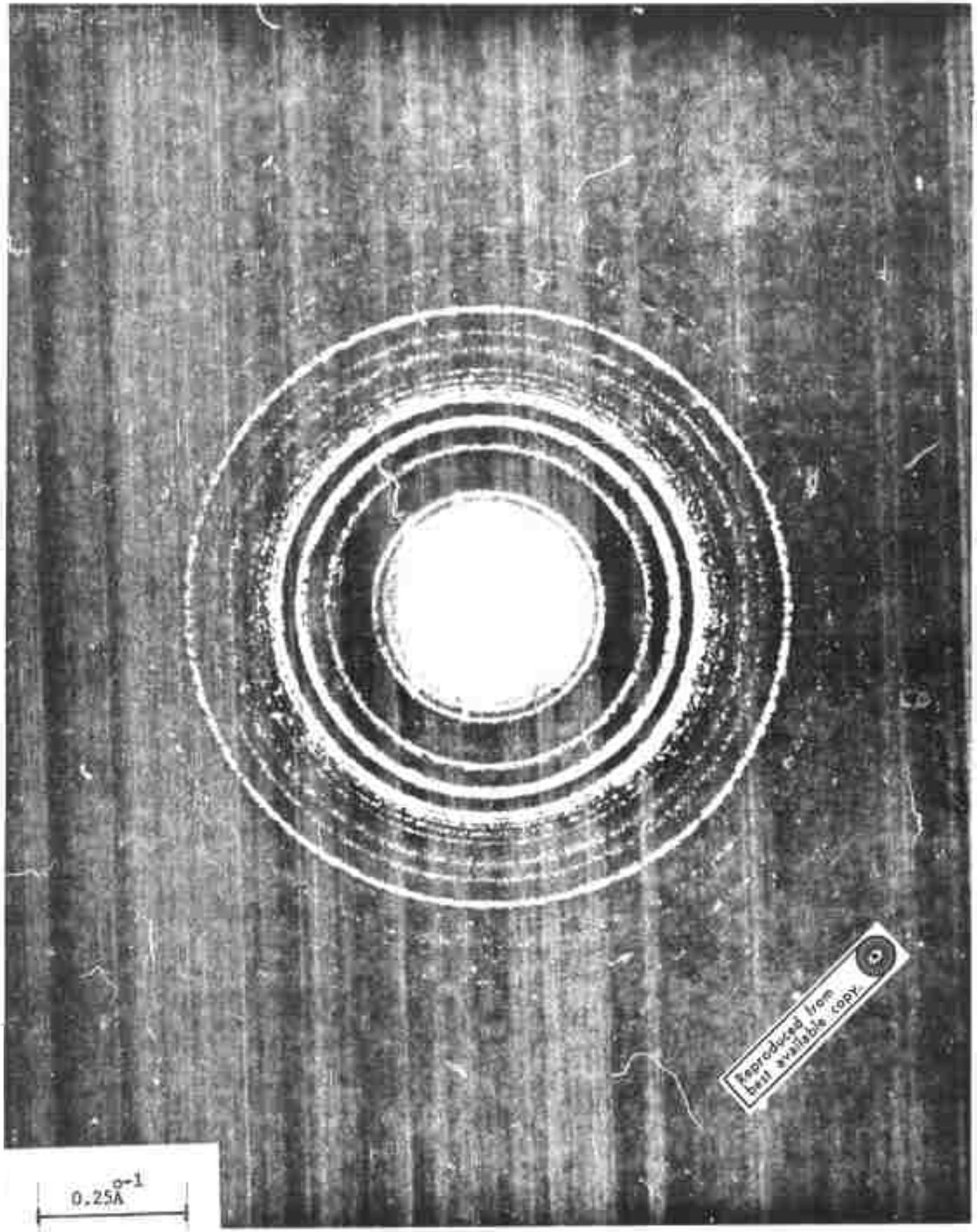

FIG. 19

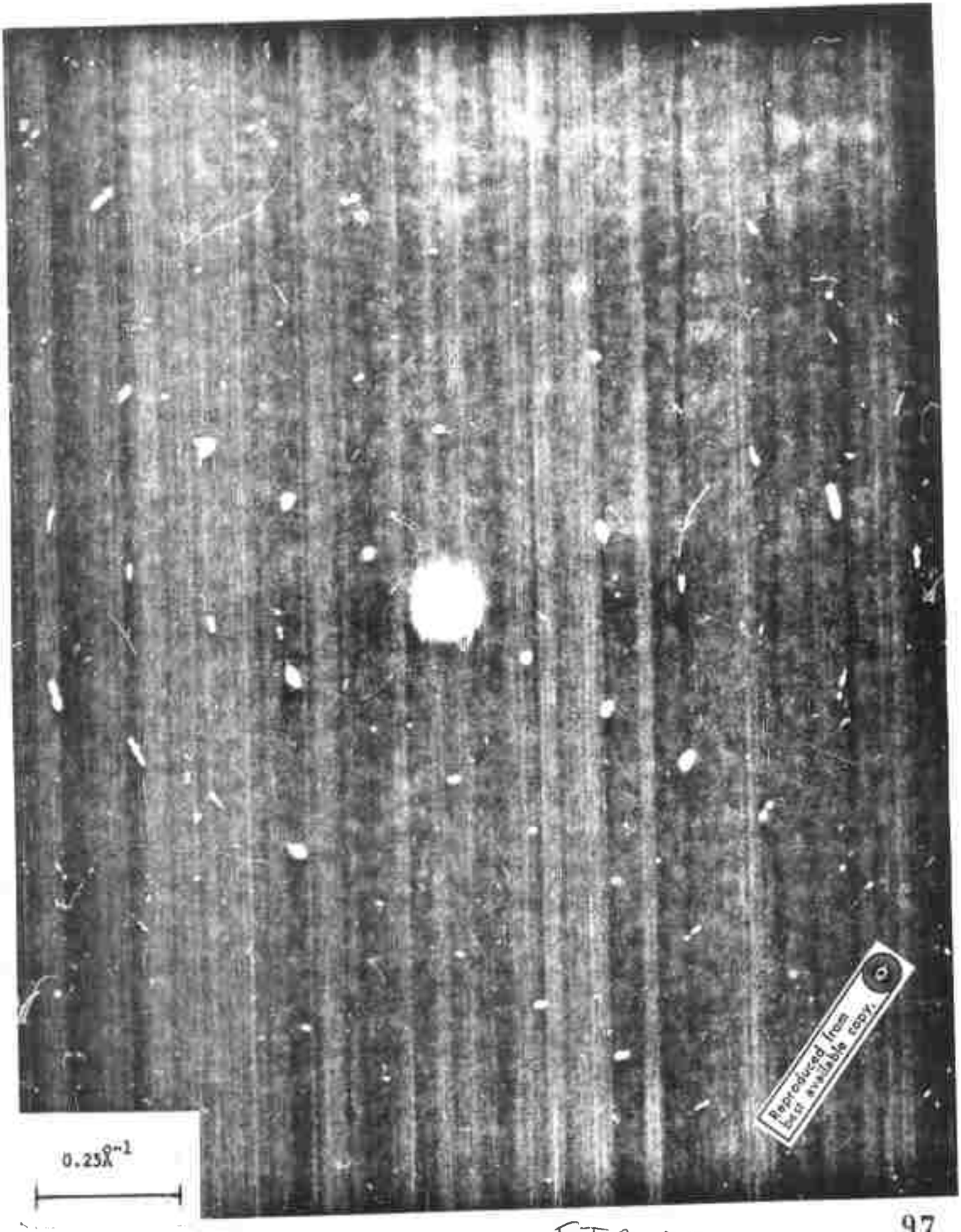

FIG. 20

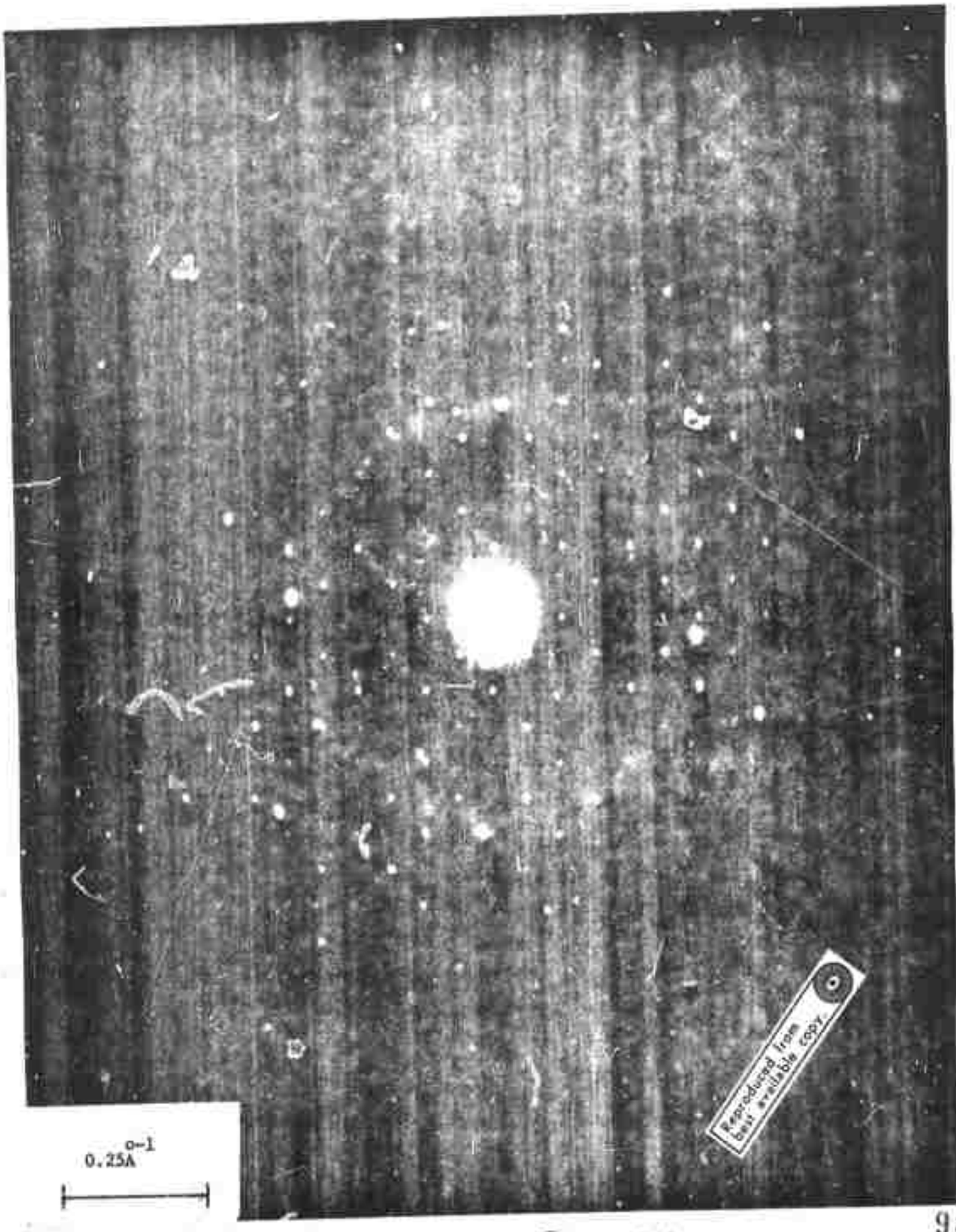

FIG. 21

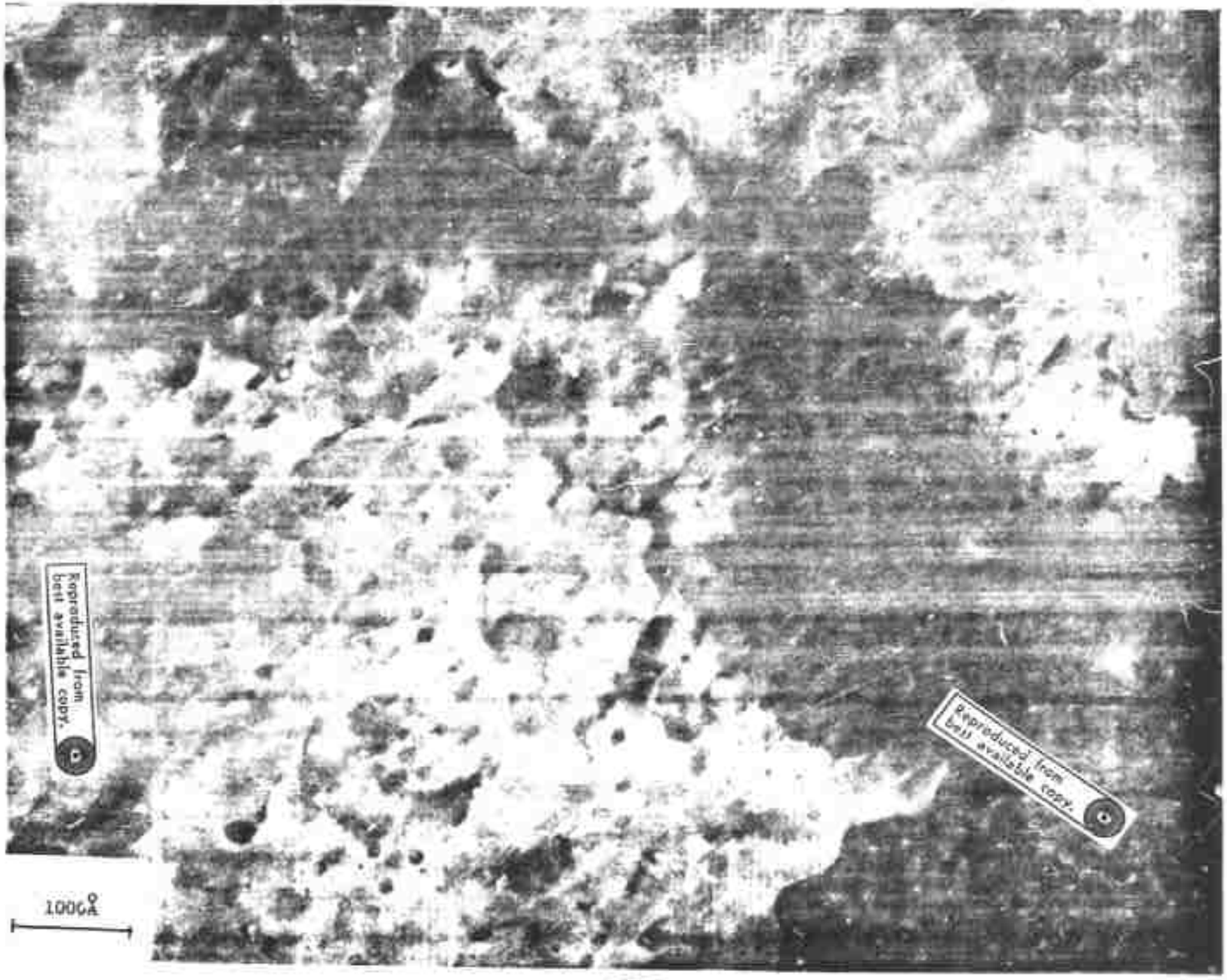
1000Å
Reproduced from best available copy.
Reproduced from best available copy.

FIG. 22

Appendix F

Determination of the Optical Constants of Thin Films from Reflectivity and Transmission Data by a Quadratic Fitting Procedure

L. R. Gilbert and J. C. Shaffer
Physics Department
Northern Illinois University
DeKalb, Illinois

and

F. M. Mueller
Physics Department
Northern Illinois University
DeKalb, Illinois
and
Argonne National Laboratory
Argonne, Illinois

I. Introduction

The determination of the optical constants of thin films mounted upon substrates with known optical properties is of great technical importance. Many amorphous materials can be prepared only in the form of thin evaporated films. To characterize their electronic structure it is important to obtain their optical functions at frequencies below and in the neighborhood of the fundamental absorption edge. In these regions multiple reflections contribute significantly to the measured reflectance and transmittance, and under certain conditions, interference maxima and minima are observed over wide spectral ranges. Several methods have been proposed for circumventing these problems. Among these are ellipsometric measurements,[1] Kramers-Kronig analyses of transmission,[2] measurement of the phase change upon reflection,[3] the use of approximate analyses which neglect interference,[4] and others.

In this paper we present a computational technique to obtain the optical functions of thin films directly from inversion of the exact equations for the normal incidence reflectance and transmittance of a multi-layer. The method, which may be described as a local quadratic fitting procedure, is designed to exploit the continuity of the complex index of refraction in wavelength in order to avoid the pitfalls associated with the fact that the exact equations do not possess unique solutions for n and k given R and T at a particular wavelength.

The method is described in sections II and III with the computational details emphasized in the latter section and is applied to reflectivity and transmission data generated from classical dispersion theory as well as to data measured upon thin films of selenium. The results are compared with those from other approaches and the utility and accuracy of the computational technique discussed.

II. Basic Formalism

The optical properties of plane parallel stratified media are easily handled by the characteristic matrix method[5-10]. A homogeneous medium of thickness z with complex refractive index $\hat{n}$, has a characteristic matrix $\hat{M}(z)$, for light of propagation number k, of the form

$$\hat{M}(z) = \begin{pmatrix} \cos(k\hat{n}z\cos\theta) & -\frac{i}{\hat{p}}\sin(k\hat{n}z\cos\theta) \\ -i\hat{p}\sin(k\hat{n}z\cos\theta) & \cos(k\hat{n}z\cos\theta) \end{pmatrix} \qquad (1)$$

in which θ is the angle of incidence upon the medium and

$$p = \sqrt{\hat{\varepsilon}} \quad \cos\theta = \hat{n} \cos\theta \tag{2}$$

for a medium of dielectric function $\hat{\varepsilon}$ and magnetic permeability $\mu = 1$. The characteristic matrix of a multilayer of total thickness, D with N media is of the form

$$\hat{M}(D) = \hat{M}_1(z_1)\,\hat{M}_2(z_2) \ldots \hat{M}_N(z_\ell) \tag{3}$$

in which

$$z_1 + z_2 + \ldots z_\ell = D.$$

If the elements of the 2 x 2 matrix $\hat{M}$ (D) are given in the array,

$$\hat{M}(D) = \begin{pmatrix} m_{11} & m_{12} \\ m_{21} & m_{22} \end{pmatrix} \tag{4}$$

then the complex transmission and reflection coefficients are

$$r = \frac{(m_{11} + m_{12}\,p_\ell)\,p_1 - (m_{21} + m_{22}\,p_\ell)}{(m_{11} + m_{12}\,p_\ell)\,p_1 + (m_{21} + m_{22}\,p_\ell)}$$

$$t = \frac{2p_1}{(m_{11} + m_{12}\,p_\ell)\,p_1 + (m_{21} + m_{22}\,p_\ell)} \tag{5}$$

where 1 and ℓ are indices referring to the first and last (semi-infinite) media. For normal incidence ($\cos\theta_1 = \cos\theta_2 = \ldots = \cos\theta_\ell = 1$) on non-magnetic media $p_i = n_i$. Thus, given the complex index of refraction for each medium, we

can easily obtain

$$T = n_\ell/n_1 \ |t|^2$$
$$R = |r|^2 \qquad (6)$$

the reflectance and transmittance of the multi-layer. For the case of an absorbing film of thickness z_1, on a dielectric slab of thickness z_2, embedded in a medium with $\hat{n}_1 = 1 = \hat{n}_\ell$ we can write

$$M\ (z_1 + z_2) = M_1\ (z_1)\ M_2\ (z_2).$$

In the study made in this paper the dielectric is quartz and its optical properties are well known in the region of interest. By matrix multiplication we can obtain the M_{ij} as functions of $k = 2\pi/\lambda$, and $\hat{n} = n + k\ K$, the unknown complex refractive index of the material. We assume here that the thicknesses, z_2 of the substrate, and z_1, of the film, can be accurately determined independently by, e.g., interferometric or mechanical means, and, if not, by the methods discussed in sec. III. If it were possible to invert equs. (6) for n and K, the problem would be completed. A study of that possibility leads to the conclusion that for a given $T_{obs}(\lambda)$ and $R_{obs}(\lambda)$, from experiment, more than a single set of $n(\lambda)$ and $K(\lambda)$ can be found. Thus the inverted multilayer problem does not have a unique solution in $\hat{n}(\lambda)$. Our aim is to overcome this difficulty by exploiting the fact that the solution path $\hat{n}(\lambda)$ in the complex $\hat{n}$-plane must be continuous in λ and that a approximately correct unique solution can be obtained for $\hat{n}(\lambda)$ in some absorbing region such that interference and multiple reflections are of negligible importance. This provides a unique initialization for $\hat{n}(\lambda) = n(\lambda) +$

i $k(\lambda)$. Our procedure is to generate solutions for each successive wavelength point using the solution for the last point as an initial estimate. The details of the technique are given in the next section.

III. Computational Technique

It is not possible to analytically invert the equations for normal incidence transmissivity and reflectivity,

$$\begin{aligned} T_{obs}(\lambda) &= T(n, k, \lambda) \\ R_{obs}(\lambda) &= R(n, k, \lambda) \end{aligned} \tag{7}$$

to obtain

$$\begin{aligned} n(\lambda) &= n(T_{obs}, R_{obs}, \lambda) \\ k(\lambda) &= R(T_{obs}, R_{obs}, \lambda) \end{aligned} \tag{8}$$

and, therefore, the procedure for solving (7) must be one of numerical interpolation. Such a procedure is known to lead to multiple solutions and hence it is necessary to choose from these the correct solution. There apprears to be no absolute criterion for electing the appropriate solution at a particular wavelength.

In order to invert these equations for a given λ, a local quadratic approximation to the exact equations is made. If some initial estimate of $n(\lambda)$ and $k(\lambda)$, say n_o and k_o is available then in some rectangular region, Ω, sufficiently

small and centered at (n_0, k_0) in the n-k plane we may write

$$T(n, k, \lambda) \cong C_1 n^2 + C_2 k^2 + C_3 nk + C_4 n + C_5 k + C_6$$
$$R(n, k, \lambda) \cong C_7 n^2 + C_8 k^2 + C_9 nk + C_{10} n + C_{11} k + C_{12} \quad (9)$$

If we now choose 6 (non-collimar) points in Ω and evaluate $R(n,k,\lambda)$ and $T(n,k,\lambda)$ at each of these using the exact characteristic matrix method, we can invert (9) to obtain the twelve constants above.

In Ω we also have

$$\delta T = (2C_1 n_0 + C_3 k_0 + C_4)\ \delta n + (2C_2 k_0 + C_3 n_0 + C_5)\ \delta k$$
$$\delta R = (2C_7 n_0 + C_9 k_0 + C_{10})\ \delta n + (2C_8 k_0 + C_9 n_0 + C_{11})\ \delta k \quad (10)$$

We can define,

$$\Delta T = T_{exp}(\lambda) - T(n_0, k_0, \lambda)$$
$$\Delta R = R_{exp}(\lambda) - R(n_0, k_0, \lambda) \quad (11)$$

in which T_{exp} and R_{exp} are the observed reflectivity and transmission at wavelength λ. If we choose $\delta n = N^* - N_o$ and $\delta R = R^* - R_o$ then we can equate ΔT and δT and ΔR and δR invert (10) above to obtain n^*, R^* which are improved estimates of $n(\lambda)$ and $k(\lambda)$. If $T_{exp} - T(n^*, k^*, \lambda)$ and $R_{exp} - R(n, k, \lambda)$ are not sufficiently small then we take n^* and k^* as new initial estimates and repeat the process, by setting $n_0 = n^*$ and $k_0 = k^*$. Normally we have found that 3 to 6 cycles are required at a given wavelength (provided the initial n_0 and k_0 are well chosen) to obtain

$$1 - \frac{R\ (n^*,\ k^*,\ \lambda)}{R_{exp}\ (\lambda)} \quad + \quad 1 - \frac{T\ (n^*,\ k^*,\ \lambda)}{T} \quad \leq \quad 10^{-7} \qquad (12)$$

Once we have obtained a value of n* and k* satisfying this criterion we move to the next wavelength point using n* and k* as the initial estimate for $n_0\ (\lambda + \Delta\lambda)$, $k_0\ (\lambda + \Delta\lambda)$. The size of the rectangle Ω has been found not to be critical if the mesh size in λ is chosen small enrough and we typically choose Ω to be a square with sides less than 10^{-5}.

In order to initiate the entire procedure, we must obtain some independent initial estimate of n and k at some value of the wavelength. If we initiate the calculation in the region in which the absorbance, R + T, is low and interference maxima and minima are present we may estimate n from the location of these interference maxima and minima or from the magnitude of the reflectivity maxima [7] from the equation

$$n^2 = n_0\, n_s\, \frac{1 + \sqrt{Rm}}{1 - \sqrt{Rm}} \qquad (13)$$

where in most cases $n_0 = 1$. On the other hand we may initiate the calculation in the shorter wavelength region for which interference is no longer observable and the reflectivity and transmission may be evaluated from multiple <u>intensity</u> reflections. Then

$$k = \alpha\lambda/4\pi$$

$$n = \frac{1 + R}{1 - R} + \sqrt{\frac{4R}{(1-R)^2} - k^2} \qquad (14)$$

where

$$\alpha = \frac{1}{d} \log \left[\frac{(1 - R)^2}{2T} + \sqrt{\left[\frac{(1 - R)^2}{2T} \right]^2 + R^2} \right] \qquad (15)$$

d being the thickness of the film. These equations are precisely correct only for a free-standing film and if necessary should be modified to account for the presence of the substrate as has been done by Bennett et. al.

We have found it more reliable to calculate an initial value for n from the interference in the long wavelength region and to simply assign k a small initial value of about 10^{-3} in most practical cases. Fortunately, the program, as we shall indicate in the next section, quickly converges toward an excellent estimate of n and k allowing considerable latitude in the starting values of n and k.

IV. Results and Discussion

We have subjected our procedure to two tests. In the first place we have generated by computer reflectivity and transmission data on thin films whose n and k are those from classical dispersion theory for a dilute system of charged harmonic oscillators. With suitable choices of the parameters upon which n and k depend, we can simulate systems which either have large spectral ranges with observable interference or in which interference is not observed due to high absorption. This approach has several advantages. First of all, we can test our procedure in the case that R and T and d, the film thickness, are known with precision and for which exact initial estimates of n and k can be made. Fig. 1 shows such a simulated R and T displaying marked interference, while Fig. 2 shows R and T in a region of high absorption and shows no interference. Our procedure

reproduces both the correct n and k exactly to a large number of significant figures, in each of these regions. We conclude, therefore, that if experimental reflectivity and transmission data of very high precision were available, if the thickness of the film were known with sufficient accuracy, and if a precise initial estimate of n and k could be obtained, our procedure is capable of producing exact results. In practice this will not be the situation and one or more of the above conditions will not be satisfied. We have studied the influence of introducing arbitrary errors into the experimental data, i.e., into R and T. These errors are generated by a random number algorithm. Our procedure is stable, i.e,, the solutions $n(\lambda)$, $k(\lambda)$ remain close to the correct solutions for random errors in both R and T up to 1%. If the errors are larger than this correct solutions may not be obtained. An example of a solution which diverges from the correct solution is illustrated in Fig. 2. If the error in R and T which we introduce is sufficiently large and if the solutions are being generated in a spectral region in which $\frac{dn}{d\lambda}$ and $\frac{dk}{d\lambda}$ are large in absolute magnitude the solution will often diverge from the physically correct one as does n' in this figure. A reasonably careful study of this kind of behavior has led us to conclude that we can tolerate errors of up to 1 or 2 % in R and T over the region below the absorption edge but that R and T should be accurate to ½% in the absorbing region. We have also studied the influence of inaccuracies in the initial estimates of n and k and of the film thickness. The values of n and k may be inaccurate by as much as 25% providing the thickness is known accurately. The solutions converge virtually immediately to the correct solution, i.e., in the computation for the very first wavelength. The difficulties with inaccurate knowledge of the film thickness are the most problematical. In

our study of the simulated data on films we found that errors of greater than a ½% in the thickness estimate for a film of 5μ led to serious instability in the values of n and k obtained from the procedure. Even smaller errors in the film thickness may introduce oscallations about the correct values into the computed n and k.

FIG. 1

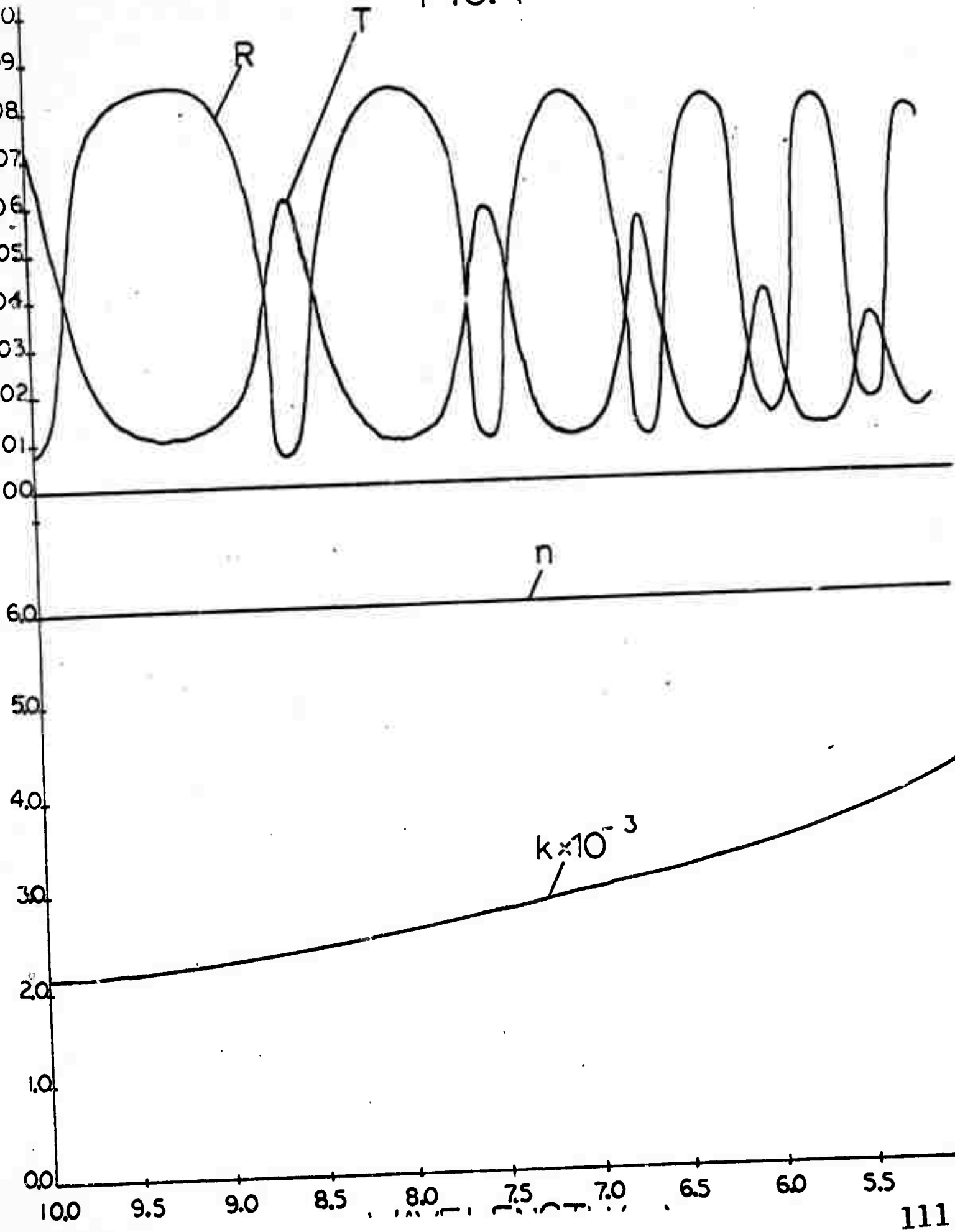

FIG. 2

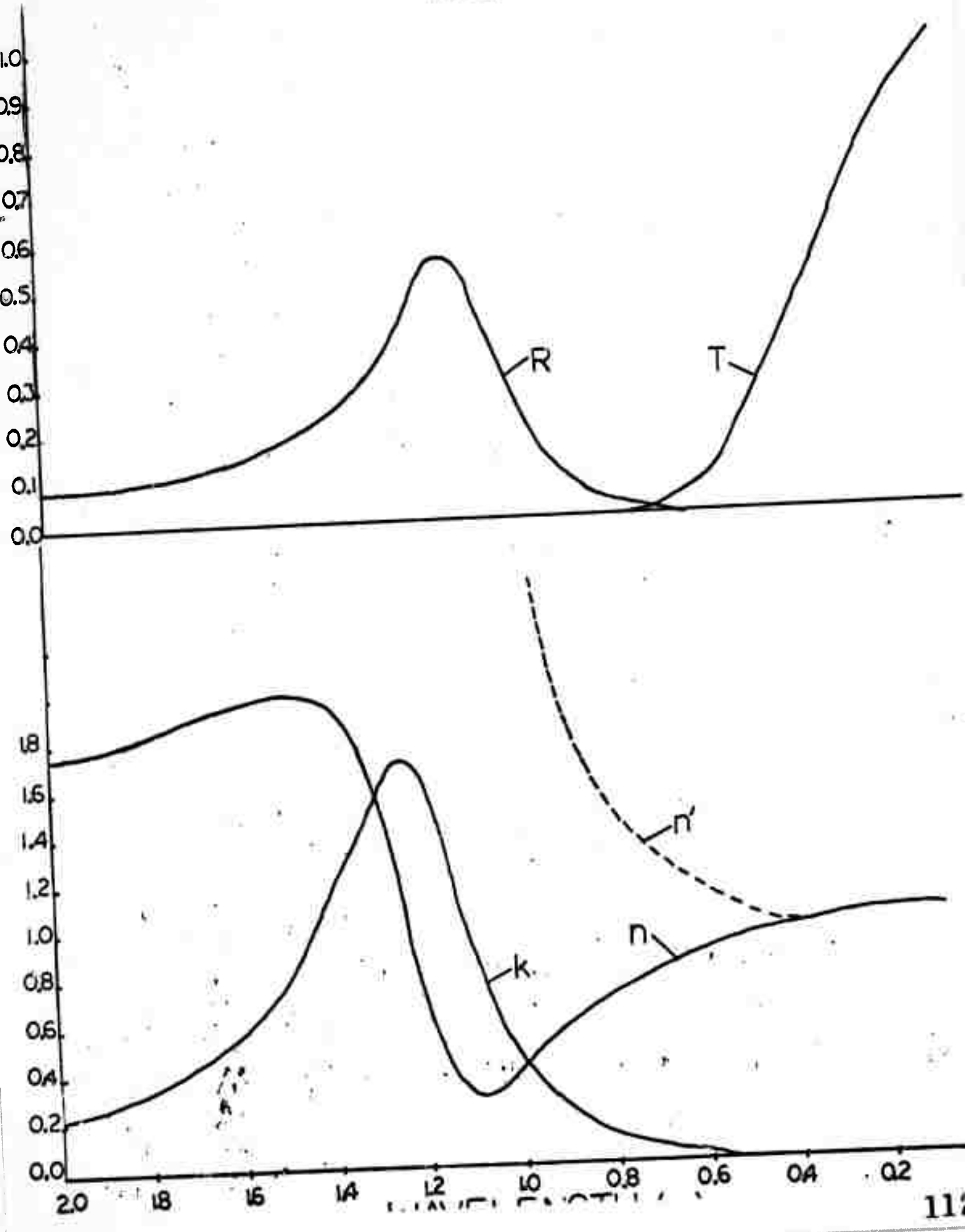
1.0
0.9
0.8
0.7
0.6
0.5
0.4
0.3
0.2
0.1
0.0
R
T
1.8
1.6
1.4
1.2
1.0
0.8
0.6
0.4
0.2
0.0
n'
n
k
2.0
1.8
1.6
1.4
1.2
1.0
0.8
0.6
0.4
0.2

Appendix G

A METHOD FOR DETERMINING PHOTOCONDUCTIVE RESPONSE TIMES*

Z. Hurych, Department of Physics
Northern Illinois University, DeKalb, Illinois 60115

A standard method of measuring ac photocurrents which employs chopped light, can be easily modified to yield also the photoconductive response time τ_o. If a photoconductor with response time τ_o is illuminated by symmetrical square wave pulses of frequency f, the first harmonic frequency of the photocurrent is delayed with respect to the exciting radiation by a phase ϕ_o, where

$$tg\ \phi_o = 2\pi f\tau_o \quad . \tag{1}$$

This phase shift ϕ_o can be easily measured using a lock-in amplifier as a phase sensitive detector. In order to obtain good accuracy in ϕ_o, f must be chosen of the order of $1/\tau_o$. This paper indicates how additional phase changes due to the electronic equipment, can be eliminated.

In ac photoconductivity measurements, the exciting light pulses are usually produced by a light chopper, where the same blade chops the light illuminating the sample and also the light from an auxiliary light source which is placed in front of a photosensitive detector P. P thus provides a signal coherent with the exciting light, which is used as a reference for the lock-in amplifier. In photocurrent measurements, the phase of the lock-in amplifier is adjusted to the value ϕ_1 for maximum mixer output.

---

* This research was supported by the Advanced Research Projects Agency of the Department of Defense and was monitored by the Army Research Office, Durham, under Contract No. DA-ARO-D-31-124-70-G77.

Clearly,

$$\phi_1 = \phi_0 + \phi_E + \phi_G + \phi_P \quad , \tag{2}$$

where the subscripts 0,E,G,P are symbols for the phase shifts due to the sample, electronic equipment, geometry of the light chopper and the photodetector P with its electronic circuit, respectively.

The sample is subsequently replaced by another "reference" photodetector R, with a very short response time τ_R such, that the corresponding phase delay

$$\phi_R = \text{arctg } 2\pi f\tau_R \tag{3}$$

is much smaller than ϕ_0. Then without any change in electronic circuits or geometry of the equipment, the phase of the lock-in amplifier is again adjusted to a value ϕ_2 for maximum mixer output, so that according to eq. (2)

$$\phi_2 = \phi_R + \phi_E + \phi_G + \phi_P \tag{4}$$

From (2) and (4) we obtain

$$\phi_0 = (\phi_1 - \phi_2) + \phi_R \quad , \tag{5}$$

and the photoconductive response time τ_0 is then determined from eq. (1). If $\tau_R \ll \tau_0$, ϕ_R in eq. (5) can be neglected.

A trigonal Se single crystal was used to compare this technique with the "graphical" method, where τ_0 is determined from the decay of the photocurrent pulses observed on an oscilloscope. Very good agreement was obtained for τ_0 in the range 3 msec up to 100 msec using a PAR HR-8 lock-in amplifier and f = 17 cps. As the "reference" photodetector R, a TI planar silicon light sensor LS 600 with a response time of 15 μsec was used.

Due to the use of a lock-in amplifier, the method described above can be used for measurements of τ_0 even in the case of photosignals well below

the noise level. Thus this method is applicable to very poor photoconductors, and can be applied to good photoconductors at very low light levels or low drift fields when one wants to eliminate space charge effects.

A few errors are associated with this method; for example, eq. (1) neglects the finite width d (usually a few mm) of the illuminated part of the sample. This introduces an error $\Delta\phi_o$ of the order of a few percent as $\Delta\phi_o \approx d/L$, where L (typically 10-20cm) is the length of the segment of the chopping blade corresponding to one light pulse. Another source of error ($\sim$1%) is the reproducibility of the phase shift dial of the lock-in amplifier. (Since this method measures the difference $\phi_1 - \phi_2$, an absolute accuracy of the phase shifter is not important.) Finally, the value τ_o determined from eqs. (1) and (5) is the exact response time only if the rise and fall of the photocurrent are symmetrical and obey the $(1-e^{-t/\tau_o})$ or e^{-t/τ_o} law, respectively, otherwise τ_o would be an "effective" or average response time.

The author would like to thank Dr. C. Wood for valuable discussions.

Appendix H

OPTICAL AND TRANSPORT PROPERTIES OF AMORPHOUS Sb_2Se_3*

C. Wood, Z. Hurych and J. C. Shaffer
Physics Department, Northern Illinois University
DeKalb, Illinois 60115

Abstract

The optical absorption, reflectivity, electrical conductivity, photoconductivity, and photoemission have been studied in amorphous films of Sb_2Se_3. The films were prepared by coevaporation thus allowing strict control of composition, in contradistinction to previous methods of preparation. Comparison with data on Sb_2Se_3 single crystals show marked similarity of properties and in particular, show that the forbidden energy gap values closely correspond. Furthermore, in contrast to published data, on similar amorphous systems such as As_2Te_3[1]), the structure at the band edges appears to be quite sharp, thus showing no evidence of a mobility gap.

1. Materials Preparation

Throughout the work described in this contribution the intent has been to compare the properties of amorphous thin films of antimony selenide with crystalline Sb_2Se_3. Much effort has been made to ensure that the composition of the films can be made closely approximate to that of the crystal and that the films are, indeed, amorphous. Thus a brief description of the preparation and the structural and compositional investigation of the films is in order.

* This research was supported by the Advanced Research Projects Agency of the Department of Defense and was monitored by the Army Research Office Durham, under Contract No. D-ARO-D-31-124-71-G132.

The films were prepared by the technique of coevaporation onto fused quartz substrates. Separate quartz crystal oscillators monitored and controlled the rates of deposition of Sb evaporated from an electron-beam gun and Se from a resistance heated crucible, thus allowing a high degree of control of composition of the resultant films. Films can be obtained with a variety of compositions, and though the principal interest herein is with films of composition near to that of the stoichiometric crystal, we report some results on other samples.

The degree of order of these films has been checked by electron diffraction[2]) and the stoichiometric films were found to be amorphous to the resolution of this technique (~20 Å). Mossbauer spectroscopy has been carried out[3]) on both crystalline and amorphous samples and indicates that the short-range order of Sb in the amorphous films differs from that in the crystals. Differential thermal analysis of the samples allowed a determination of a crystallization temperature, of ~180°K; however, no softening temperature (T_g)has been determined due to the small mass of the samples. The composition of the samples has been determined by both micro-probe analysis and by conventional X-ray emission methods. The compositions are probably accurate to the order of 1 at. %.

2. The Energy Band Gap

It has been known for some time that Sb_2Se_3 is a semiconducting compound with a band gap 1.0-1.2eV at room temperature[4]). The photoconductivity spectra of amorphous and polycrystalline films have been

measured[4]) and, from the threshold, the band gap of the amorphous samples was found to be 1.6eV and that of the polycrystalline samples 1.3eV. As will be pointed out below, these results are not consistent with those reported here and may be explained by wide compositional deviations in the samples used in previous work.

In Fig. 1 the absorption constant, determined from reflectivity and transmission measurements, of a thin (250 Å) and thick (5.8μ) film of composition approximating that of the crystalline material is compared with single crystal data using unpolarized light. Similar data for an Sb excess and a Se excess film are also displayed. The absorption constant in the region of the edge shows an $\alpha^{\frac{1}{2}}$ dependence on photon energy, for the single crystal. It is apparent from this dependence and the reflectivity curves that the transition giving rise to the edge at ∿1.1eV in the crystal is a direct one with a superimposed indirect tail[5]). The absorption coefficient for the amorphous films exhibits no simple relationship with energy.

The resistivity of the stoichiometric amorphous films is comparable to that of the crystal. Preliminary values of the thermal activation energies computed from the slopes of the resistivity versus temperature curves are ∿1.0eV and ∿0.5eV for the crystal and amorphous films, respectively. The former value is in good agreement with published values[6]) and with the optical data. For the films, a value of approximately one-half the estimated band gap appears to be commonly found for amorphous materials[7]).

In Fig. 2 the photocurrent response spectra of a crystalline sample and several amorphous films of different compositions Sb_xSe_y are shown. The photoconductive activation energy ($\lambda_{\frac{1}{2}}$)[8]) of the crystalline sample and for the stoichiometric amorphous film of composition Sb_2Se_3 are 1.1eV and 1.3eV, respectively. There appears to be no evidence of band tailing in the spectral distribution curves.

3. Visible to Ultraviolet Optical Properties

The near normal incidence reflectivity of the natural cleavage plane of Sb_2Se_3 to unpolarized light and for light polarized ||a and ||c orientations is shown in Fig. 3 for the spectral region 0eV to 11.0eV. The data is less reliable in the unpolarized light case because of a wavelength-dependent horizontal polarizing component in the Cary 14-R spectrophotometer[9]). The data exhibits a broad region of high reflectivity extending from about 1.0eV to about 7.0eV. In addition much individual structure associated with critical points may be discerned in this region which is in essential agreement with the data of Shutov et al[5]). The front surface reflectivity of an amorphous film of Sb_2Se_3, 5.8μ thick, is also presented in Fig. 3 over the same spectral region. For the particular film there is no measurable transmission in this range and therefore, the measured reflectivity can be compared to that of the bulk single crystal. The reflectivity was found to be somewhat lower than that of the single crystal in agreement with results on other amorphous materials[10]). In Fig. 4 we show ε_1 and ε_2 for the crystal and film as obtained from a Kramers-Kronig analysis of

the reflectivity data. The technique for Kramers-Kronig analysis has been reported elsewhere[11]. It can be seen that $\varepsilon_2(\omega)$ for the film and for the crystal differ in detail although their overall behavior is quite similar. Note that in either case the region of high absorption as reflected in $\varepsilon_2(\omega)$ extends from about 1eV to about 4.5eV indicating rather narrow bands are responsible for this region of the spectra.

4. Photoemission

The results of some preliminary photoemission measurements are presented in Fig. 5. The photoelectric yield (Y) and the energy distribution curves (EDC) of photoemitted electrons were measured and compared for single crystalline and amorphous Sb_2Se_3. The measurements were performed in vacuum in the range 10^{-10} torr. The single crystals were cleaved in the natural cleavage plane ($\perp$b) in situ. The amorphous films of composition Sb_2Se_3 were prepared in the bell-jar apparatus and transferred under a dry inert atmosphere to the photoemission chamber and, therefore, because of this exposure, the data is less reliable. The chamber is being modified to prepare the films in situ.

The values of photoelectric threshold as obtained from the $Y^{1/3}$ vs. $h\nu$ extrapolation[12] were 5.7eV for films and 6.4eV for crystals.

From the EDC which represent the joint density of electronic states (JDOES) between the valence and conduction bands, an attempt was made to construct the effective valence and conduction band density of states. In the case of the amorphous material, the JDOES could be satisfactorily

interpreted in terms of indirect transitions, i.e., no pronounced dependence of matrix elements on k (but possibly a dependence on hν), for photon energies of 7eV to 11.8eV, with no evidence of sharp structure in the valence or conduction band. For the single crystal, direct transitions were dominant together with slight additional structure which could be explained in terms of indirect transitions, with constant matrix elements due probably to a localized or flat E vs. k band. A more detailed assignment of these transitions at present is a difficult task as the band structure calculations are not available, and the results of group theory selection rules have been applied so far only to the region of the interband minimum, which is inaccessible to photoemission measurements due to the work function of investigated materials.

5. Conclusions

In summary we find marked similarities between the properties of single crystal and amorphous Sb_2Se_3 and little evidence of extensive band tailing into the forbidden band gap as one would expect to find from a mobility gap consideration.

Acknowledgements

The authors wish to acknowledge the valuable assistance of the following graduate students: R. Afshar, D. Buczek, L. Gilbert, R. Mueller, B. Van Pelt and C. Wang.

References

1) K. Weiser and M. H. Brodsky, Phys. Rev. B 1 (1970) 791.

2) B. Krause, to be published.

3) S. L. Ruby, L. R. Gilbert and C. Wood, Bull. Am. Phys. Soc. 16 (1971) 303.

4) N. Kh. Abrikosov, V. F. Bankina, L. V. Poretskaya, L. E. Shelimova and E. V. Skudnova, Semiconducting II-VI, IV-VI and V-VI Compounds (Plenum Press, New York, 1969) 187.

5) S. D. Shutov, V. V. Sobolev, Y. V. Popov and S. N. Shestatskii, Phys. Stat. Sol. 31 (1969) K23.

6) M. V. Kot and S. D. Shutov, Trudy po fizike poluprovodnikov, Kishinevskii Universitet 1 (1962) 47.

7) E. A. Fagen and H. Fritzsche, J. Non-Crystalline Solids 2 (1970) 170.

8) T. S. Moss, Photoconductivity in the Elements (Academic Press, New York, 1952).

9) M. E. Hill, A. L. Olson, and L. W. Nichols, Appl. Optics 7 (1968) 1437.

10) J. Tauc, Optical Properties of Solids, Ed. S. Nudelman and S. S. Mitra, (Plenum Press, New York, 1969).

11) J. C. Shaffer and R. Afshar, Bull. Am. Phys. Soc. 16 (1971) 374.

12) R. C. Eden, Ph.D. Thesis, Stanford University, (1967) 249.

Captions

Fig. 1 The optical absorption spectra of single crystal Sb_2Se_3 and amorphous films of Sb_xSe_y.

Fig. 2 The photoconducting spectral response of single crystal Sb_2Se_3 and amorphous films Sb_xSe_y.

Fig. 3 Near-normal incidence optical reflectivity spectra of single crystal and amorphous Sb_2Se_3.

Fig. 4 Real (ε_1) and imaginary (ε_2) parts of the dielectric constants of single crystal and amorphous Sb_2Se_3.

Fig. 5 Photoemission energy distribution N(E) versus energy (E) above the top of the valence band of single crystal and amorphous Sb_2Se_3.

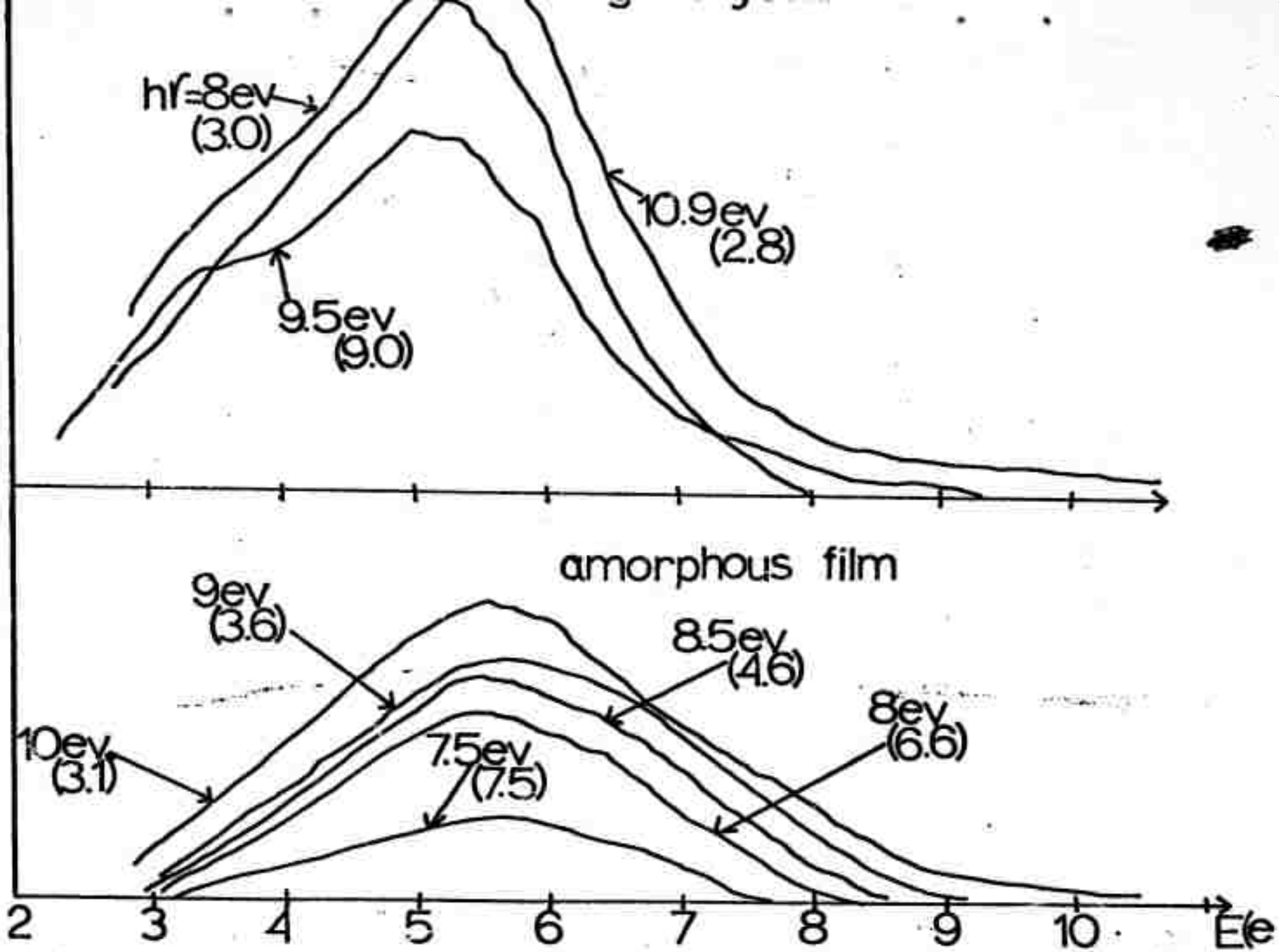
hν=8ev
(3.0)
10.9ev
(2.8)
9.5ev
(9.0)
amorphous film
9ev
(3.6)
8.5ev
(4.6)
8ev
(6.6)
10ev
(3.1)
7.5ev
(7.5)
2
3
4
5
6
7
8
9
10
E(e

FIG. 1.

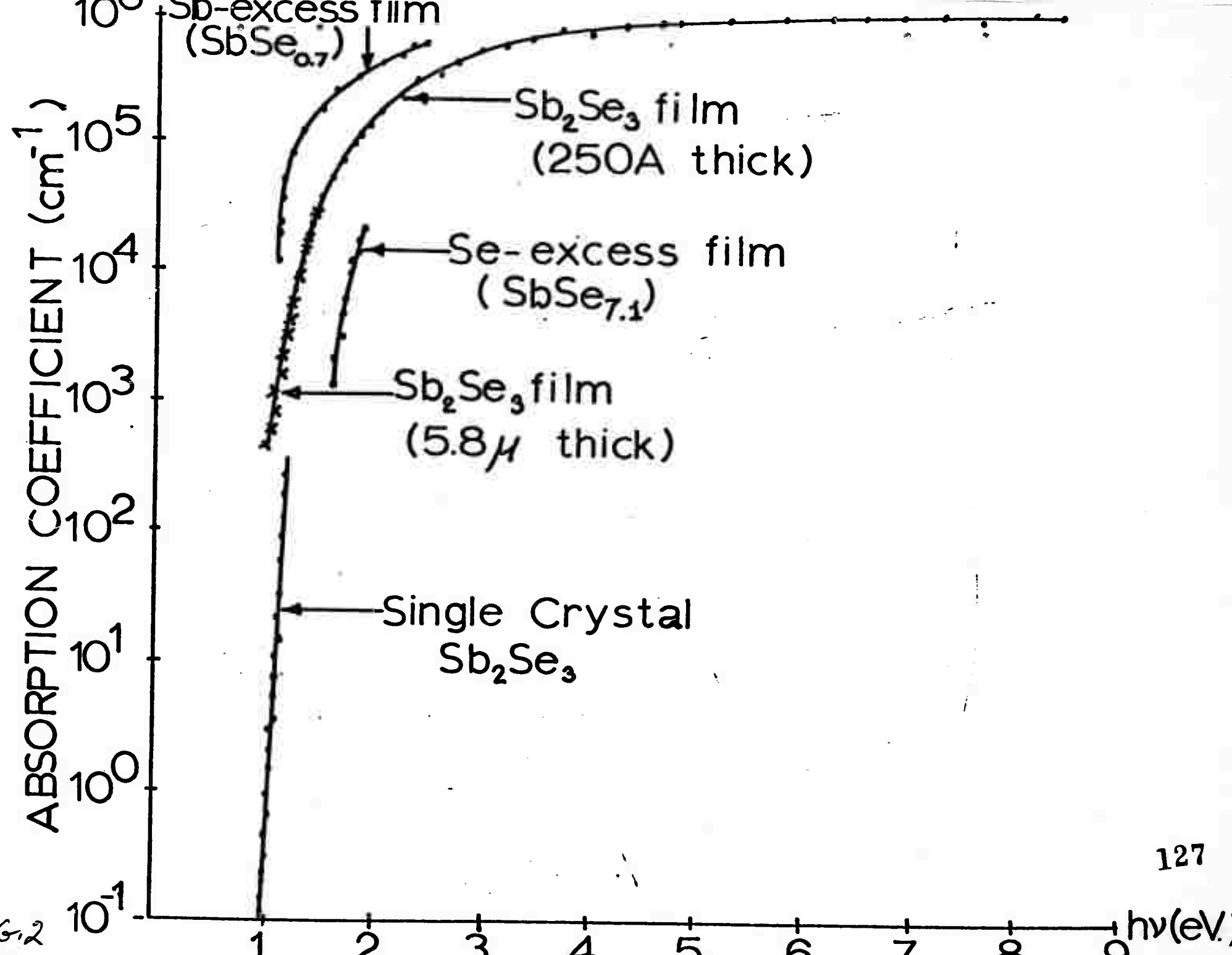
Sb-excess film
(SbSe0.7)
Sb2Se3 film
(250A thick)
Se-excess film
(SbSe7.1)
Sb2Se3 film
(5.8μ thick)
Single Crystal
Sb2Se3
ABSORPTION COEFFICIENT (cm-1)
10^0
10^5
10^4
10^3
10^2
10^1
10^0
10^-1
1
2
3
4
5
6
7
8
9
hν(eV)

FIG.2

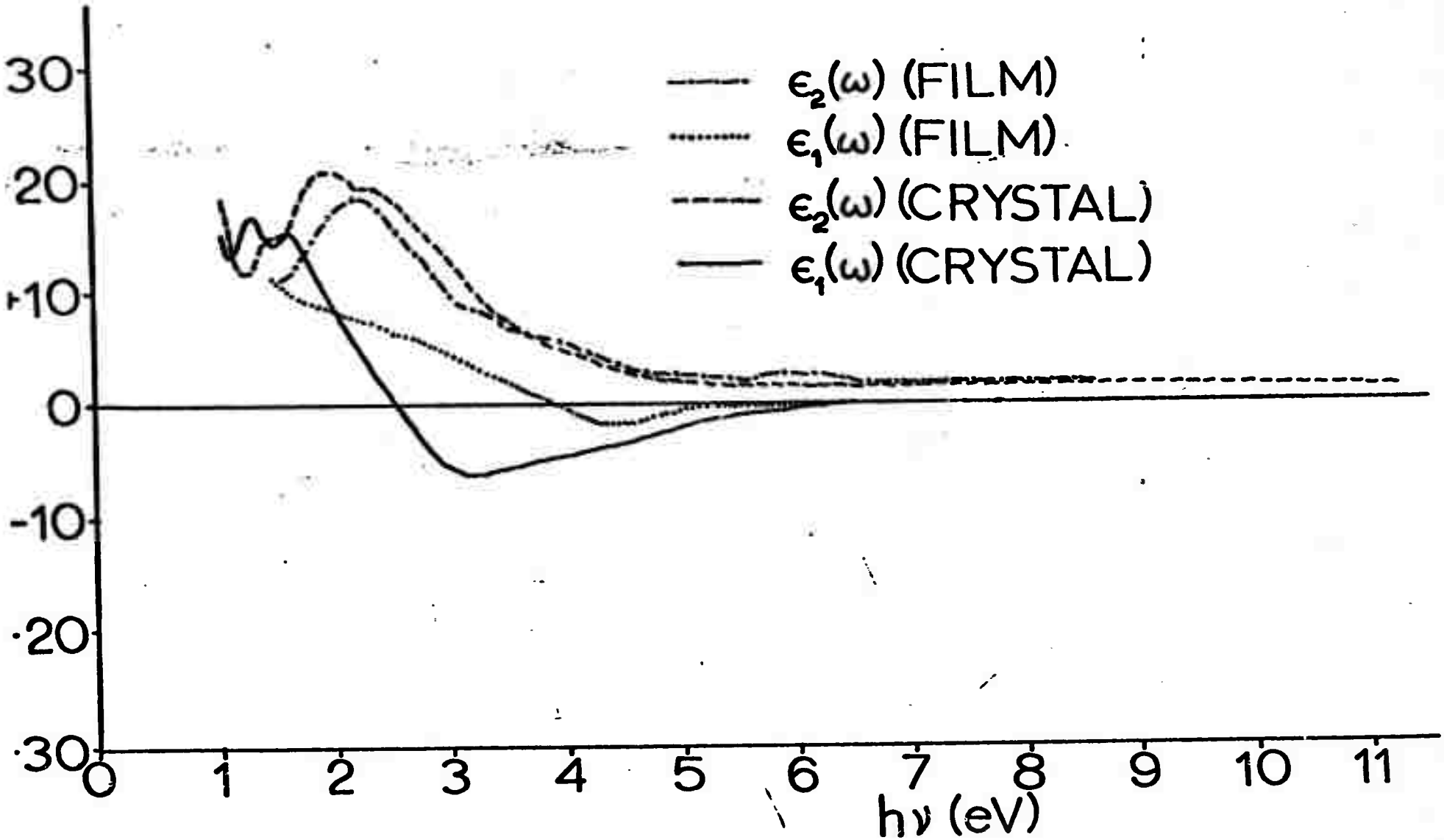
30
20
10
0
-10
-20
-30
0
1
2
3
4
5
6
7
8
9
10
11
hν (eV)
$\epsilon_2(\omega)$ (FILM)
$\epsilon_1(\omega)$ (FILM)
$\epsilon_2(\omega)$ (CRYSTAL)
$\epsilon_1(\omega)$ (CRYSTAL)

FIG. 3

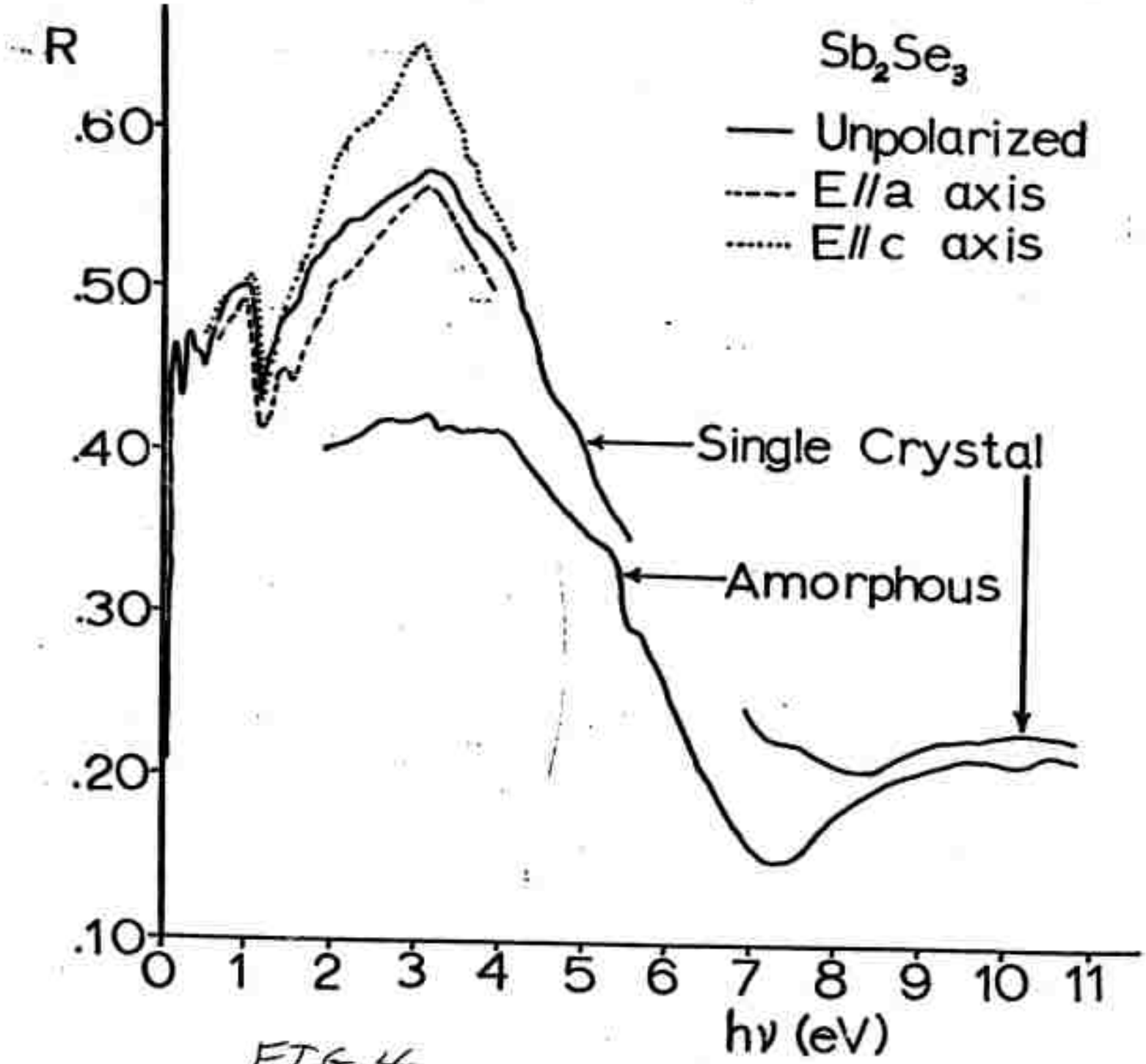
R
.60
.50
.40
.30
.20
.10
0 1 2 3 4 5 6 7 8 9 10 11
hν (eV)
Sb_2Se_3
— Unpolarized
---- E//a axis
..... E//c axis
Single Crystal
Amorphous

FIG. 4

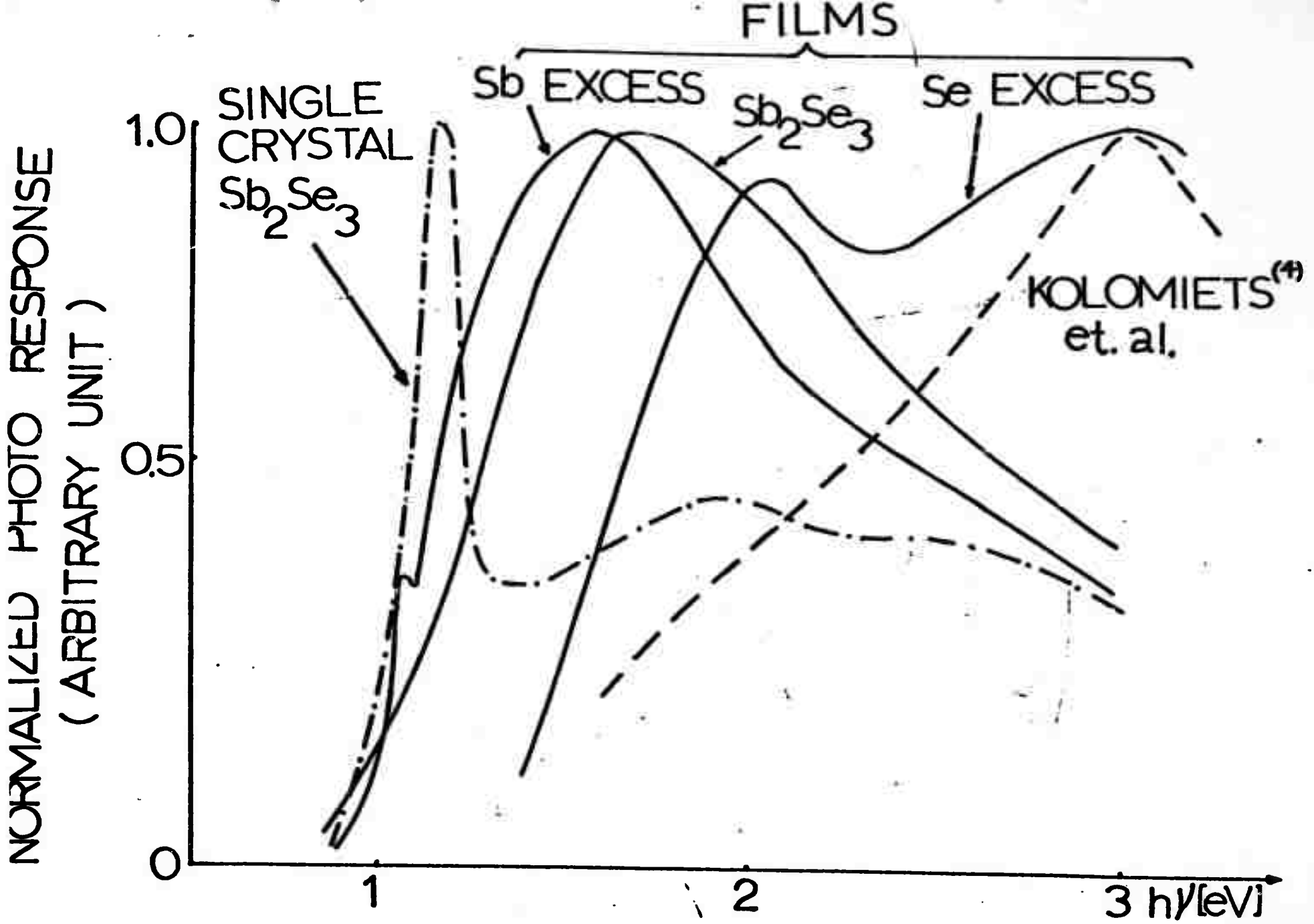
FILMS
Sb EXCESS
Se EXCESS
SINGLE CRYSTAL Sb_2Se_3
Sb_2Se_3
KOLOMIETS[4] et. al.
NORMALIZED PHOTO RESPONSE (ARBITRARY UNIT)
1.0
0.5
0
1
2
3
hν[eV]

FIG. 5

Appendix I

Photoconductivity in Amorphous $Sb_{1-x}Se_x$ Layers*

Z. Hurych, R. Mueller, C. C. Wang and C. Wood
Department of Physics
Northern Illinois University
DeKalb, Illinois 60115

Abstract

The photoconductive spectral response of amorphous $Sb_{1-x}Se_x$ films as a function of composition shows that an excess of Sb or Se causes a shift toward smaller or larger activation energies, respectively, when compared with stoichiometric Sb_2Se_3 films ($x = 0.60$). This shift agrees with the shift of the optical absorption edge. The similarity between the sharpness of the photoconductive onset and optical absorption edge of amorphous and crystalline Sb_2Se_3 is not inconsistent with the presence of localized states inside the pseudogap. An estimate of the density of states at the quasi-Fermi level for amorphous Sb_2Se_3 gives values of at least 10^4 greater than the single crystal material.

Introduction

Amorphous Sb_2Se_3 is one of the least investigated of the V-VI compound semicondcutors. There exist little experimental data on photoconductivity (1), (2), and there the sample compositions were not well defined. Because of large difference in the vapor pressure of the two constituents, evaporation from a

* This research was supported by the Advanced Research Projects Agency of the Department of Defense and was monitored by the Army Research Office, Durham, under Contract No. DA-ARO-D-31-127-71-G132.

single source of Sb_2Se_3 does not yield stoichiometric Sb_2Se_3 films. Using a controlled co-evaporation procedure we have produced $Sb_{1-x}Se_x$ films in a large range of compositions with x-values from 0.52 up to 0.86, so that the effect of the x-value on photoconductive spectral response and the photosensitivity ($\mu\tau$) could be investigated.

Preparation of Samples

Samples were prepared by co-evaporation of Sb from an electron beam gun and Se from a resistor heater onto room temperature quartz substrates. Two Sloan ONMI II quartz crystal monitors and controllers were used, and the evaporation rate of both Sb and Se separately monitored and recorded on x-t plotters. Gold contacts were evaporated onto the substrates in a separate vacuum system prior to film deposition. Antimony contacts were evaporated onto substrates during the same vacuum cycle before the $Sb_{1-x}Se_x$ films were deposited. The background pressure was $\sim 10^{-8}$ torr. The composition of samples was determined by electron microprobe with an accuracy of ~ 1 at. %. The films were found to be amorphous both by X-ray and electron diffraction (3).

Photoconductivity

Photoconductivity of $Sb_{1-x}Se_x$ films was investigated for various compositions corresponding to the x-values in the range of 0.52 up to 0.86. The spectral dependence of photoconductivity was measured using Baush and Lomb High Intensity Grating Monochromators. Light was mechanically chopped at various frequencies between 16 and 80 cps and the photosignal was synchronously detected using PAR

HR-8 lock-in amplifier. The results are plotted as a change in conductivity per incident photon flux versus photon energy in Fig. 1. This figure clearly shows the strong dependence of the photoconductive spectral response on sample composition. The set of curves in Figs. 1 and 2 is divided by the curve for the stoichiometric Sb_2Se_3 film (x = 0.60) with a photoconductivity activation energy E_a = 1.4 eV as determined by Moss' criterion. It is seen that with increasing Sb content (x < 0.60) the activation energy and the photoconductivity onset move toward lower energy, while the higher Se content (x > 0.60) shifts the response toward higher energies with respect to Sb_2Se_3 film. The effect of composition on the position of the photoconductivity onset was always found to correspond to the change in fundamental optical absorption edge position (4). This dependence of E_a on composition is similar to that of melt-quenched amorphous $Sb_{1-x}S_x$ published by Mostovskii et. al (5). The structure present on the onset edge of some films is due to the optical interference as shown by comparison with the absorptance (Fig. 2). For comparison, Fig. 1 also shows the photosensitivity of single crystalline Sb_2Se_3 with E_a = 1.1 eV.

The lux-ampere characteristics were investigated and were found linear over 2 orders of magnitude. It was difficult to extend these measurements to lower light intensities due to the low photosensitivity of films.

Even though the contacts were carefully shielded from illumination during measurements to avoid any photovoltic effects, some effect of contact material was observed on the spectral response (Fig. 3) when Sb or Au contacts were used. However, we found this contact effect was much weaker than that reported in (2).

The absolute photoconductivity was measured at hν = 1.65 eV. The chopped

light illuminated the sample through a light pipe of known diameter. From the absolute photoconductivity $\Delta\sigma$, the product $(\mu\tau)$ was calculated using a relation

$$\Delta\sigma = \eta q\ (\mu\tau)\ AI_o/th\nu$$

where A is the sample absorptance, t is the sample thickness, q is the electronic charge and I_o is the light flux. The quantum efficiency η was assumed to be one. The light flux was determined using a calibrated thermopile.

The values of the $(\mu\tau)$(τ is the lifetime of excess carriers) were found to be in the range of 6×10^{-10} up to 2×10^{-9} cm^2/V. The value of $(\mu\tau)$ for single crystalline Sb_2Se_3 was found to be 3×10^{-5} cm^2/V.

A direct display of the decay of the photoconductive pulse was generally impossible because the photosensitivity of the films was very low and the signal was often below the noise level. The photoconductive response time was measured from the phase shift between the light pulse and the photoconductive response using a method described in (6). The values of the response time were 10^{-3} up to 10^{-2} sec for films compared to 400 μ sec for single crystal. It should be noted that this method measured the "effective" response time, i.e. those components of the pulse which contribute to the largest area of the pulse. This means that this method cannot resolve the very fast initial rise and fall of the pulse which is found for e.g., for amorphous As_2Te_3 (7) or GeTe (8) and which was associated with the recombination lifetime.

Discussion

The photoconductivity spectral response shows a strong dependence on com-

position which can be used to explain the difference in spectral response between our stoichiometric Sb_2Se_3 films and those reported by Kolomiets et. al. (1), (2). Their films were prepared by evaporation from a source of Sb_2Se_3 which we found produces nonstoichiometric films with composition depending on the temperature of the source and the stage of the evaporation cycle due to preferential evaporation of Se. The discrepancy between their results and ours can therefore be explained by an excess of Se in their samples.

Comparing the spectral response of amorphous with crystalline Sb_2Se_3, one finds no significant difference between the sharpness of the onset for these two different modifications. Even though a diffuse onset of photoconductivity (or of optical absorption) is usually considered as a proof for the existence of localized states in the gap, the presence of a sharp onset does not preclude the existence of these states. The explanation is given by much lower values of matrix elements for electronic transitions between localized and extended states (9), (10). Similarly, sharp onsets of photoconductivity and optical absorption edge were found previously for amorphous Si (11) Ge (12). All these measurements suggest that even though the process of photoconductivity includes both optical and transport properties, the information about the localized states from the photoconductive edge coincides with the optical densities rather than with the densities obtained from electrical or magnetic measurements. It is known (9) that the effective "optical" density of localized states in the gap can be a few orders of magnitude lower than the density obtained from transport measurements.

While from the absolute photoconductivity one can easily obtain the product

($\mu\tau$), the separation of this product into its two constituents has to include some model for transport of carriers. For example, the model proposed by Weisser and Brodsky (7) for amorphous As_2Te_3 assumes that exited carriers move along or just above the "mobility edge", and τ was equated to the carrier lifetime having a value of $<10^{-8}$ sec thus giving mobility values of the order of 0.1 to 1 cm^2/V sec, which is just on the boundary between a localized and delocalized conductivity mechanism. The opposite approach was taken by Kolomiets (13) who associates τ with the response time of $\sim 10^{-3}$ sec, controlled by trapping effects, and completely neglects the initial fast part of the photopulse. The corresponding values of μ are thus in the 10^{-4} to 10^{-3} cm^2/V sec region corresponding to localized mobility. The time 10^{-3} sec then corresponds to the "lifetime" of a hopping carrier between traps.

If we assume a delocalized mobility value of the order 1 cm^2/V sec in our films then, because the ($\mu\tau$) product has values of the order 10^{-9} to 10^{-10} cm^2/V, the recombination lifetime has to be in the range 10^{-9} to 10^{-10} sec. The immediate consequence is that there must then exist recombination centers or deep traps of very large cross-section approximately in the middle of the pseudogap. The order of magnitude of the density of traps can be estimated from following kinetic conditions. The light intensity used corresponds to the generation rate $g \sim 10^{19}/cm^3$ sec averaged over the absorption length. In the steady state condition the density of free carriers n must be $n = \tau.g$, where τ is the free carrier lifetime. Taking the average value of ($\mu\tau$) to be 1×10^{-9} cm^2/V, the lifetime of nonlocalized carriers has a value $\tau \sim 10^{-9}$ sec, yielding $n = 10^{10}/cm^3$. Now trapped carriers of density n_t result in a response time τ_{resp} longer than τ

by the factor $\tau_{resp}/\tau = (n_t + n)/n \sim n_t/n$. In our case $\tau_{resp}/\tau = 10^{-3}/10^{-9} \sim 10^6$, yielding $n_t = 10^{16}/cm^3$. From the total number of trapped carriers n_t we can then estimate the total number of trapping states N_t between the mobility edges assuming that the trapped carriers are in thermal equilibrium with the conduction or valence bands. Even though the trapping states should be thought to be distributed continuously throughout the gap with the density N_t/cm^3 eV, the major part of carriers are trapped at the levels within a slice kT of the quasi-Fermi level E_F^*. The condition of thermal equilibrium then yields (14)

$$\frac{n_t}{n} = \frac{N_t kT}{Nc} e^{E_F^*/kT}$$

with $N_c \sim 10^{19}/cm^3$ being the effective density of states in the conduction band. Because the above equation includes two unknowns (N_t,E_F^*) it is useful to consider E_F^* as a parameter and calculate the corresponding values of N_F^*. This is done in the following Table 1, which clearly indicates that $E_F^* \leq 0.3$ eV, since the density of states inside the gap cannot exceed the band densities. There must exist, also, a lower limit for E_F^* because the very low lifetime 10^{-9} sec requires the existence of recombination centers of rather high concentration which would lie between the quasi-Fermi levels for electrons and holes (assuming equal recombination cross-sections for electrons and holes). Assuming that E_F^* is somewhere in the interval 0.3 eV to 0.5 eV from the non-localized states, we get rather high densities of states (10^{18} up to $10^{21}/cm^3$) deep inside the pseudo-gap.

Similar calculations were performed for single crystalline Sb_2Se_3 comparing again the response time and the internal photosensitivity $\mu\tau$, assuming a mobility

of 45 cm^2/volt sec (15). In this case we found that the density of trapping states at the quasi-Fermi level must be lower by at least a factor of 2×10^4 than that for the amorphous films thus giving values 10^{14} up $10^{16}/cm^3$ eV for crystalline Sb_2Se_3. This fact is of particular importance if we realize that both amorphous and crystalline Sb_2Se_3 exhibit the photoconductive onset of similar sharpness despite quite different values of states inside the gap.

Conclusion

It is shown that for amorphous $Sb_{1-x}Se_x$ films the position of the photoconductive edge coincides with the optical absorption edge and depends strongly on film composition. This edge is located at 1.4 eV for stoichiometric Sb_2Se_3 films. The sharpness of the photoconductive onset for amorphous Sb_2Se_3 is similar to that of single crystal Sb_2Se_3, thus giving no evidence for the band tailing into the pseudogap. On the other hand, the analysis of the photoconductivity kinetics yields much higher density states deep inside the pseudogap, with values $\sim 8 \times 10^{17}$ to 10^{21}/eV cm^3 which are closer to densities of states obtained from transport rather than from optical measurements.

References

1. B. T. Kolomiets, V. M. Lyubin and D. V. Tarkhin, Fit. Tverd. Tela. 1, 899 (1959) [Sov. Phys. Sol. St. 1, 819 (1960)].

2. V. M. Lyubin and V. S. Maidzinskii, Sov. Phys. - Semiconductors 3, 11, 1408 (1970).

3. B. Krause, to be published.

4. R. Mueller and C. Wood, to be published.

5. A. A. Mostovskii, L. G. Timoteeva, and O. A. Timoteev, Sov. Phys. - Solid State 6, 389 (1964).

6. Z. Hurych and C. Wang, to be published in J. of Scient. Instru.

7. K. Weiser and M. H. Brodsky, Phys. Rev. B1, 791 (1970).

8. W. E. Howard and R. Tsu, Phys. Rev. B1, 4709 (1970).

9. H. Fritsche, J. Noncryst. Solids, 6, 49 (1971).

10. J. D. Dow and Y. Y. Hopfield, Proc. of 4th Inter. Conf. on Amorphous and Liquid Semiconductors, Ann Arbor, Michigan, 1971 (to be published).

11. D. T. Pierce, C. G. Ribbing and W. C. Spicer, Proc. of the 4th Intern. Conf. on Amorphous and Liquid Semiconductors 1971 (to be published).

12. T. M. Donovan, W. E. Spicer and J. M. Bennet, Phys. Rev. Lett. 22 1058 (1969).

13. J. Black, E. M. Conwell, L. Seige, and C. W. Spencer, J. Phys. Chem. Solids, 2, 240 (1957).

Table I.

E_F^* [eV] from the band edge	N_t^* [11 eV cm^3]
0.1	8×10^{29}
0.2	1.3×10^{23}
0.3	2.5×10^{21}
0.4	4×10^{19}
0.5	8×10^{17}
0.6	1.3×10^{16}
0.7	8×10^{15}

Figure Captions

Figure 1 Relative photosensitivity of $Sb_{1-x}Se_x$ films.

a) Se rich films.

b) Sb rich films.

Figure 2 Relative photoresponse and optical absorptance A for $Sb_{1-x}Se_x$ film with $x = 0.524$.

Figure 3 Effect of Sb or Au contacts on the spectral photoconductive response of $Sb_{1-x}Se_x$ films.

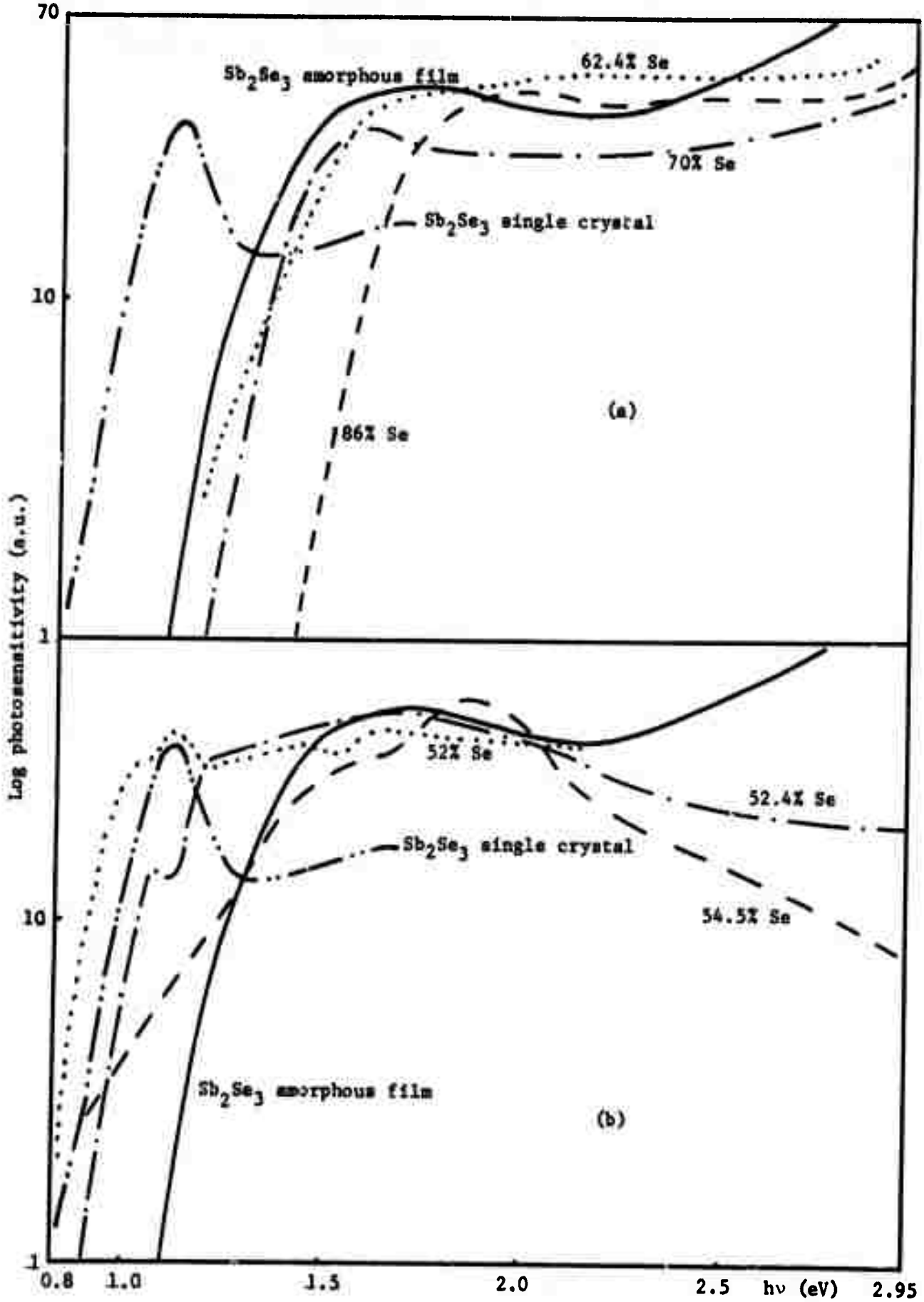
70
10
1
Log photosensitivity (a.u.)
Sb_2Se_3 amorphous film
62.4% Se
70% Se
Sb_2Se_3 single crystal
86% Se
(a)
52% Se
52.4% Se
Sb_2Se_3 single crystal
54.5% Se
Sb_2Se_3 amorphous film
(b)
0.8
1.0
1.5
2.0
2.5
hν (eV)
2.95

FIG. 1

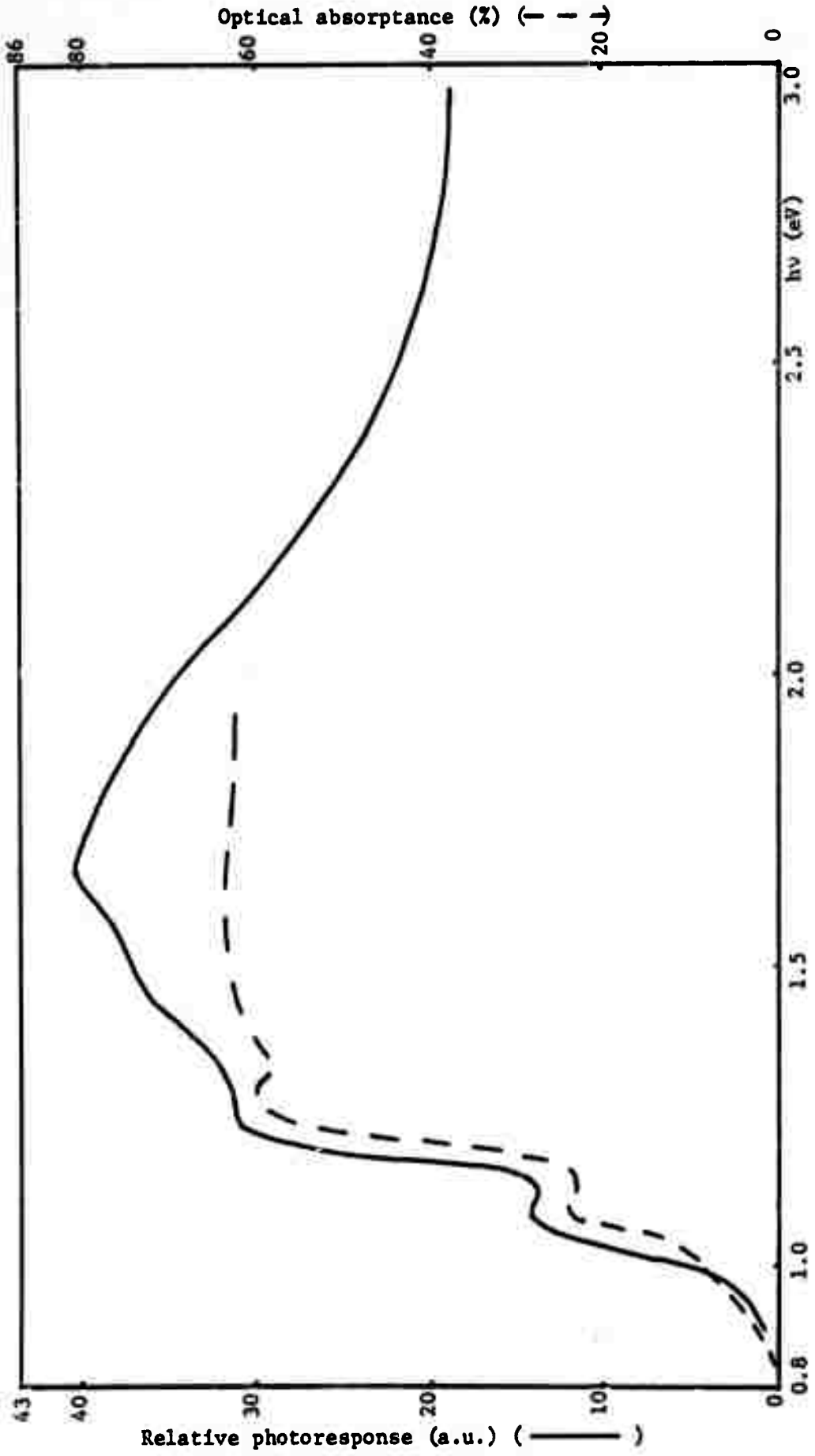
Optical absorptance (%) (— — —)
86
80
60
40
20
0
3.0
2.5
2.0
1.5
1.0
0.8
hν (eV)
43
40
30
20
10
0
Relative photoresponse (a.u.) (——)

FIG. 2

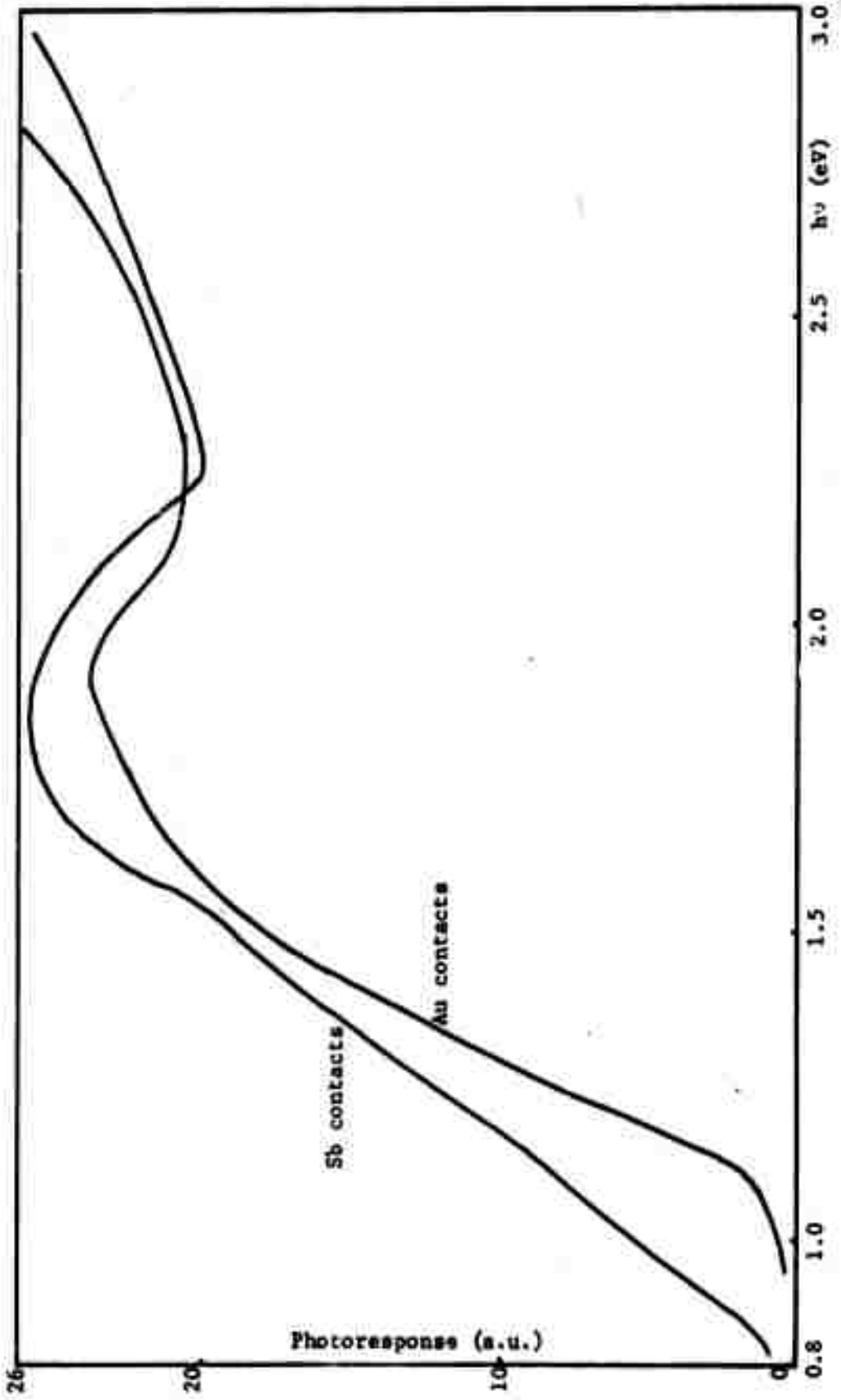
Photoresponse (a.u.)
0
10
20
26
0.8
1.0
1.5
2.0
2.5
3.0
hν (eV)
Au contacts
Sb contacts

FIG. 3